UNIVERSITÀ DEGLI STUDI DI CAGLIARI

Dipartimento di Fisica

Dottorato di ricerca in Fisica

XIX Ciclo (2003-2006)

Tesi di Dottorato

Porous Silicon applications in biotechnology

Relatore

Dott. Guido Mula

Dottoranda

Valeria Demontis

Acknowledgements

Vorrei innanzitutto ringraziare il mio supervisore di tesi, il Dott. Guido Mula, che mi ha dato l'opportunità di lavorare su un tema di ricerca estremamente interessante e che mi ha sempre sostenuto e incoraggiato con pazienza durante tutto il percorso di studi.

Un ringraziamento particolare alla D.ssa Susanna Setzu, che mi ha introdotto allo studio Silicio Poroso e che mi ha seguito per tutto il lavoro con costanza ed entusiasmo.

Vorrei poi ringraziare la D.ssa Silvia Salis, il Dott. Gianluca Manunza e il Dott. Daniele Chiriu con i quali ho collaborato in alcune fasi del lavoro sperimentale.

Un grosso contributo alla ricerca è stato dato dalla Prof.ssa Maura Monduzzi e dal Dott. Andrea Salis, che mi hanno guidato nella fase di realizzazione e caratterizzazione del biosensore. Ringrazio entrambi per la grande disponibilità dimostratami e per le preziose discussioni scientifiche svolte.

Je voudrais remercier Dr. Thierry Pagnier et Dr. Pierre Bouvier pour m'avoir accueilli dans le Laboratoire d'Electrochimie et Physico-chimie des Materiaux et des Interfaces (LEPMI) de l' Institute Nationale Polytechnique de Grenoble (France). Je les remercie pour m'avoir transmise un petite peu de leurs connaissances dans le domaine de la spectroscopie Raman et de la Photoelectrochimie et pour leurs conseilles qui m'ont aidée pendant le reste de mon travaille. J'adresse aussi mes remerciement au Prof. Didier Delabouglise qui m'a aidée pour l'étude de immobilisation d'ADN sur le silicium poreux.

Ringrazio inoltre la Prof. A. M. Fadda e la D.ssa C. Sinico del Dipartimento Farmaco Chimico Tecnologico dell'Università degli Studi di Cagliari per lo studio di realizzazione di un sistema Drug Delivery in Silicio poroso.

Infine ringrazio il nostro coordinatore di dottorato, il Prof Luciano Colombo, che ha seguito con grande dedizione il nostro percorso di studi, e tutti i docenti del corso.

Contents

Introduction

Biotechnology is nowadays a field in great expansion and the continuous boost for obtaining smaller and more efficient devices stimulates an always increasing interest from the research community. The fields of application of biotechnological devices are very numerous, ranging from industry, medicine, environmental studies, pharmacology etc.

The use of nanostructured materials in biotechnology is very attractive, since their unique properties offer excellent prospects for interfacing biological recognition events with electronic signal transduction and for designing a new generation of bioelectronic devices exhibiting novel functions[1].

The field of biosensing devices (*biosensors*), i.e. sensors which use a biological component to exert their functioning, is a very attractive field of research. In fact biosensors couple the selectively and sensitivity of a biological component with the power of detection of a technological device.

In this thesis we will mainly focus our attention to the realization of a porous silicon-based biosensor for triglycerides analysis.

Porous silicon (PS), discovered[2] in 1956, has been widely studied mainly for its optical properties (the room temperature luminescence[5] and the possibility to modulate the refractive index in a simple way during formation[3]), but since the interest of the scientific community has been triggered to its potential biotechnological applications, PS has shown many advantages respect to standard materials.

In particular porous silicon appears a to be a good candidate for coupling with biological molecules because of its peculiar characteristics. The most noticeable are the very large specific area, reaching 900 m^2/cm^3 for nanoporous Si, which allows the loading of large amounts of biological material in a very small volume and the possibility to easily tailor the pore size and morphology[30] as function of the kind of molecules to be introduced. Besides, the proven biocompatibility[34] and non toxicity[4] of PS layers allow

the possibility to develop devices to be directly implanted into living organisms without risk of rejection[53].

Moreover, the possibility to integrate the PS-based biotechnological device in the traditional silicon-based electronics, opens the way to the realization of compact systems for the *in vivo* and *online* diagnostics and treatments.

The first chapter of this manuscript is dedicated to porous silicon. We will start with a general description of the interfaces between a semiconductor and an electrolyte and then we will consider the particular case of the PS/electrolyte interface. The anodic formation in HF solution and the main properties of this attracting material will be discussed in detail.

In chapter 2 we will give a short overview on biosensors. We will describe the main elements that constitute those devices and we will make a brief introduction to enzymatic catalysis, that is the biochemical process on which our device is based. Then, we will discuss the state of art of porous silicon applications in the field of biosensors.

In Chapter 3 we will show the experimental methods used to realize and characterize our biosensor.

In Chapter 4 we will firstly deal with the process of formation of our PS samples, discussing the choice of the formation parameters (HF concentration, current density, anodization time etc.) and morphological properties (porosity, specific area, thickness etc.) for the realization of the biosensor. Then, the results of High Resolution X-ray Diffraction (HRXRD), Field Emission Gun Scanning Electron Microscopy (SEM-FEG) and N_2 adsorption method characterizations will be presented.

In chapter 5 we will discuss the process of stabilization of the porous silicon surface through oxidation, needed to protect the samples against dissolution in aqueous solutions.

In chapter 6 we will then describe the immobilization of lipase on PS layers. The method we used is physical adsorption, which has been preferred with respect to other techniques because it is based on weak interactions between the surface and the biological molecules, with very limited or no interferences on the biological functioning of the enzyme. We will then describe optimization of the immobilization process with respect to the

immobilization duration and the pH. The goodness of PS as matrices for enzyme immobilization will be demonstrated by measurement of the catalytic activity of the lipase-loaded PS system performed with standard techniques of analytical chemistry. The sensitivity of the device towards different triglycerides concentration will be shown. We will see that the velocity with which our system transforms a given quantity of triglycerides is a function of their concentration in the emulsion. This function, as we will see, very well match the Michaelis-Menten equation, that is the equation on which is based the theory of enzymatic catalysis in case of free enzymes.

Finally in chapter 7 we will describe the realization of the potentiometric biosensor. The loaded porous silicon samples will be used as electrodes in an electrochemical cell containing an emulsions where triglycerides act as electrolytes. The operation of our device is based on the sensitivity of PS / electrolyte interface to changes in the pH of the electrolyte solution. First of all we will describe the sensitivity of our system to changes in the pH of test solutions, by using buffer solutions with different pH. Then will describe the calibration of the device made using emulsions with different concentrations of tributyrin, showing the reliability and efficiency of our biosensor.

In Appendix A and a B we will describe two more applications of PS we investigated, that are at a very early stage of development. In Appendix A will be described the use of PS as a material for drug delivery systems, while in Appendix B we will present the use of PS for the realization of a DNA-biochip.

Chapter 1:

1 Porous Silicon

1.1 Introduction

Porous silicon (PS) was first observed more than 50 years ago by Uhlir[2] during some experiments of electropolishing of crystalline silicon in aqueous hydrofluoric acid solutions. However, since crystalline silicon, due to its indirect bandgap, do not show luminescence even at low temperature, the interest of the scientific community on PS was only triggered when its room temperature visible luminescence was discovered in 1990[5].

1.2 Electrochemical formation of Porous Silicon

1.2.1 Fundamental properties of SC/ Electrolyte Interfaces

The properties of semiconductor (SC)/electrolyte interface have been extensively reviewed[6], and here we will describe briefly the main characteristics needed for a better understanding of the porous silicon formation process and of its applications.

The diagram of the energy levels in an electrolyte may be described in a way similar to that used for the description of the energy levels in a solid[7]. A redox system (that is a system composed by two or more elements which can change their oxidation number during a reaction) is represented by an energy level that corresponds to an occupied electronic state for the reduced form and to an empty state for the oxidized form. In this representation, we can define the redox Fermi level ($E_{F,\,red}$), that is the equivalent for the electrolyte of the Fermi level, as the energy level at which the probabilities to find oxidized or reduced species in solution are the same (Fig. 1.1 (b)).

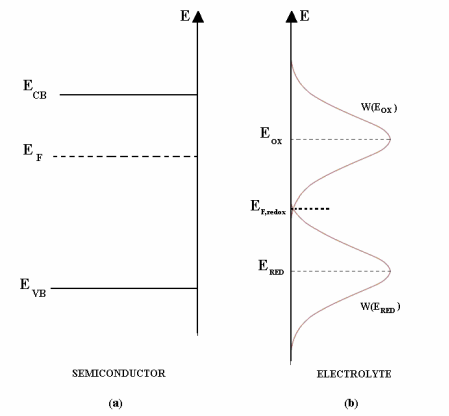

Fig. 1.1: Schematic representation of the energetic levels of a *n*-type semiconductor (a) and an electrolyte (b) before contact. E_{CB} and E_{VC} are the energies of the conduction and valence bands, E_F is the Fermi level. W (E_{OX}) and W (E_{RED}) are Gaussian functions which represent the probability to find the oxidized or reduced species at energy E. $E_{F,\,redox}$, is the redox Fermi level and corresponds to the energy at which the probabilities are equal.

When a semiconductor electrode is brought in contact with an electrolyte, an equilibrium is established through a mechanism of charge transport between the two phases, leading to a band bending which continues until the Fermi level of the semiconductor equals the Redox Fermi level of the electrolyte.

This transport is carried out by electron transfer through the conduction band or by hole transfer through the valence band. In general, the net result of the redistribution of charges at the interface is the formation of an electric double - layer, with three distinct zones: the Space Charge Layer (SCL) in the semiconductor side, the Helmholtz layer (HL) and the diffuse layer (DL) in the

solution side. The definition of these three layers is given in the following discussion.

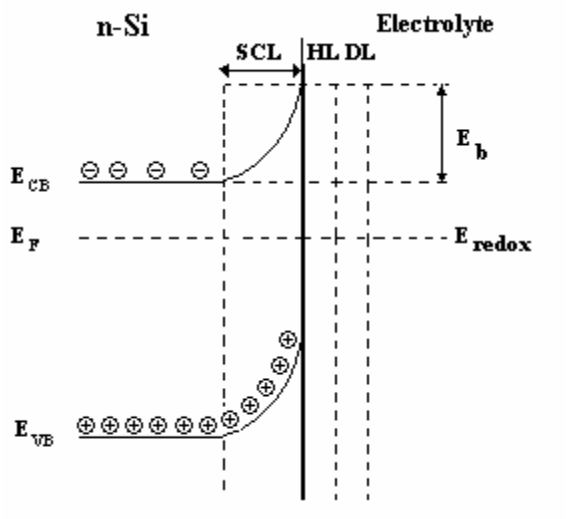

Fig. 1.2: The energy levels across an *n*-Si / Electrolyte interface; E_b is the band bending energy.

According to the relative position of the Fermi Level and the Redox Fermi Level, three different situations are possible (Fig. 1.3):

$E_F > E_{F,redox}$. Inversion (Fig. 1.3 a): there is a flow of electrons from the semiconductor into the electrolyte. As a consequence, electrons are drained from the surface, giving rise to a depletion layer in the semiconductor, called Space Charge Layer (SCL), which typically extends from a few tens to a few hundreds of nm in depth. Since surface is depleted from electrons, it remains positively charged. The electric field in this region is a function of the distance from the surface. On the electrolyte side, this mechanism is followed by a reorientation of dipoles and ions, so that a negative charge accumulates to form the Helmholtz layer (HL). It contains ions that are specifically adsorbed on the electrode (protons on an amphoteric surface for example) and polarized solvent molecules. The concentration of these ions defines the potential drop across the Helmoltz layer and controls the position of the contact potential at the surface of the semiconductor (as we will see in the following paragraphs, the flatband potential); the depth of this region is less than 1nm. The region between the Helmoltz layer and the bulk electrolyte is characterized by a deviation of ion

concentration with respect to the bulk values and is called Diffuse layer (DL) or Gouy-Chapman region.

The space charge layer within the semiconductor leads to a dependence of electron energy on distance, which is referred to as band bending at the surface. Band bending causes the majority carriers at the surface to move towards the bulk of the semiconductor, while holes are attracted to the surface. The semiconductor electrodes is then said to be in depletion mode because electrons are drained away from the surface.

$\mathbf{E_f < E_{F,redox}}$. Accumulation (Fig. 1.3 b): Electrons flow from the electrolyte towards the semiconductor. As a consequence, at equilibrium there is an accumulation of majority carrier in the Space Charge Layer, whose depth is in this case shorter than in the case of inversion.

$\mathbf{E_F = E_{F,\ redox}}$. Flat band (Fig. 1.3 c): The two phases are in equilibrium and there is no charge transfer, nor an electric double-layer; this condition is called *flat band.*

Different kinds of band bending are shown in Fig. 1.3 for *n*-type silicon.

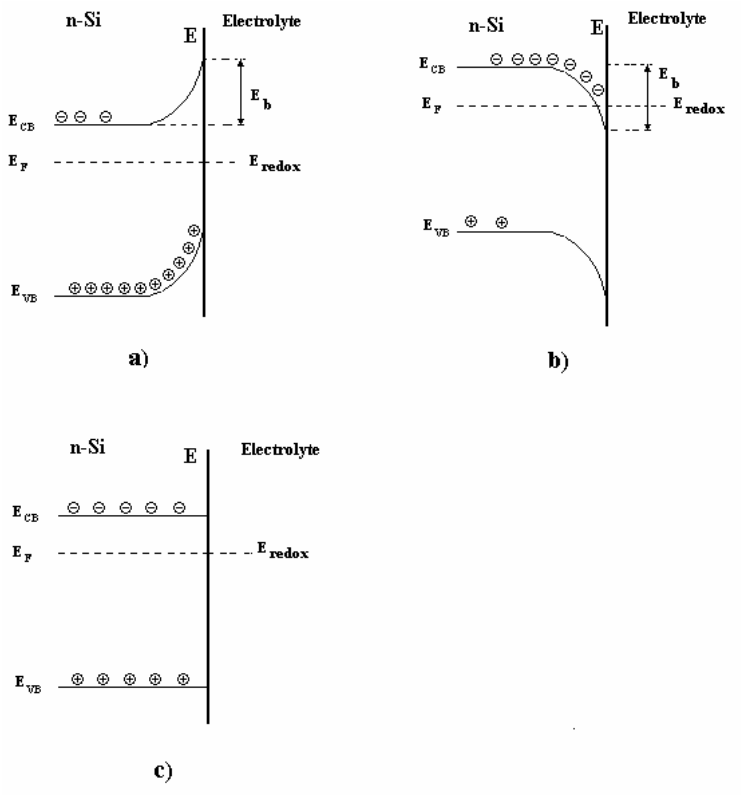

Fig. 1.3: Different types of band bending for an n-type Si electrode in equilibrium with an electrolyte. a) Inversion; b) Accumulation; c) Flat band. E_{VB} is the valence band energy, E_{CB} is the conduction band energy, E_F is the Fermi level in the semiconductor and $E_{F,redox}$ is the redox Fermi level of the electrolyte.

The potential difference between the semiconductor and solution phases can be varied by applying an external potential and the junction can be modified from accumulation to flatband and inversion.

1.2.2 Flatband potential

The applied potential at which there is no band bending is called *flatband potential* and is a quantity of great relevance in electrochemistry. Indeed, since the flatband potential is determined by the potential drop across the Helmoltz layer, it depends on the concentration of ions adsorbed onto the surface, that is in turn influenced by the reactions occurring at the interface.

In general, if X is the ion that can be adsorbed onto the surface, the potential drop across the interface is described by a nernstian equation:

$$V_s - V_{sol} = const. - \frac{RT}{nF}\log(a_X)_{sol}$$

where V_s and V_{sol} are the potential in solid phase and in the electrolyte phase, respectively, R is the gas constant, T is the temperature (in this case 298 K), n is the number of exchanged electron, F is the Faraday constant and a_X is the activity of the ion X, that is the concentration of the ion X in the solution[8]. In general, it is commonly used the following approximated form:

$$V_s - V_{sol} = const. + \frac{0.059[V]}{n} \cdot pX$$

If $X = H^+$, the flatband potential is expected to shift cathodically by 59 mV when the pH of the electrolyte is increased by one unit at T= 298 K:

$$V_{fb} = const. + \frac{0.059}{n}[V] \cdot pH$$

This is the case of semiconductors covered by a thin oxide layer in contact with an aqueous electrolyte (that is also the case for the system we want to study) for which the flat band potential shows a strong dependence on the pH of the electrolyte.

It is commonly accepted[8] that this phenomenon is due to the fact that the oxide's surface in contact with aqueous solutions is positively charged, negatively charged or neutral depending on the pH of the solution, as shown in Fig. 1.4. The blue rectangles indicate the surface of the oxide, while p_0 is the zero charge point.

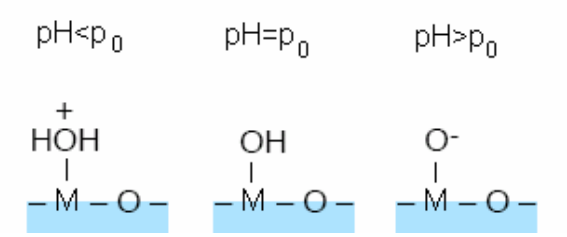

Fig. 1.4: Scheme of the behaviour of the oxide's surface in contact with solutions at different pH.

Indeed for several semiconductors the plot of flatband as function on pH shows the expected linear behaviour with a slope of 60 mV per pH unit.

However, its is very difficult to know exactly the reactions occuring at a semiconductor/ electrolyte interface and deviations from the nernstian behaviour are often observed[9]. For example, for TiO_2 the dependence of V_{fb} on pH is 50 mV per pH unit, for 6H-SiC is 40 mV/pH unit, for GaP is 37 mV/pH unit etc.

In case of Si/ aqueous electrolyte interface, a weaker sensitivity of flaband potential on pH has been observed[10]. Experimental measurements show, in fact, slopes of about 30 mV per pH unit. Even in this case the main reaction which determines the V_{fb} variation on pH is attributed to the amphoteric behaviour of the Si–OH (silanol) groups on the Si surface. The frequent deviations from nernstian behaviour have not been yet clearly explained.

V_{fb} is also influenced by other parameters that can modify the interface, such as the doping level, oxidation of the surface, adsorption of charged species and variations in the concentration of the electrolyte. Then since the V_{fb} is highly sensitive to the surface modifications it is a good parameter to study electrochemical processes involving a semiconductor as one of the electrodes.

One of the most used techniques to determine the flatband potential is photoelectrochemistry. The semiconductor/electrolyte junction at inversion regime is a photoconductive system: when lightened using photons with energy larger than the electronic band-gap, electron-hole pairs are created and, due to the band bending, charges can diffuse in the material. These charges give rise to an electric current, called photocurrent, which is greater for higher band bending. Photocurrent decreases when an external potential is applied in such way to reduce the band bending and is zero when the applied potential equals the flatband potential. The photoelectrochemical study of the evolution of the flatband potential during a reaction is not possible because the light beam used to excite the electron-hole pairs can interfere with the system. It is instead possible to take advantage of another simple and powerful technique to investigate and characterize a semiconductor surface immersed in an electrolyte. This technique, introduced in 1995[11], consists in measuring the time evolution of the open-circuit potential (OCP).

1.2.3 Open Circuit Potential

The open-circuit potential (OCP) (also referred to as equilibrium potential or rest potential) of an electrode, is the overall voltage generated in the electrochemical cell measured with respect to the potential of a reference electrode. This voltage is measured in the open circuit configuration using a high-impedance voltmeter, so that only a negligible current can flow through the cell. OCP is the most easily measurable electrochemical parameter, but at the same time is a complex quantity as it is the sum of all possible potential drops in the system. In fact, in such experimental setup additional potential drops (V_0) are involved respect to V_{fb}, for example potential drops at electrolyte/reference electrode and semiconductor/ metal interfaces.

$$OCP = V_{fb} + V_0$$

The absolute value of OCP gives no useful information about interface reactions. However, as we are interested in the differences of the potential drop across the interface, OCP variation is a good parameter to investigate reactions. In fact, the only contribution to OCP that can vary as a consequence of a reaction at the electrode is V_{fb}, because all other possible potential drops are on first approximation not affected by interface modifications. The study of the time evolution of OCP is then equivalent to the study of the time evolution of the flatband potential.

An electrode in the open circuit configuration is in equilibrium if no net chemical change occurs in the system during the time of measurement. This is the case for example when the Fermi level of the semiconductor has the same value of the redox Fermi level of an electrolyte. In many situations, and almost always for crystalline silicon, the electrode/ electrolyte interface at open circuit is at a nonequilibrium condition and a net chemical change in the system occurs when two or more redox couples are present in the electrolyte. In this cases OCP is not a constant parameter.

When one of the redox couples is associated with the dissolution of the electrode, OCP is also called corrosion potential (it is the case of a silicon electrode at OCP in aqueous solution).

Any change in the system, such as surface preparation, solution composition and concentration, pH, temperature, convection, lighting, and so on, can affect the OCP. For applications like biosensing, in case of non

equilibrium electrodes, i. e. red-ox or dissolution reactions, a surface stabilization is required in order to eliminate the contributions to OCP due to interface modifications.

All this considerations make the OCP a very important parameter in many applications, such as standard pH measurements with glass membrane electrodes, and will be used in the course of this thesis as a key parameter for the characterization and calibration of biosensors.

1.2.4 The Si/ Electrolyte interface

Silicon is known to be a highly oxidizable material so that the surface stability has been a major issue for electrochemists. In presence of water silicon reacts forming an oxide layer with passivating nature, that prevents silicon from further etchings. The great likelihood of the silicon oxidation reaction and the stability of SiO_2 explains why under ambient conditions silicon is almost always found with a native surface oxide layer, of a typical thickness of about 2nm. HF is one of the few substances that can dissolve this SiO_2 layer at room temperature, leading to a prevalence of silicon hydride species on the surface. Aqueous HF solutions are also most widely used to perform the dissolution of crystalline silicon to form porous silicon.

1.3 Porous silicon formation

1.3.1 Formation regime by anodization

Since early studies Porous Silicon (PS) has been mainly obtained by electrochemical etching of crystalline silicon in aqueous or ethanolic HF solutions. Several reports[12] show the possibility to form PS by chemical reactions, commonly called “stain etching”, where dissolution is carried out in a mixture of HF and a strong oxidizing agent, such as KNO_3, with no current flow. These techniques however are not so versatile or reproducible as anodic etching, that still remains the most used technique.

The anodic dissolution is carried out in a cell where the silicon wafer acts as anode and a HF-resistant electrode (generally made of platinum) acts as

cathode. The cell body is constructed with a highly acid resistant material, as Teflon.

Porous silicon preparation in aqueous HF electrolyte is now controlled up to a very high level of reproducibility, permitting also the construction of complex structures (for example superlattices). However, the formation parameters are only known on empirical basis, while the exact formation mechanism, after an almost fifty years long debate, is still not completely understood[13, 14, 15, 16, 17, 18, 19, 20].

A basic knowledge of Si/ HF electrochemistry is the starting point for any understanding of pore formation.

Is useful to define the four categories in which silicon wafers are classified according to the doping type and level:

p-type: *p*-doped samples with a resistivity of the order of the Ωcm;

p^+-type: heavily doped *p*-type samples with resistivity of the order of 10^{-3} Ωcm;

n-type: *n*-doped samples with resistivity of the order of the Ωcm;

n^+-type: heavily *n*-doped samples with resistivity of the order of 10^{-3} Ωcm.

Fig. 1.5 shows the typical *i-V* curves for *n*- and *p*-type doped silicon in aqueous HF.

These curves show some similarities with the Schottky diode model, expected for a semiconductor/electrolyte interface, including photogenerated currents. However, there are also significant differences: for example, the fact that even if the sign of majority carries is different in *n* and *p*- type silicon, the reactions at Si/ HF interface remain the same or the three order of magnitude higher current values with respect to normal Shottky diode, which indicates a possible surface state contribution [21].

Under cathodic polarization both *n* and *p*-type silicon are normally stable, that is silicon doesn't dissolve. The only reaction that takes place in this region is the reduction of water with the subsequent liberation of hydrogen gas. It is only under anodic polarization that silicon dissolution occurs, but porous silicon formation takes place only in a particular region of the anodic regime.

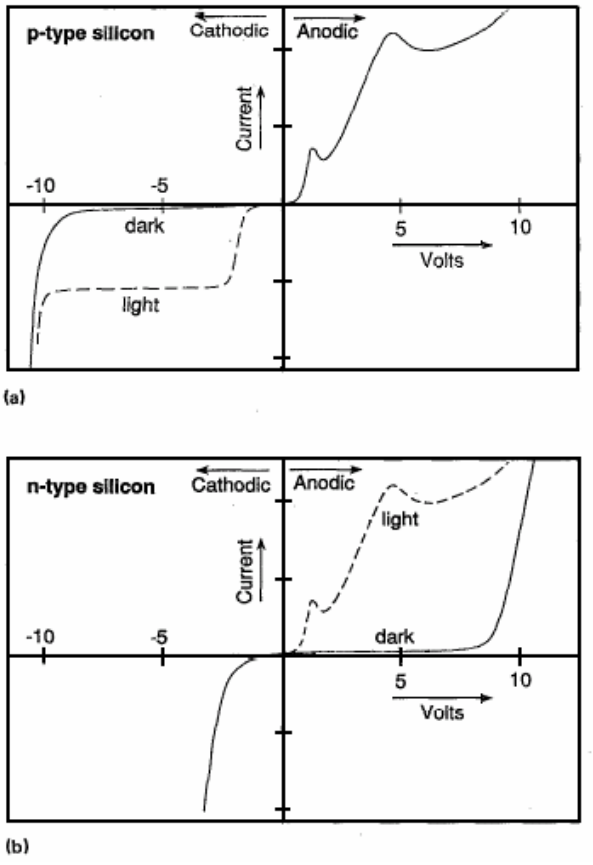

Fig. 1.5: Typical *i-V* curves for (a) *p*- type and (b) *n*- type silicon in aqueous HF solutions[21]. The solid line indicates the dark response and the dashed line indicates the light response.

Fig. 1.6 shows a magnification of the part of the anodic potential region interesting for porous silicon formation. Three regions must be distinguished, labelled with the three letters A, B and C.

Pore formation takes place in region A, where *i-V* characteristics show an exponential behaviour. In region C, at high potential values, there is the silicon electropolishing. Region B is a transition region, where the process of PS formation and electropolishing compete.

The curve in Fig. 1.6 is the same for both *p*- type, p^+-type and n^+-type, except for *n*-type silicon (poorly doped *n* silicon), for which the process of

pores formation does not take place without illumination. The *i-V* curve for this type of wafer became similar to the others only under illumination.

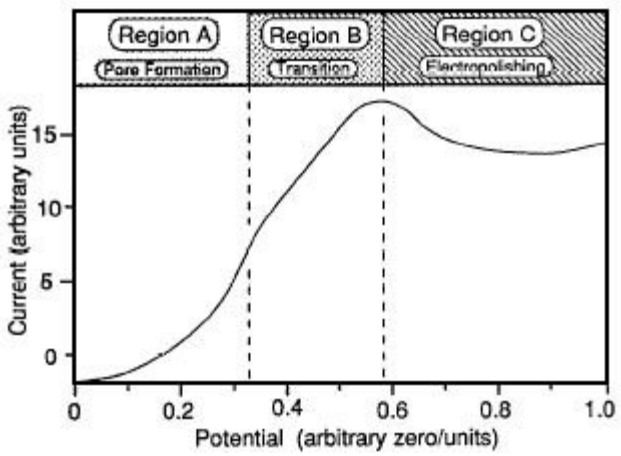

Fig. 1.6: Typical anodic *i-V* curve, showing the salient region of silicon dissolution in aqueous HF. In region A porous silicon formation occurs, in region C silicon electropolishes and region B is a transition region[21].

The formation of porous silicon has been a subject of investigation for many decades, but still no agreement on the exact mechanism has been obtained. In the electrochemical formation of PS two aspects must be distinguished: the pore initiation and their subsequent propagation. As far as the the pores initiation is concerned, it is commonly accepted that it will occur in presence of surface defects or inhomogeneities.

1.3.2 Dissolution chemistry

The most accepted model for the dissolution chemistry of silicon during anodic etching in HF is that proposed by Lehmann and Gösele[16] shown in Fig. 1.7.

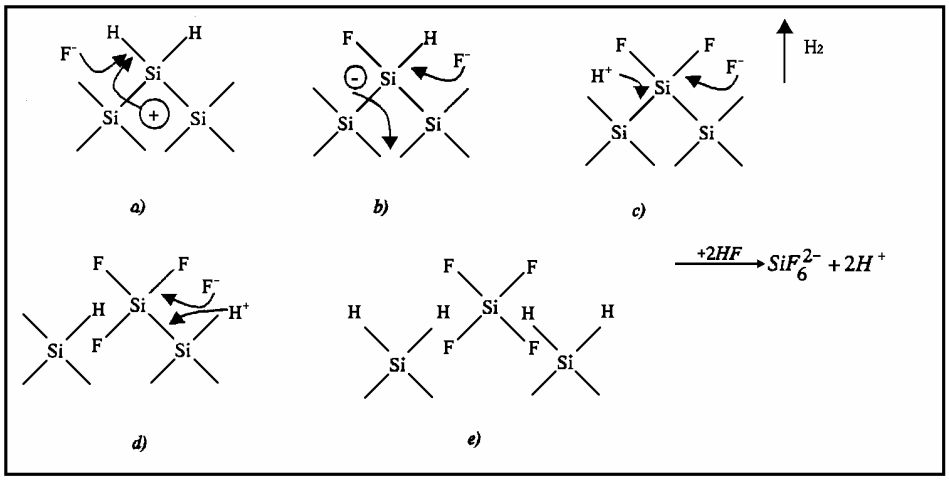

Fig. 1.7: Reaction model proposed for the silicon electrodes dissolution in aqueous HF solutions, associated with porous silicon formation[16].The description is in the text.

When PS is immersed in HF solution it is characterized by hydrogen-terminated surface.

When a hole reaches the hydrogen saturated surface, attack of the Si-H bonds by fluoride ions can occur and a Si-F bond is established (Step a). The bonded F exerts a polarising influence so that another F^- ion can bond to silicon, with the generation of an H_2 molecule and the injection of one electron into the electrode (step b and step c). The polarization induced by the two Si-F bonds weakens the Si-Si backbonds that are easily attacked by HF or H_2O, in presence of a second hole (Steps d and e); then one silicon atom remains bonded to fluorine atoms and disperse in the solution (Step e). The SiF_4 is not stable and reacts with HF forming H_2SiF_6.

The hole process requires two holes to take a silicon atom in solution.

When a silicon atom is removed from the surface, it leaves an atomic size dip that causes a change in surface geometry and in the electric field distribution. In particular, as in correspondence of a dip the surface has a smaller curvature radius, the electric field lines are concentrated in these locations. As a consequence, a preferential hole transfer will occur, amplifying surface inhomogeneities and causing the gradual formation of the porous structure.

1.3.3 Theories of pore formation

If the chemistry of the formation process is reasonably well understood, the mechanisms behind pore propagation are still unclear and several models have been proposed.

All proposed theories agree to the fact that at the semiconductor/electrolyte interface the formation mechanisms are more easily explained by taking into account the physical parameters (such as band bending, electric field lines, depletion layers, tunnelling, …) than the specific chemical reactions that are involved in the dissolution of the semiconductor. As a matter of fact, it seems that the mechanisms driving the pores' formation are similar whatever the semiconductor (Si, GaN, GaAs, …)[18].

At present, the Beale model is one of the most accepted theories. It considers the semiconductor depletion layer as the parameter determining the distribution of the electric field and then the pore propagation. As we have just seen, for the dissolution to occur the presence of holes is needed, and the pores propagate until holes are available. When the diameter of crystallites (silicon skeleton) is of the order of two times the space charge layer thickness, a depletion of the remaining silicon occurs, because of the overlapping of the space charge regions at the pore surfaces.

When this condition is reached the structure becomes inert towards further electrochemical etching and the formed layer doesn't participate at the reaction anymore. In the bottom of pores, where the curvature of the surface is smaller and the electric field more intense, the depletion layer is thinner and the probability for a hole to reach the surface through tunnel effect is greater. Then, it is there that the reaction propagate.

1.4 Characteristics of PS layers: dependence on anodization conditions

1.4.1 Morphology

The microstructure of porous silicon has been extensively studied by many groups by means of microscopy techniques. Beale et al[18], characterized several

porous silicon layers obtained with different substrate doping and different anodization currents by Transmission Electron Microscopy (TEM). They observed that the doping level, and therefore the substrate resistivity, is the parameter which determines the morphology of the formed layer.

Fig. 1.8 show the typical morphologies of the four different wafer types. In *p*-type porous silicon both the pore diameter and the crystallite sizes are very small, generally between 1 and 5 nm. The morphology is characterized by a homogeneous and highly interconnected pore network, that is often referred to as 'sponge' structure.

In *n*-type porous silicon the pore sizes are considerably larger than in *p*-type and they tend to form straight channels in the direction of the crystallographic axis. In general the structure is macroporous, but the pore formation process shows two phases: at the beginning (the first few hundreds of nm) the formed layer is nanoporous, after this nanoporous layer, macropores are formed.

Both heavily *n*- and *p*- doped silicon samples give rise to porous films with a microstructure characterised by many long voids running perpendicular to the surface, with occasional branches and numerous small buds on the side of the main pores. Main columns have in general a diameter of a few tens of nanometers, that is larger than that of *p*-type PS nanopores, and these materials are therefore classified as "mesoporous".

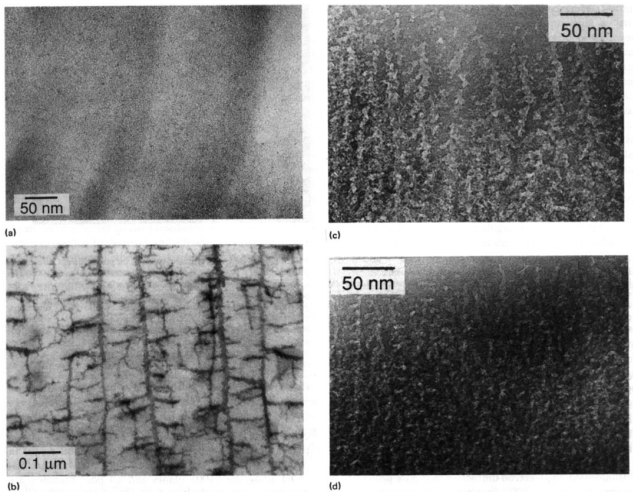

Fig. 1.8: XTEM micrographs showing different morphologies obtainable with p, n, p^+, n^{+21}.

The difference in pore size between various morphologies can be evaluated by the analysis of the gas adsorption isotherms by using the BJH (Barett-Joyner-Halend) method[22] and the D.H. (Dollimore- Heal) extension method[23].

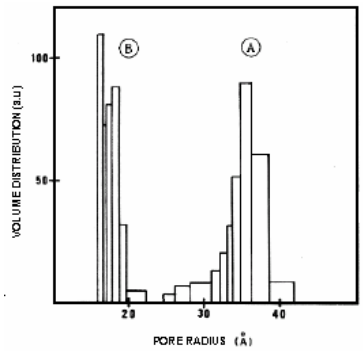

Fig. 1.9: Pore size distribution of (A) p^+-type and (B) p-type porous silicon obtained by BJH method[24].

Almost all literature studies refer to p-type porous silicon, that has been studied more in detail than n- type. As we can see in Fig. 1.9, the pore size distribution in lightly doped samples is remarkably lower than in heavily doped samples under the same anodization conditions.

1.4.2 Porosity

Porosity is defined as the fraction of void in the porous silicon layer[30]. Porosity is a combined function of HF concentration in the etching solution and of current density. The measured porosity as a function of these two parameters is shown for p and p^+-type PS in Fig. 1.10.

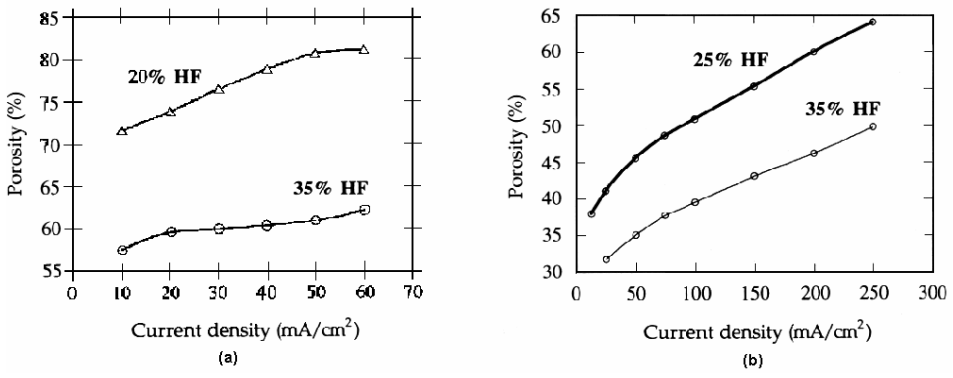

Fig. 1.10: Porosity as a function of current density for two different HF concentration for *p*-type (a) and p^+-type PS[30].

For a given HF concentration, porosity increases with increasing current density and for a fixed current density the porosity decreases with increasing HF concentration. Not all the porosity values are accessible experimentally, since below a critical porosity value there is no dissolution, while an upper level is imposed by the low mechanical stability of the high porous layers. This is an empirical limitation due to the fact that the high stresses to whom the structure is exposed during the drying phase can cause the cracking of the layer. A great care must be taken in this phase in order to obtain levels of porosity very close to 100%.

1.4.3 Crystalline properties

One important property of porous silicon is that its skeleton maintains the structure of a single crystal after anodization, as shown by X-ray topography studies. Fig. 1.11 shows the typical diffraction pattern of PS[25]. When studying a porous silicon layer on the crystalline silicon substrate, two distinct diffraction peaks occur for each X- ray reflection: one from the crystalline silicon and the other from the porous layer, located at a smaller Bragg angle.

The shift of the PS-related Bragg peak towards smaller angles indicates that the pore formation affects the silicon lattice by slightly expanding its lattice parameter by an amount that depends on the details of the pore structure.

Moreover, the width at half maximum of the porous silicon peak (7'') is not too different from that relative to crystalline silicon (5''), which confirms that the porous silicon skeleton is a nearly perfect crystal despites its porosity.

As far as the elastic properties are concerned, PS differs from crystalline silicon. These properties have been studied from the measured strains produced by the lattice mismatch and the results demonstrate that porous silicon is less stiff than crystalline silicon, and stiffness decreases with porosity[25]. This property seems to be very useful for using porous silicon as a substrate for molecular beam epitaxy. For instance the use of porous materials as a substrate for epitaxy has been suggested for a few materials[26, 27, 28].

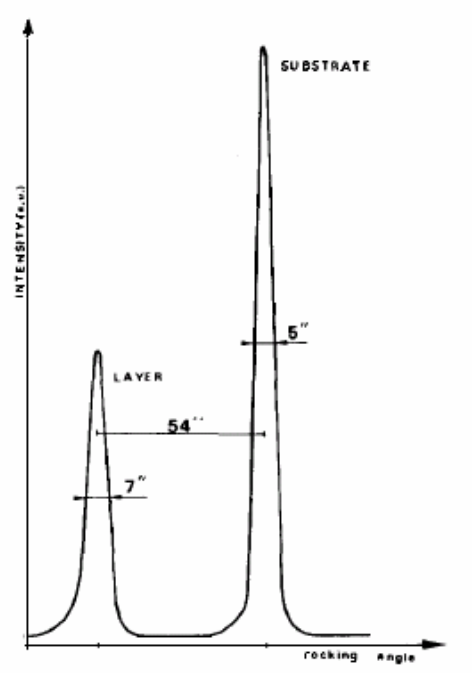

Fig. 1.11: X-Ray diffraction pattern of p^+-type porous silicon layer on a silicon substrate[25].

1.4.4 Thickness

The thickness of porous silicon layers increases linearly with increasing anodization time[30], as shown in Fig. 1.12. This means that the formation velocity is constant and that the thickness of a sample is determined only by the anodization time once the formation parameters are fixed. Typical values of the formation velocity are of some tens of nanometers per second, but slow variations occurs by changing the substrate doping.

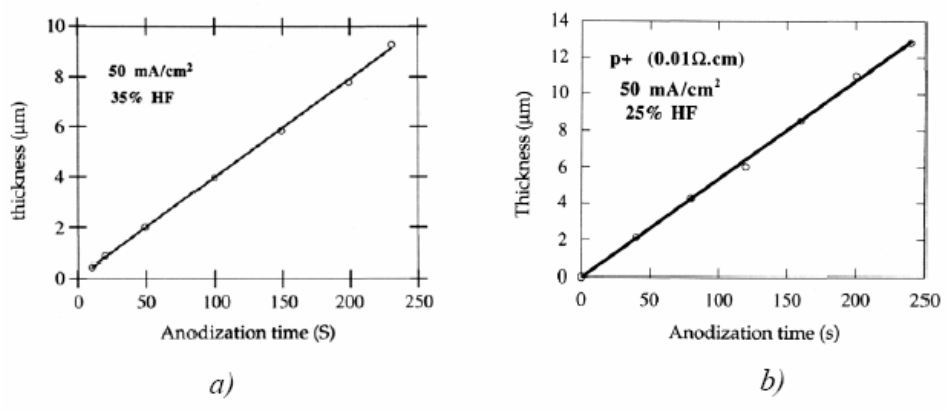

Fig. 1.12: Thickness of the porous silicon layers as a function of anodization time for a) *p*-substrate and b) p^+-substrate[30].

1.4.5 Surface area

The specific surface area of porous silicon is defined as the accessible area of solid surface per unit volume of material[29]. Its values are very high and can range from ~100 m^2cm^{-3} for macroporous silicon to ~900 $m^2\,cm^{-3}$ for nanoporous. Measurements by N_2 adsorption method (BET) have shown that specific surface depends on porosity. In particular, beyond a value of porosity of 50%, specific surface decreases with increasing porosity. In Fig. 1.13 is represented the evolution of the specific surface of two lightly doped *p*-type samples with different starting porosity (51% and 65%) as a function of porosity[30]. The porosity of the samples was then varied by chemical dissolution. For all values of porosity the two samples have the same specific surface, as a demonstration that in this case the porosity is the relevant parameter for specific surface independently on other anodization conditions.

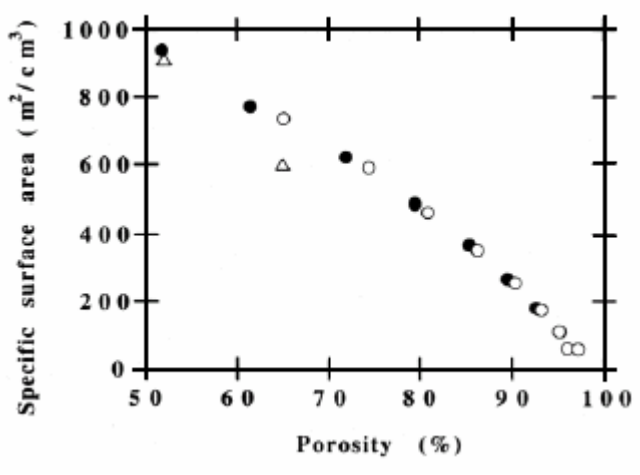

Fig. 1.13: Specific surface area as a function of porosity for 1 μm-thick *p*-type PS sample and starting porosity of 51% (●) and 65% (○)[30].

As we can see maximum of specific surface is found in correspondence of 50% of porosity, and the value of this maximum is at about 900 m^2cm^{-3}. The high values of specific surface make porous silicon a material suitable for many application, especially in biotechnology.

1.5 Porous silicon surface modification

As prepared PS layers show a great reactivity due to the instability of the surface just after formation and rapid modification of the surface occurs if the surface is not intentionally passivated.

1.5.1 Aging

The surface of fresh porous silicon (that is PS shortly after formation) is almost completely covered by hydride species (SiH, SiH_2, and SiH_3 groups), as evidenced by infrared vibrational spectroscopy[31]. Hydrogen-terminated porous silicon, which exhibits a highly hydrophobic character, has been shown to be sufficiently stable to perform studies on this material in inert atmospheres or in air for short periods of time.

Longterm use of as-formed PS is precluded due to its great propensity to oxidize. In fact, it has been observed[5,32] that the storage in ambient air at room temperature (aging) causes natural oxidation and contamination by chemical species from the atmosphere, giving rise to a passivated surface of highly variable composition. The resulting surface is mainly covered with surface hydroxyl groups (Si-OH) called silanol groups and, opposite to fresh PS, shows hydrophilic properties.

Fig. 1.14 shows infrared transmission spectra of fresh and aged *p*-type PS; we can see that changes concerns mainly hydrogen and oxygen content.

As-formed PS shows the absorption bands associated with vibrations of the $Si\text{-}H_x$ (2115, 2090, 906, and 630-670 cm^{-1}) and, but only for this particular sample, the bands associated with Si-F bonds (815 cm^{-1}). During aging, absorption bands associated with Si-O groups (1050-1200 and 450 cm^{-1}) appear while absorption of $Si\text{-}H_x$ groups decrease; also Si-F bands disappears, because they are progressively replaced by Si-OH bonds.

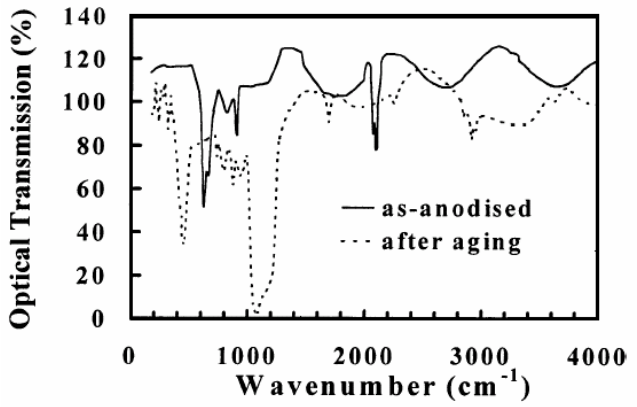

Fig. 1.14: Infrared transmission spectra of as-formed 80% porosity PS layer and the same after aging over 92 weeks in air[32].

The aging process is affected by illumination conditions, humidity, temperature and sample porosity and, since it is very difficult to control all storage conditions, this prevents the obtainment of identical layers.

1.5.2 Dissolution of porous silicon in aqueous solutions

The instability of PS silicon surface is increased by contact with aqueous solutions. It is well known that PS dissolves in alkaline solutions, but more recent papers[33,34,35] showed that dissolution also occurs in aqueous solution and under simulated physiological conditions. Unfortunately, even if many articles refers to it, this process has not been yet extensively studied.

Anderson et al[34] studied the process of dissolution for *p*-type PS, observing that dissolution is dependent on the layer porosity an on the pH of the solution. Fig. 1.15 shows the dissolution kinetics of three porous silicon layers with medium(62%), high (80%) and very high porosity (88%) in solution at pH = 7.

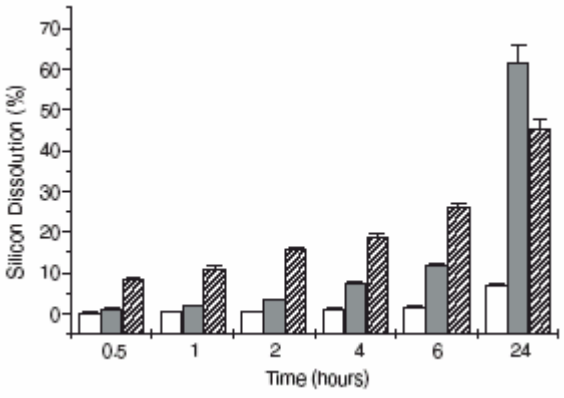

Fig. 1.15: Dissolution kinetics of *p*-type porous silicon layers at pH = 7 for Medium (62%) silicon porosity film (white); high (83%) porosity film (grey); and very high (88%) porosity film (hatched) [34].

The dissolution rate is besides affected by the pH of the solution, in particular it increases by increasing the pH value. For medium porosity samples (≈ 60%) the dissolution process is not appreciable for solution having pH values smaller than 6, while for pH > 6 the dissolution effects are already visible after a few hours.

In our case, we observed this phenomenon in acetate buffer at pH 4 and pH 5 and in phosphate buffer at pH 6, pH 7 and pH 8.

If for some biomedical application (for example drug delivery) material corrosion may even be desirable, for others, such as biosensensing, a stable interface between the pores and an aqueous environment is necessary.

One strategy to obtain long-term stability is to intentionally oxidize the surface under controlled conditions[36]. Three approaches are possible:

1. Thermal oxidation
2. Electrochemical oxidation
3. Chemical oxidation

1.5.3 Thermal oxidation

Thermal oxidation is the most commonly used technique for the passivation of silicon in microelectronics. This technique has been applied to the oxidation of porous silicon since many decades in order to provide a stabilization of the luminescence[41]. It consists in the annealing of porous samples at high temperature in ambient air or under controlled O_2 atmosphere for time intervals ranging from a few tens of minutes to a few hours. In general, the temperatures used are within the 300 °C ÷ 1000 °C range. PS layers are then partially or totally transformed in SiO_2:

$$Si + O_2 \rightarrow SiO_2$$

depending on the formation parameters. The oxidation temperature must not exceed 1000 °C, unless a pre-oxidation step at 300°C is performed, since the porous structure can be modified and the pores can collapse[41]. The content of oxygen at the end of the process varies with substrate, oxidation temperature and duration, but it is uniform aver all the surface. In mesoporous material formed on n^+-type doped substrates and oxidized at 1050 °C, more than 90% of the Si is oxidized within 30 s[37].

1.5.4 Anodic oxidation

Electrochemical oxidation of porous silicon occurs in electrolyte solutions under anodic polarization, and is therefore called “anodic oxidation”. Generally, the process is carried out at constant current density using a 0.1 M aqueous KNO_3 solution[38]. Since fresh porous silicon surface is hydrophobic, electrolyte must be gradually substituted avoiding the air exposure of the pores’ surface.

Several articles[38, 39, 40, 41] report that anodic oxidation of *p* and p^+-type PS proceeds with slow variations of potential during time, until a critical value of potential V_0 is reached. Beyond that critical value a sharp increase of potential occurs, which is interpreted as the breaking of the electrical contact in the porous layer. The oxidation process, in fact, causes the electrical isolation of parts of the Si-skeleton that prevents the achievement of a complete layer oxidation. In general 40-50% of the structure remains unoxided at the end of the process.

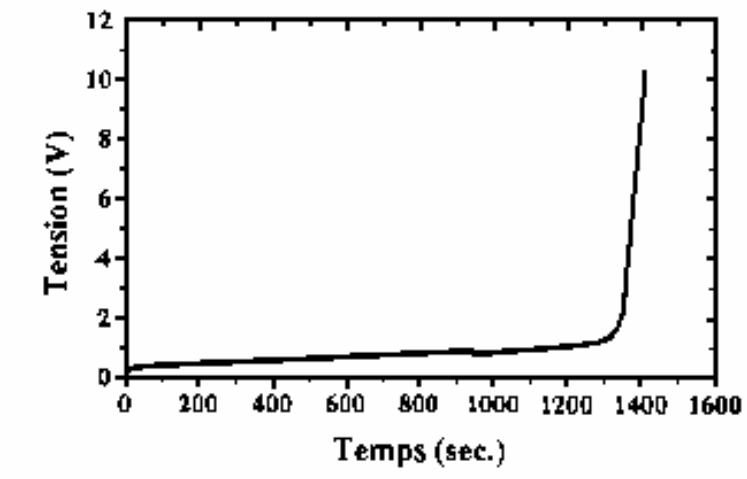

Fig. 1.16: Time evolution of the anodization potential during oxidation at constant current density of 0.3 mAcm-2 for a 1 μm-thick p-type sample of 65% of porosity[41].

The value V_0 at which the interruption of the electric contact occurs for p^+ samples is comprises between 7 V and 10 V at 5 mA cm^{-2} [38].

A good parameter that as been appointed for the description of the anodic oxidation is the *exchanged charge* during the process. If the oxidation process is stopped before the break of the electric contact, exchanged charge can also been chosen to measure the anodic oxidation level of the sample[41].

The *anodic oxidation level* (*q*) is defined as the ratio between the exchanged charge at the moment of oxidation process interruption (*Q*) and the maximum exchanged charge for a process where the contact breaking is reached (Q_0):

$$\text{Oxidation level} = q = \frac{Q}{Q_0}$$

The exchanged charge Q_0 is in a first approximation independent on current density, but depends on the layer thickness[42]. Fig. 1.17 shows the complete plots of the anodization potential as a function of the exchanged charge for *p*-type PS samples oxidized using a constant current density of 0.1 mA/cm^2. We can see that the potential V_0 at which the breaking of the electric contact occurs is equal to 3V for all samples, but the total exchanged charge increases when increasing the sample thickness.

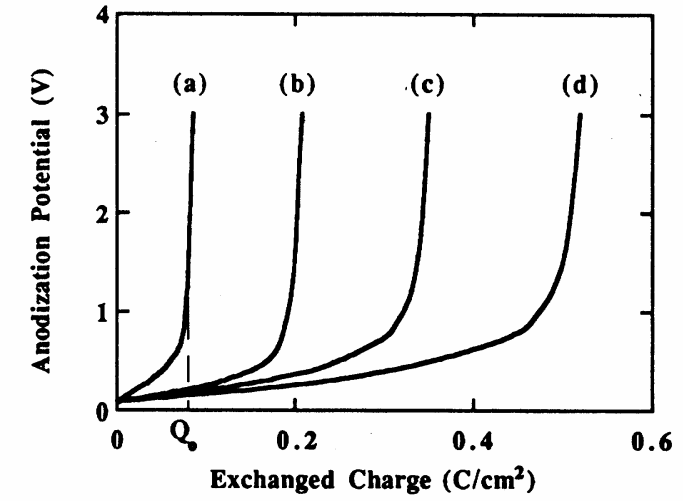

Fig. 1.17: Anodization potential as a function of exchanged charge for four *p*-type samples of different thickness: a) 0.3 μm, b) 1 μm, c) 3μm, d) 5μm[43].

In contrast with thermal oxidation, complete conversion of PS to silica is not achieved, because electrical isolation of parts of PS skeleton occurs preventing further current flow and thereby oxidation. In mesoporous p^+ samples of 65% porosity for example, about 40% of the structure remains unoxidized by the end of the anodization process[40].

Surface composition of anodically oxidized PS has been studied, and it was shown to depend on the oxidation conditions. A constant oxygen distribution over the thickness of the layer is not guaranteed and observations revealed that

in some cases oxidation takes place at the bottom of the pores and remains confined mainly in that region[38].

FTIR analysis performed on samples showed that the oxygen present in the anodically oxidized layers is not all incorporated in the form of SiO_2.

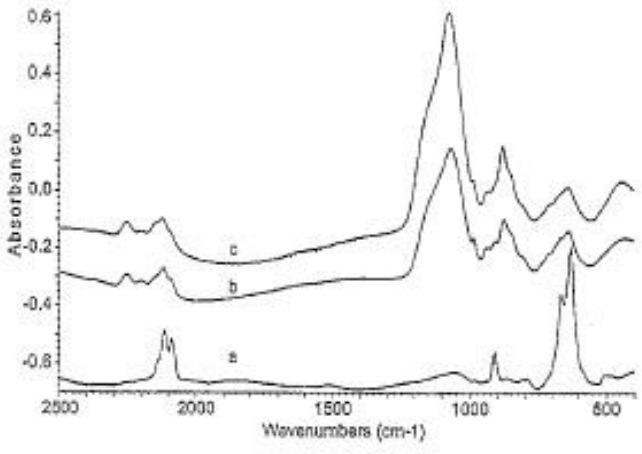

Fig. 1.18: FTIR spectra of PS layers freshly prepared (a), oxidized at 0.5 $mAcm^{-2}$.

The porous silicon surface after any oxidation process, appears hydrophilic, i.e., a layer of water is absorbed when the sample is removed from an aqueous solution. This fact favour the introduction of the solution within the pores.

1.5.5 Chemical oxidation

A wide range of chemical oxidation of PS have been developed. Among them we can remember the immersion in H_2O_2 solution for a time varying from a few seconds to a few tens of minutes[44], the immersion in KNO_3[45], the immersion in boiling water[46]. In the most cases the oxidation degree of the structure obtained with chemical methods is qualitatively reviewed. In general however only a partial oxidation of the structure is obtainable[47].

1.5.6 Other techniques for surface stabilization

Besides oxidation, other techniques are available to stabilize PS surface; here we limited to a short overview, suggesting the article of J.N. Chazaviel et al[31] in "Properties of porous Silicon" for a more complete review:

Capping (epitaxially deposited layers ($CoSi_2$, SiGe, Si on PS, GaAs etc) organic/polymeric layers, metallic layers (Ti and Co silicides));

Nitridation (rapid thermal annealing in N_2 or NH_3);

Organic chemical derivatization (stabilization by organic groups, process stopped at a monolayer).

These techniques have not been considered in the course of this thesis, but they will be an subject of study in future work.

1.6 Porous silicon as a biomaterial

1.6.1 Biocompatibility and bioactivity

Biocompatibility is the ability of a material to interface with a natural substance without provoking a defence response. The human body typically responds to contact with synthetic materials by depositing proteins and cells at the surface of the materials. This can cause infection and rejection of devices manufactured from non-compatible materials. The majority of today medical devices are made from 'bioinert' materials such as titanium, stainless steel etc. that not interact with the biological environment and are 'tolerated' by the human body.

A biomaterial can be biocompatible even if it is 'bioactive', that is if it bonds to living tissue. The success of any medical implant depends on the behaviour of cells in the vicinity of the interface between the host and the biomaterial used in the device. All biomaterials have morphological, chemical and electrical surface characteristics that influence the response of cells to the implant. The initial event is the adsorption of a layer of protein on to the biomaterial.

Porous silicon can be either a bioactive, a bioinert or a 'resorbable' material, depending on the characteristics of the layer and on the environment in which it is inserted[48].

We have already explained that PS completely dissolves in aqueous solutions, in physiological simulated conditions, showing a complete biodegradability[34]. We have also seen that modification of the surface through oxidation can transform the layer in an inert material. Studies of the behaviour of aged PS in simulated human plasma shows rapid dissolution[49].

Cahnam et al[50] showed that the rate at which PS is degraded by the body is tunable by surface chemistry.

Studies in vitro involving the immersion of various kinds of material in simulated body fluids show that the immersion of meso- and nano-porous silicon with suitable porosity, induces in some cases the precipitation of a form of hydroxyapatite, that is the mineral phase of bone, on its surface[51].

The bioactivity towards living cellular systems has also been investigated and, until now, no toxic effects have been observed from the silicon structure or its degradation products on the adhered cells[52].

All these observations demonstrate the potentialities of porous silicon for the construction of *in-vivo* implantable devices for controlled release of drugs, diagnostics of the bodily functions, replacements of failed bodily processes etc[53]. At present, a particular kind of nanostructured silicon (BioSilicon^{TM}) has already been patented by the company PSiVida mainly for drug delivery applications within the human body.

Chapter 2:

2 Biosensors

2.1 Introduction

Biosensors are a special class of sensing devices which use a biological mechanism to recognise a test species in a mixture. According to IUPAC definition, a biosensor is precisely defined as a self-containing integrated device, capable of providing specific quantitative or semi-quantitative analytical information using a biological recognition element which is in contact with a transduction element [54].

The biological recognition system is usually a receptor protein, an enzyme, an antibody etc. with intrinsic selective properties, that confer high selectivity to the biosensors in comparison with other chemical sensors. This property together with compact size, one-step reagentless analysis, sensitivity and reusability, make biosensors very attractive alternatives to conventional analysis techniques.

Some interesting commercial biosensors are already available for the detection of glucose, lactate, penicillin and urea, but their number is very small in comparison with theoretical efforts in their development.

In the last decades the potential use of biosensor in many fields (such as industry, medicine, environmental control etc.) has led to a great deal of research activity, that is characterized by a strong multidisciplinarity, spanning physics, biochemistry, chemistry, electrochemistry, electronics and software engineering

In order to get an idea of the development that this field is reaching, we can look at the trend of the number of articles, having biosensors as subject, published in the last 15 years (Fig. 2.1). The data have been obtained by a search on the Ovid database using the keyword "biosensor".

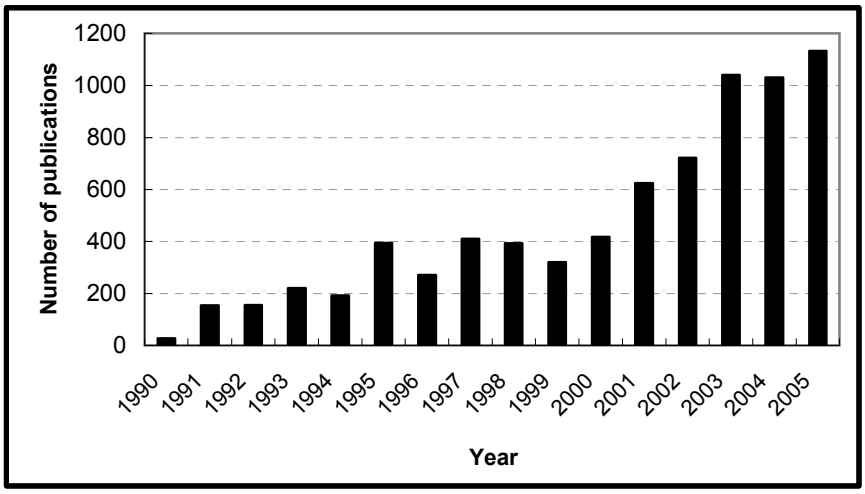

Fig. 2.1: Number of publication dealing with biosensors in the last fifteen years.

Nanotechnology is playing an always increasingly important role in the development of biosensing[55]. In particular, the use of nanomaterials appears very advantageous because it allows the introduction of many new signal transduction technologies. Because of their submicron dimensions, nanosensors, nanoprobes and other nanosystems can be constructed. Preferably, nanotechnology-based biosensors should be integrated within tiny biochips with on-board electronics, sample handling and analysis. This will greatly enhance functionality, by providing devices that are small, portable, easy to use, low cost, disposable, and highly versatile diagnostic instruments. Medicine is one of the fields with the main interest in developing biosensors, because stable and reliable devices would make

possible *on-line* and *in-vivo* monitoring of important substances for the living organism, such as metabolites, hormones and drugs. For instance, one could think to integrate an *in-vivo* blood sugar monitor with an automatic insulin delivery for patients suffering from diabetes.

The work presented in this thesis is also inserted in the field of research on biosensors development. In particular our goal was to couple a nanostructured material, such as porous silicon, with a biological element, an enzyme, in order to fabricate a new biosensor, suitable for quantitative analysis of triglycerides, that should be compact and re-usable, allowing a significant cost reduction while maintaining a high detection efficiency.

In this chapter we will make first a short general overview on biosensors and the state of art of porous silicon application in this field; then we will describe the basic mechanisms governing the enzymatic catalysis, to have all ingredients for the development of our enzymatic biosensor.

2.2 Biosensors: generalities

Biosensors are basically made up of three elements:

The *selector*, that is the biological component creating the recognition event when in contact with the substance to be detected;

The *transducer*, which transforms the interaction between the selector and the analyte in a physically measurable signal;

The *detector*, which allows to process and display the physical chemical signal in a suitable form.

The biological component may be constituted by a tissue, a microorganism, a cell receptor, an enzyme, an antibody, a nucleic acid etc. When it interacts with the substance to be revealed (that is generally dispersed in a mixture) there is a change in some physico-chemical parameters associated with the interaction, that can be revealed by the transducer. The detector then provides a useful signal, by working in a physicochemical, optical, electrochemical, thermometric, magnetic way etc.

In Table 1 some transduction methods are reported. One of the most useful is the transformation of a biochemical reaction into an electric signal,

current or potential, because on one hand it is relatively simple to construct and handle electrochemical devices, on the other they can be miniaturized and integrated in electronic devices.

Selector	Transducer	Detector
Enzyme	Current	Amperometric electrode
Antibody	Potential	Potentiometric electrode
DNA, RNA	Surface plasmon	Laser light reflectometer
Receptor	Impedance	Conductometer

Table 1: Basic elements of a biosensor: some examples[56].

Biosensor are in general classified on the basis of the nature of the transduction method. Therefore one can distinguish electrochemical biosensors, amperometric biosensor, interferometric biosensor and so on. Another classification can also been made on the basis of the nature of the biological element, so there are enzymatic biosensors, immunosensors etc.

2.2.1 Characterization of the biosensors response

The main parameters characterizing the performances of a biosensor are the selectivity, the sensitivity, the reproducibility, the time response, the stability and the life time. Some of them depends upon the choice of the biological element used as selector, others on the system geometry, others on the working and storage conditions. For example, selectivity is the ability of a device to recognise a specific element in a mixture, without interferences in the device performances deriving from addition of other substances. This property is strictly connected with the selectivity of the biological element used as selector, for example enzymatic biosensors have in general a high selectivity, deriving from the selectivity of enzymes. Sensitivity, reproducibility and time response are respectively defined, as for other type of detectors, as the smaller amount of substance that can be detected, as the measure of the scattering of a series of observations performed in the same conditions, and as the time necessary to reach the 90% of the response; they all depend both on the biological element, on the geometry of the system and

on the detection methods. For what concerns stability we can distinguish operational stability and life time. Operational stability is the preservation of the good performances of the device for multiple or lengthy measurements, while the life time is the storage or operational time during which the device keeps its performances unaltered. These parameters depend mainly on the storage condition, i. e. dry or wet, temperature, pH etc.

2.3 Enzymatic biosensors

Among various kind of biosensors we focus our attention to the class of enzymatic biosensors, which includes the biosensor that we developed in this thesis. Let us make a brief recall on catalysis and on fundamentals of the kinetics of enzyme-catalyses reaction at the basis of our work.

2.3.1 Catalysis

The term catalysis was coined in 1836 by Jons Jacob Berzelius, who observed for the first time that some substances, called catalysts, can accelerate the velocity of a reaction.

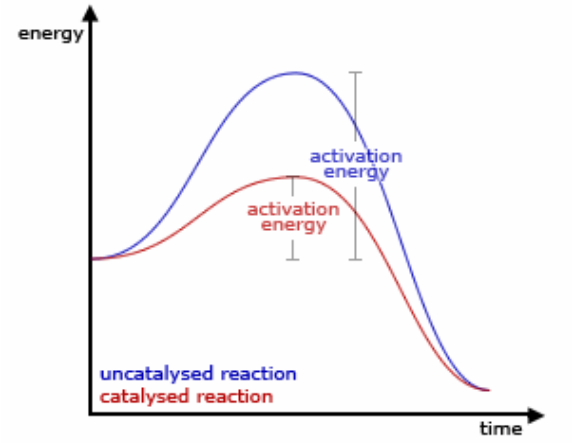

Fig. 2.2: Reaction profiles showing a higher energy barrier for an uncatalysed reaction with respect to a catalysed reactions.

A catalyst is a substance that increases the rate at which a chemical reaction approaches equilibrium without becoming itself permanently involved. It acts by lowering the barrier of activation of a reaction, that is by lowering the activation energy, as shown in Fig. 2.2.

2.3.2 Enzymes

Enzymes are biological catalysts. Like all catalysts, they are not themselves consumed in the reaction in which they participate, but are regenerated to take part in multiple cycles. Very slow reactions can be accelerated by many orders of magnitude by an appropriate enzyme. A given enzyme may be very selective, both in the substances with which it interacts and in the reaction that it catalyzes. The substances upon which an enzyme acts are traditionally called *substrates*.

Most of enzymes are proteins and thus are made up of amino acids. In general, there is a specific binding site for capturing the substrate and executing the chemical transformation through various polar and non polar interaction.

As already mentioned, an important property of enzymes is selectivity, that is the ability to discriminate among various kind of substrates. The selective qualities of an enzyme are collectively recognized as its *specificity*. Specificity has its basis on the fact that intimate interaction between an enzyme and its substrates occurs through molecular recognition, that is strongly dependent on structural complementarities. Then the products formed by a given enzyme are also very specific and therefore clearly identifiable.

2.3.3 Kinetics of enzyme-catalysed reactions

The reaction velocity, v, of an enzyme-catalysed reaction depends on the substrate concentration, [S]. Experimental observations show that at low substrate concentrations [S], v is proportional to [S]. However, v does not increase proportionally as [S] increases, but instead begins to level off. At high [S], v becomes virtually independent of [S] and approaches asymptotically a maximum. The value of v at this limit is called V_{MAX}. This behaviour is a saturation effect: when v shows no increase even though [S] is

increased, the system is saturated with substrate. Such plots are called substrate saturation curves (Fig. 2.3). The physical interpretation is that every enzyme molecule in the reaction mixture has its substrate-binding site occupied by S.

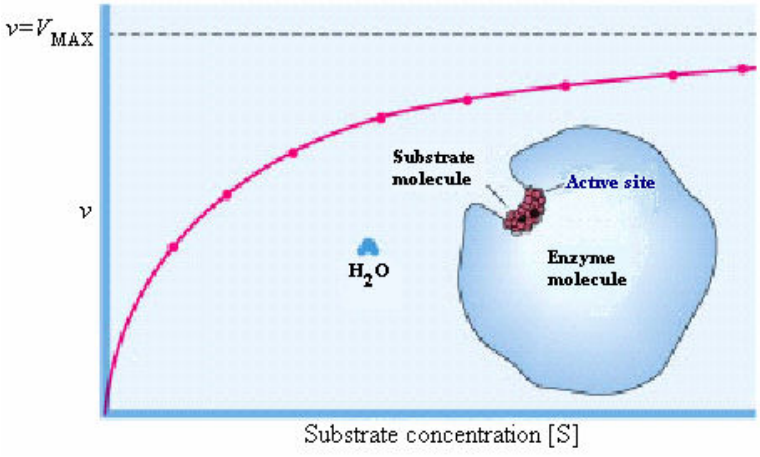

Fig. 2.3: Substrate saturation curve for an enzyme-catalysed reaction. The amount of enzyme is constant, and the velocity of the reaction is determined at various substrate concentrations. The reaction rate, v, as a function of [S] is described by a rectangular hyperbola. At very high [S], $v = V_{MAX}$, that is v becomes independent of [S]. The H_2O molecule provides a rough guide to scale. The substrate is bound at the active site of the enzyme.

2.3.4 The Michaelis- Menten theory

The general theory to describe the enzyme kinetics was proposes in 1913 by Lenore Michaelis and Maud L. Menten.

Their theory was based on the assumption, proposed by Brown in 1902, that the enzyme, E, and its substrate, S, associate reversibly to form an enzyme-substrate complex, ES:

$$E + S \underset{k-1}{\overset{k1}{\rightleftarrows}} ES$$

The product P is formed in a second step when ES breaks down to yield E + P:

$$E + S \underset{k-1}{\overset{k1}{\rightleftarrows}} ES \xrightarrow{k_2} E + P$$

After the reaction the enzyme is then free to interact with another molecule of substrate. The rate constants k_1, k_{-1}, k_2, describe the rate at each step in the reaction.

The model of Michaelis and Menten was refined and extended in 1925 by Briggs and Haldane, who introduced the *steady-state assumption.* They assumed the concentration of the enzyme-substrate complex ES quickly reaches a constant value in such a dynamic system. That is, ES is formed as rapidly as it disappears by a dissociation to regenerate E + S, or by the reaction to form E + P:

$$\frac{d[ES]}{dt} = 0$$

One other simplification advantageous to study enzyme kinetics is to observe only *initial velocity*, v_0. Since enzymes accelerate the rate of the reverse reaction as well as the forward reaction, it would be helpful to ignore any back reaction by which E+P might form ES. The velocity of this back reaction would be given by $v = k_{-2}$[E][P]. However, if we observe only the initial velocity for the reaction immediately after E and S are mixed in the absence of P, the rate of any back reaction is negligible because its rate will be proportional to [P], and [P] is essentially 0.

Given these assumptions, the expression which correlates the reaction velocity to the substrate concentration is given by the so called *Michaelis-Menten equation*:

$$\boxed{v_0 = \frac{V_{MAX}[S]}{K_M + [S]}}$$

where, $V_{MAX} = k_2 \cdot [E_0]$, with $[E_0]$ equal to the enzyme concentration, and $K_M = \frac{(k_{-2} + k_2)}{k_1}$.

The Michaelis- Menten equation states that the rate of an enzyme-catalysed reaction, v, at any moment is determined by two constants, K_M and V_{MAX}, and the concentration of substrate at that moment.

K_M is called Michaelis- Menten constant and is very important because it corresponds to the substrate concentration at which the reaction velocity is a half of V_{MAX}.

The Michaelis-Menten equation perfectly fits the plot in Fig. 2.3.

2.4 Enzyme immobilization

One possible way to improve biosensing performances is to immobilize the enzyme on a support. The main advantage in employing immobilized catalysts is that they are not mixed with other reagents and can be easily recovered after use, for example by filtration if the support is a powder. Moreover, it has been demonstrated that immobilization can improve the stability of the catalyst[57, 58].

Both the choice of the support material and the immobilization method can affect the performances of a biosensor. The potential advantages offered by the use of supports with a large developed surface, has suggested the employment of porous materials, which allows the immobilization of larger amounts of enzyme molecules with respect to conventional supports. At present, sensor industry uses materials such as porous glasses and polymers as supports for the realization of biosensing devices.

There are five principal methods to immobilize an enzyme on a support: physical adsorption, covalent binding, entrapment, encapsulation and cross linking (Fig. 2.4). The detailed description of all these methods goes beyond the scope of this thesis. We discuss here only covalent bonding and physical adsorption.

Enzymes are usually immobilized on solid matrices by physical adsorption or by formation of covalent bonds. The choice of one method rather than the other depends on different factors. Enzymes and proteins in general, are low stable molecules. They can lose their biological function if subjected to harsh treatments, such as extreme pH values, high temperatures,

and presence of highly reactive chemical agents. Covalent bonding produces a stable biocatalyst, but sometimes a lot of the initial activity is lost during the immobilization process. This happens since the enzyme molecule can be distorted during the formation of the covalent bonds with the chemically modified support surface.

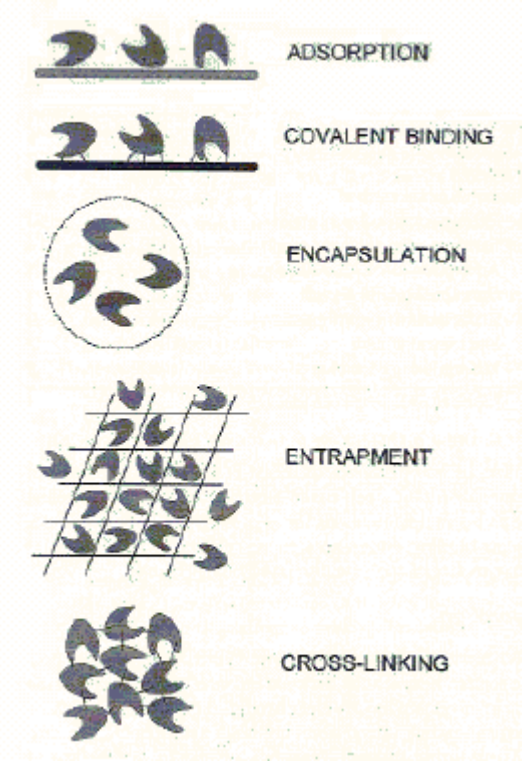

Fig. 2.4: Most used methods of immobilization

Physical adsorption is instead a more gentle method that is obtained just impregnating the porous support with the enzyme solution. Obviously only physical interactions (electrostatic interactions, dipole-dipole, hydrogen bonding, dipole-dipole induced, hydrophobic interactions etc.) are present in this case, but they are usually strong enough to bind the enzyme to the support surface without leaching during operation. This method has also the advantage that the enzyme may likely be removed when it loses the catalytic activity allowing the re-use of the immobilization matrix. In fact the

desorption of protein from the support can be induced by adding a surfactant to the solution[59].

Physical adsorption is the immobilization method that we used in this work, while other techniques are at the moment under investigation.

Another reason for the use of the physical adsorption method is that chemical modification of the surface can reduce the matrix pore diameter. Thus, if they are of the same order of magnitude of the size of the enzyme molecules - as in this case - it may happen that after chemical immobilization the pores turn out to be occluded. This fact would not allow the diffusion of the substrate inside the pore channels where the biocatalyst is located. In this case only external bounded enzyme molecules would work, leading to a significant loss of catalytic efficiency[60].

2.4.1 State of art of PS application in biosensing

Porous silicon has attracted the interest of the scientific world for possible applications in biosensing since 1995, when its abilitity in gas sensing was observed [61]. The first biosensor having porous silicon as substrate for molecules immobilization (in that case a penicillase enzyme) appeared in 1997[62]. After this date an increasing attention has been reserved to this material.

In fact it possess characteristics suitable for biosensing applications, that are its high surface to volume ratio (as much as 900 m^2 cm^{-3}), the possibility to modify the surface after formation to adapt the sample to the application, and the fact that it can be easily integrated in the usual silicon technology.

Porous silicon has been used as an optical interferometric transducer for detecting small organic molecules, DNA, and proteins at pico- and femtomolar analyte concentrations[63, 64].

Fig. 2.5 shows on the left a scheme of a PS based interferometric biosensor for DNA recognition, realized by V. S.-Y. Lin et al. (1997)[63]. Sensing measurements consist in evaluating the differences in the reflectance spectra due to the analyzed event. The interference spectrum of white light reflected at the top and bottom of a PSi layer depends on the optical thickness (product of the refractive index n and thickness L) of the film

according to the following relation $m\lambda = 2nL$, where *m* is the spectral order and λ is the wavelength of light.

On the right the results obtained by using this biosensor are shown. A given DNA sequence was immobilized on porous silicon pores, and the device was then exposed to other DNA sequences. The binding of a DNA strand to its complementary, immobilized on the PSi substrate, causes a change in the refractive index of the layer that is detected through a shift in the interference pattern. If the solution does not contain the complementary sequences, spectra before and after the analyte exposure are superimposable.

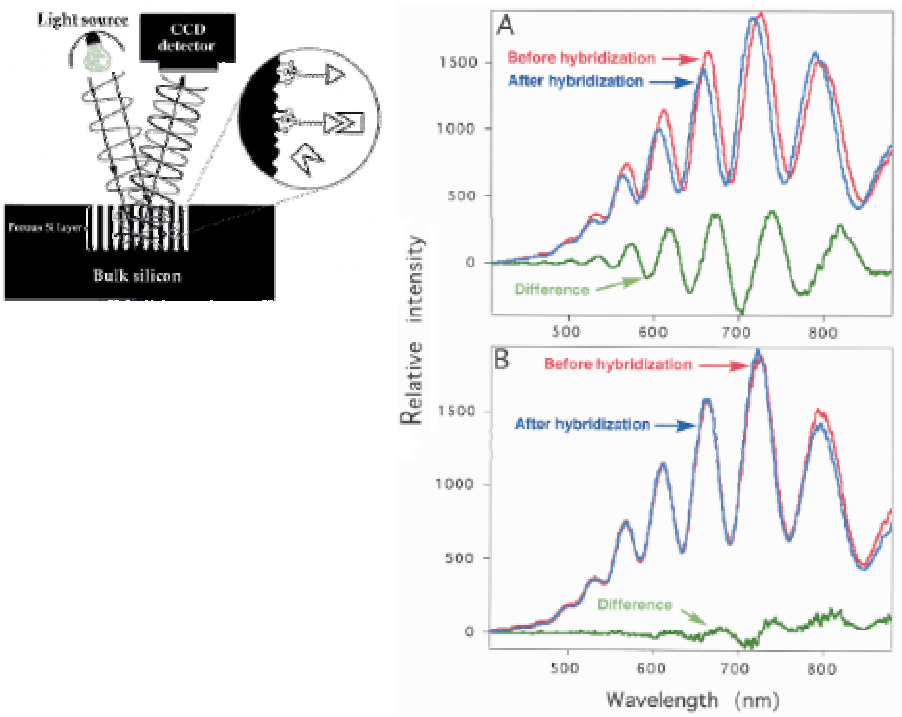

Fig. 2.5: Scheme of a PS based interferometric biosensor (left); interferometric reflectance spectra of a DNA-modified PS layer before and after hibrydization (right). In spectrum A, hybridization takes place in presence of a complementary DNA sequences respect to that immobilized on the pores; in spectrum B is presented the case of a non complementary DNA sequence[63].

Microcavity resonators made of porous silicon have also been used in biosensing[65]. These resonators possess the characteristics of line

narrowing which allows a better sensitivity in detection. Chan et al. fabricated a DNA biosensor based on a porous silicon microcavity structure[66]. The microcavity structure was highly sensitive to substances introduced in the pores because any slight change in the effective optical thickness modified its reflectivity spectrum, causing a spectral shift in the interference peaks.

Potentiometric biosensors based on porous silicon have been described[67]. The enzymes penicillinase and lipase were separately used to detect penicillin[68] and triglycerides[69, 70] by exploiting the hydrolysis reaction of triglycerides in water. They observed that the capacitance–voltage (C–V) curves of a oxidized porous silicon-electrolyte system is affected by the pH of the electrolyte, and since the hydrolysis reaction of triglycerides in water leads to changes in the pH of the solution, by using as electrolyte an emulsion of tryglycerides and enzymes, they could measure the concentration of triglycerides.

The main limit from which the biosensor of Reddy et al suffers, is that the enzyme used to catalyze the hydrolysis reaction is dispersed in the analyte and can not be recovered after the measurements.

2.5 Interest in the realization of a new PS-based biosensor for triglycerides analysis

Triglycerides are triesters of fatty acids and glycerol. They are important molecules from the clinical point of view. Triglycerides can be assumed with food (exogenous) or synthesized (endogenous) by living organisms. Endogenous triglycerides are formed in adipose tissues and in the liver, mainly starting from carbohydrates. Exogenous triglycerides, instead, are hydrolyzed in their constituents during the digestive process, and re-synthesized in the cells of intestinal villus. From there, triglycerides are transported by the blood flow in the entire organism, where they are used for the various metabolic processes and deposited in the adipose tissue. As well as it happens for hyper-cholesterolemy, a high level of triglycerides enhances the exposure to the infarct of the myocardium and to

atherosclerosis. Thus, in order to find out the risk factor, it is important to quantitatively know the blood concentration of triglycerides. Triglycerides are contained in many foods, thus their quantification is also important in the field of food industries.

The great importance of triglycerides in everyday life justifies the interest for the development of more efficient detection methods, besides those already existing, for their quantitative analysis. For example, in the field of medical analysis, triglycerides concentration is commonly measured by means of four consecutive enzyme reactions. A chromogenic compound is produced leading to a modification of the absorbance value at a fixed wavelength, that is proportional to the triglycerides content in the sample (Lambert-Beer equation). This assay is rapid (about 10 min), but it is negatively affected by interfering reactions. Moreover, enzymes can be used only once, since it is practically impossible to recover them from the sampled emulsion.

All existing sensing devices for triglycerides show a main limitation that is they are not reusable in the sense that they does not allow the recovering of the enzyme after use. It is clear that the development of a new device that is reusable and compact is potentially very interesting since it will allow a significantly cost reduction.

In our work we will exploit the same reaction involved in the biosensing device of Reddy at al., but we will overcome the loss of the enzyme after the analysis by immobilizing the enzyme molecules, before the measurements, in the porous silicon surface.

One other difference is that we used potentiometric measurements as a transduction technique, that is our measurements are performed in condition of zero current flowing, without any external polarization. This is an advantage because it allows to study the reaction without influences deriving from the external applied voltage.

Chapter 3:

3 Experimental Methods

3.1 Introduction

In previous chapters we described the formation mechanism of porous silicon, its main properties and the state of art in the field of biosensors. Now, before entering in the details of the realization of our triglycerides biosensor, we will give on overview of the techniques, instruments and experimental setups we used.

3.2 Preparation of crystalline silicon wafers

As we already mentioned in § 1.3, the formation of porous silicon can be carried out in several ways. However, only the electrochemical etching gives a high level of reproducibility.

First steps before PS formation are the cleavage and cleaning of crystalline silicon wafers.

In general, crystalline silicon for microelectronic application is put on market in circular wafers, with a typical thickness in the 400 μm to 1 mm

range and a diameter of 2" to 8". Since our cell has been realised to prepare circular samples of 1cm diameter, the first step is to adapt the wafer's dimension to those of the anodization cell, that is to cut the original wafer into 1,5×1,5 cm square chips. The cleavage is carried out by engraving the surface following the crystallographic axis using a diamond-tipped pen, and by exerting a weak pressure with fingers until the wafer cleaves.

After cleavage the chips are rinsed in absolute ethanol and distilled water, in order to eliminate impurities from the surface, and dried under nitrogen flow.

3.3 Formation and anodic oxidation

3.3.1 Formation

The basic equipment to fabricate Porous Silicon consists in an anodization cell and a high-stability potentiostat.

In Fig. 3.1 is shown a cross-sectional view of the anodization cell used to form PS.

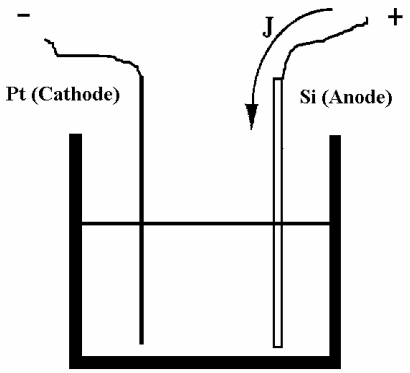

Fig. 3.1: Scheme of the anodization cell.

The body of the cell is made of grey PVC, a highly acid-resistant material, and the silicon wafer serves as anode. A stainless steel contact is made on the back-side of the wafer and the latter is sealed so that only the

front side of the wafer is exposed to the solution, in an area of 0,9 cm^2. The cathode is a grid plunged in the HF solution and is made of platinum, another acid-resistant material.

Both the cell and the platinum grid have a cylindrical geometry in order to assure a uniform electric field on the wafer.

The cell is kept at room temperature and in the dark, to avoid photogeneration of holes.

The platinum grid and the metal contact are connected respectively to the negative and positive terminals of a generator, which supplies current flow during anodization. We used a Potentiostat/Galvanostat Mod.273 from EG&G Princeton Applied Research, which ensures great stability both in galvanostat and in potentiostat modes.

A pre-anodization treatment has been performed in order to remove the native oxide on the surface of crystalline silicon wafer: wafers have been immersed in HF solution in the dark for 10 minutes before anodization.

After formation samples are accurately rinsed in deionized water to eliminate the residual HF solution.

3.3.2 Anodic oxidation

Anodic oxidation is obtained under anodic polarization of the sample in an aqueous electrolyte.

The process is performed in the anodization cell just after the rinsing of the sample in deionized H_2O. Water is rapidly replaced by a 0.1 M KNO_3 aqueous solution, taking care not to expose the porous layer to air in order to ensure a good wetting of the hydrophobic sample. The process is performed using a constant current density.

3.4 Characterization of PS layers

3.4.1 Porosity

Porosity is one of the most important parameters which characterises PS. The porosity is defined as the fraction of void within the volume of the porous silicon layer.

It can be simply determined by gravimetric method, since it is given by the following equation:

$$P(\%) = \frac{m_1 - m_2}{m_1 - m_3}$$

where m1 is the mass of the wafer before anodization, m2 is the mass just after anodization and m3 is the mass of the sample after the dissolution of the whole PS layer in a 0.1M NaOH aqueous solution.

For weight measurements we have used a Mettler AJ100 balance with a sensitivity of 10^{-4}g.

3.4.2 Thickness

The sample thickness has been determined by step-heights measurements after the dissolution of porous layer in NaOH 0.1 M. The instrument we used for such measurements was a profilometer Tencor P-10. It records vertical surface profiles by means of scanning across the sample a mechanical stylus connected to a piezoelectric transducer. Thickness is determined as the difference in level between the non-etched portion of the wafer and the bottom of the sample.

3.4.3 Pore size distribution and specific area

The knowledge of the pore size distribution is also a basic requirement when dealing with porous materials, especially when they are employed in application areas such sensing. In fact pore size determines much of the adsorption properties of a material and is therefore a parameter of great relevance in the process of immobilization of molecules.

The IUPAC guidelines make a classification of pores in three ranges according to its diameters:

Pore width (nm)	Type of pore
≤2	Micro
2-50	Meso
>50	Macro

Table 2: IUPAC classification of pore size.

Pores with diameter of the order of the nanometer are often caller "nanopores".

Unfortunately the measurement of pore sizes is not a simple task, and different methods can be used depending on the size range involved.

In case of mesoporous structures (that is the type of morphology expected for n^+-*type* porous silicon, as we will see later) the most widely used method is based on the analysis of adsorption isotherms of gases at low temperature, which present particular characteristics, with respect to non porous materials.

This technique, is a non destructive method which consists in making a gas, generally N_2, adsorb to the surface of the sample at a constant temperature, lower than the critical temperature of the used gas (460 K for N_2). The amount of adsorbed gas depends on the pressure, on the specific surface and on the interaction which are established between gas molecules and sample surface.

Gas adsorption isotherms are constructed by recording the amount of adsorbed gas at the increasing of the pressure until a pressure corresponding to the saturation equilibrium pressure of the gas at the working temperature is reached. The cycle is then completed by reducing pressure in order to make the gas desorb.

Fig. 3.2 shows a typical adsorption-desorption isotherm obtained for a mesoporous PS sample formed on p^+-type silicon.

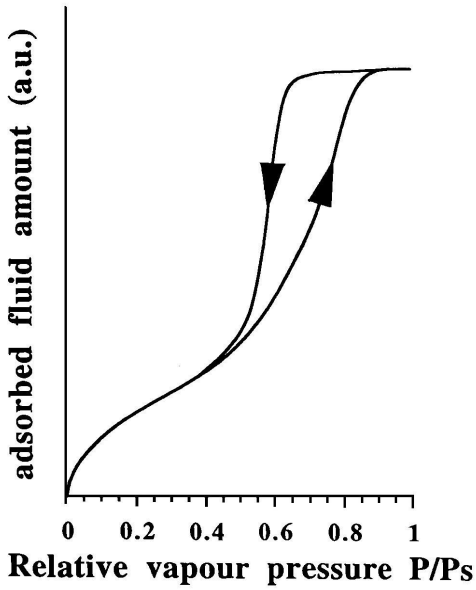

Fig. 3.2: Schematic representation of the typical adsorption isotherm of nitrogen at 77 K by a p+-type porous silicon layer[72].

In presence of mesopores, isotherms have a particular shape characterized by a hysteresis, that is the desorption curve is not superimposed on the adsorption one.

The first part of the isotherm, up to a relative pressure of 0.4, corresponds to the adsorption of nitrogen on the porous surface; this regime is very important because it allows to obtain the value of the specific surface by using the standard BET method (Brunauer- Emmett- Teller)[71]. The BET model describes the adsorption dynamics, correlating the total volume of the adsorbed gas (V) with the pressure at which the adsorption takes place (P):

$$\frac{V}{V_m} = \left(\frac{1}{1 - p / p_0} \right)$$

where V_m is the saturation volume with a monolayer of adsorbed gas and p0 is the saturation pressure of the gas. Once the value of V_m is known, the sample pores' surface can be calculated from the N_2 molecule size[71].

The increase in the relative pressure beyond 0.4 (Fig. 3.2) results in a sharp increase of the adsorbed volume. In this region the physical adsorption of gases by the surface rapidly increases as a consequence of the capillary

condensation of gas molecules in the pores, which takes place at values of relative pressure where the smallest pores begin to be filled[72]. At higher relative pressures, when all pores are filled, the curve reaches a plateau. The volume of condensed liquid corresponding to the amount of gas adsorbed at the plateau is equal to the void volume in the material and gives information about porosity.

Decreasing the relative pressure and letting the condensed gas evaporate, we can observe that the desorption curve is shifted with respect to the adsorption and there is a hysteresis loop.

The pore dimension can be determined either from desorption or adsorption branch by using the BJH (Barett-Joyner-Halend) method[22] and its extension D.H. (Dollimore- Heal) method[23].

3.5 Study of enzyme immobilization on PS

3.5.1 The enzyme: lipase from Candida rugosa

Lipases (triacyl glycerol acyl hydrolases, EC 3.1.1.3) are enzymes that in nature hydrolyze triglycerides. They are among the most used enzymes in food industries and for biotechnological applications[73] because of their ability to catalyze esterification and transesterification reactions[74]. Lipases for biotechnological applications are of microbial origin; in particular they come from bacteria, yeast and fungi[75]. Among the several lipases commonly used in biocatalysis, only in a few cases the structure has been resolved by X-ray diffraction. This knowledge is important to explore the coupling of this biological catalyst with an inorganic matrix, as porous silicon, to fabricate a biosensing nano-device for bio-medical or food applications.

The enzyme that we have used for the immobilization on porous silicon is the Lipase produced by *Candida rugosa* fermentation, an enzyme that has been investigated by mean of X-rays diffraction and whose structure is then well known. *Candida rugosa* lipase is a globular protein with a molecular weight of about 64 KDa and a length of about 5 nanometers. Two conformations (closed and open) of *Candida rugosa* lipase have been determined[76].

Fig. 3.3 shows the open structure of *Candida rugosa* lipase as determined by Grochulsky et al[77].

Fig. 3.3: Structure of Candida rugosa lipase. Lysine (pK = 10.72) is coloured in red, Arginine (pK = 12.48) is coloured in yellow and Histidine (pK = 6.04) is coloured in green.

The fundamental element of the structure is the active site, in which is located the "catalytic triad", a group of three amino acids, responsible for the catalytic action. The surface charge of the protein depends on pH, and in particular if:

pH < pI (pI: isoelectric point) the number of *positive* charges is higher than that of negative charges.

pH > pI the number of *negative* charges is higher than that of positive charges.

pH = pI the same number of positive and negative charges are present.

The main specification provided by the producer of the lipase used in this work, the "Amano Enzyme Europe L.T.D.", are:

Lipase activity: Not less than 30.000 units/g (One unit is the amount of enzyme that releases 1 μmole of fatty acid per minute at pH = 7.0)

Molecular weight: 64.000 Da

Isoelectric point: 4.30

Inactivation Conditions: 85 °C for 10 minutes.

It is well known hat the activity of lipases depends on pH. Also the different buffers used to obtain a certain pH may affect the activity (Fig. 3.4):

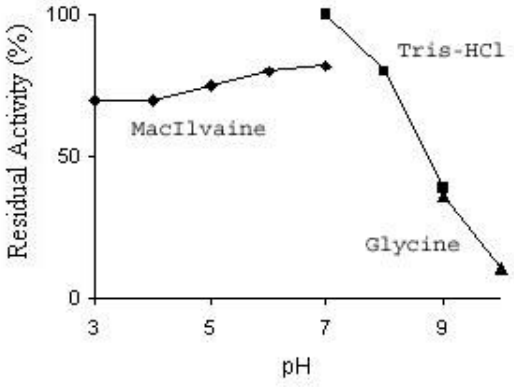

Fig. 3.4: Curve of Relative activity as a function of pH. Values are obtained with three different buffer solutions, that justifies the different values for pH = 7 [78].

The enzyme shows a maximum activity for pH = 7, which rapidly decreases towards pH = 10. Measurements were made using the same technique and three different type of buffer solution. As a matter of fact, the activity is weakly dependent on the composition of the buffer solution used for the measurements.

Another parameter that affect the enzyme activity is the temperature, as we can see in Fig. 3.5.

The enzyme activity is maximum for temperature comprises between 20-30 °C, while it is inhibited by augmenting temperature above 40 °C.

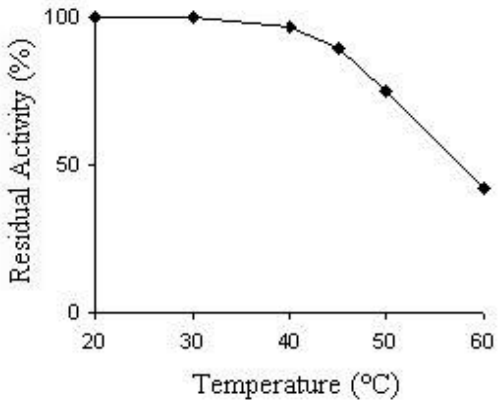

Fig. 3.5: Curve of the relative activity as a function of temperature. The activity has a maximum for a temperature of 40 to 50 °C and decreases until the enzyme inactivation beyond 70 °C[78].

3.5.2 Enzymatic activity measurements

The amount of enzyme which is adsorbed onto the support during an immobilization process is impossible to be determined in absolute terms (e.g. grams), as its purity is often low and a part may be in an inactive, or partially active, state. For this reason, enzymes are usually characterized in terms of activity rather than mass.

The determination of the enzymatic activity, which has been very important for the studies of enzyme immobilization of lipase on porous silicon, has been carried out by the pH-Stat methode[79], using 718 Stat Titrino pH-meter from Metrohm (Herisau, Switzerland).

The method of activity determination is based on lipase-cathalyzed hydrolysis of triglycerides in water emulsion (Fig. 3.6).

As we can see, in water, lipase catalyzes triglyceride hydrolysis to give glycerol and fatty acids. A common nomenclature used in biochemistry gives the name of “substrate” to the substance whose reaction is catalysed by an enzyme. In this case we can say that the triglyceride is the substrate for the lipase.

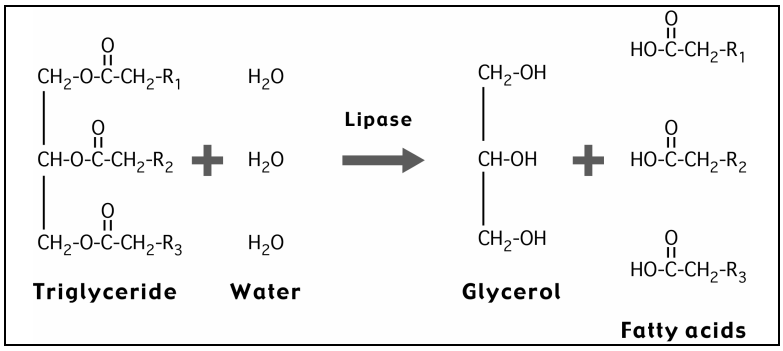

Fig. 3.6: Scheme of the hydrolysis reaction of triglycerides in water.

To test lipase activity, we used a small triglyceride, the tributyrin, that in water hydrolyses forming glycerol and butyric acid. Tributyrin was homogenized in water thanks to an emulsification reagent, prepared by dissolving gum arabic (6.0 g), glycerol (54 ml), NaCl (1.79 g) and KH_2PO_4 (0.041 g) in distilled water (40 ml). This substrate emulsion contained 3 ml of tributyrin, 10 ml of emulsification reagent and 47 ml of distilled water and was homogenized by an Ultra-Turrax homogeniser.

The product of the hydrolysis of tributyrin is butyric acid, whose presence lowers the pH of the emulsion. The enzymatic activity is defined as the μmoles of transformed substrate or formed product per minute.

The pH-stat method consists in maintaining fixed and equal to 7.00 the pH of the emulsion during hydrolysis, by continuous titration with 10 mM NaOH solution. The neutralization reaction is:

$$CH_3CH_2CH_2COOH + NaOH \longrightarrow CH_3CH_2CH_2COO^- + Na^+ + H_2O$$

that is one mole of NaOH exactly neutralises one mole of butyric acid.

The number of μmoles of NaOH per minute added to the emulsion to keep constant the pH value then equals the enzyme activity.

During measurements, the emulsion was kept under continuous stirring and at temperature of 25°C to guarantee homogeneity and optimum emulsion diffusion within the PS pores.

In Fig. 3.7 is represented a scheme of the device for activity measurements:

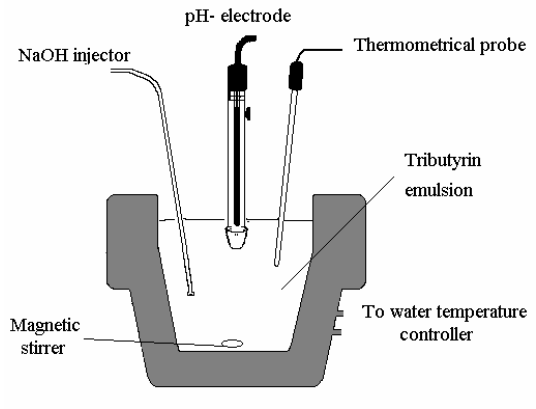

Fig. 3.7: Scheme of the pH STAT.

Particular care must be taken in the determination of the emulsion volumes used for the activity determination. In fact, since the results are given in terms of added NaOH μmoles, any error in the emulsion volume determination will directly affect the number of μmoles added. The volume of substrate emulsion, prepared according to the recipe described in § 3.5.2, was fixed at 3 ml. The volume of the sampling volumes withdrawn from the immobilization solution for the measurement of the time evolution of its activity was fixed at 100μL.

During this thesis, the pH-stat method has been used for measurements of the lipase activity in the immobilization solution, by introducing fixed quantities of enzymatic solution in the tributyrin emulsion, and for the measurements of the activity of lipase immobilized into the pores (that is for the characterization of porous silicon as a matrix for enzyme immobilization) by introducing the loaded sample directly in the emulsion (see Fig. 6.1).

3.6 Potentiometric measurements

Once verified that PS is a good nanostructured material for enzyme immobilization, the next step was the realization of the biosensor for tryglicerides analysis.

We chose to build our biosensor using a configuration for potentiometric measurements. In electrochemistry, potentiometry is a method where electrodes are used to measure voltages which are related to chemical information. The electrode potential is measured without current flow, that is in open circuit configuration, and is called Open Circuit Potential (OCP).

The OCP signal we record during experiments is then the time evolution of the PS electrode potential induced by the composition modification of the triglycerides emulsion. We are then able to transform the information about the amount of the hydrolyzed triglycerides molecules into an electric signal. As a matter of fact, the quantity of interest is not the absolute value of the OCP but only its variations ΔOCP: the absolute value depends on many parameters, and can be different for slightly different experimental conditions, while its variations are just related to the composition modifications in the emulsion. We will use then the ΔOCP to check the emulsion pH variations (see § 1.2.3).

Another advantage of using OCP as parameter to monitor hydrolysis reaction Is that we avoid electrode polarizations that may affect in a unknown way the normal development of the reaction.

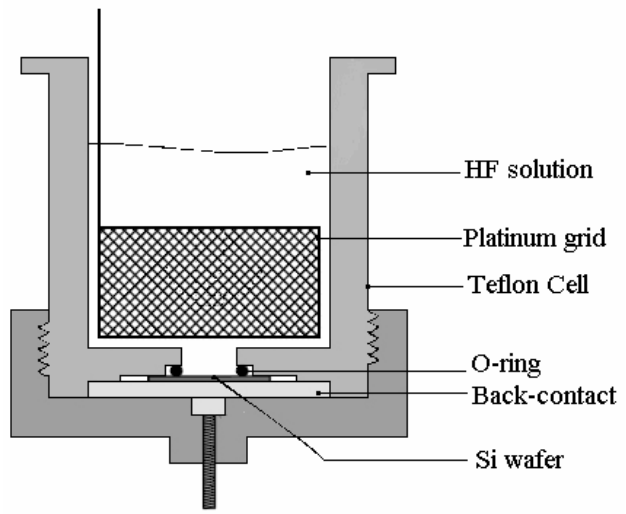

Fig. 3.8: Scheme of the electrolytic cell used for OCP measurements.

The electrochemical measurements consist in measurements of the potential of a given electrode with respect to another one, whose potential is kept constant. Due to the potential drop across the cell, however, there is the need of a third (reference) electrode to precisely control the potential of the second electrode. This three electrode configuration in general needed only for electrochemical measurements where there is a net current flow between the electrodes, while for potentiometric measurements the third electrode is generally not needed. However, in our case we noticed that the signal noise was significantly reduced when using the three-electrode configuration, and we chose then to use this configuration for our measurements.

The electrolytic cell is the same used for PS formation, adapted for the three-electrodes configuration. The experimental setup is composed by the electrolytic cell, represented in Fig. 3.8, and by a potentiostat used as a high impedance voltmeter. The PS wafer act as working electrode.

Chapter 4:

4 Preparation and characterization of n+-type Porous Silicon as a matrix for enzyme immobilization

4.1 Introduction

The aim of this work was the realization of a potentiometric biocatalytic sensor for triglycerides, with the biological sensing element integrated in the device in order to guarantee compactness, ease of use and re-usability.

The great importance of triglycerides in everyday life justifies the interest for the development of more efficient detection methods, besides those already existing, for their quantitative analysis.

In previous chapters we have explained the advantages deriving from enzyme immobilization on solid supports, and especially on porous materials.

Porous silicon is a material with great potentiality for this kind of applications because it combines the advantages deriving from the great surface area with the possibility to integrate the device in microelectronic circuits.

In this chapter we will describe all the steps involved in the preparation and characterization of porous silicon enzymatic biochips. We will first describe the preparation and characterization of PS layers and the process of enzyme immobilization in the pores' surface. Then we will show that the porous silicon matrix is a good support for enzyme immobilization, by comparing its competitive performances to those of standard supports.

The characterization and optimization of the porous silicon-enzyme system will be performed by using standard techniques of analytical chemistry used in enzymatic activity measurements. The results will be compared to those obtained with other kinds of supports. In the sixth chapter we will discuss the properties of PS biochips as electrodes for potentiometric biosensors.

4.2 Choice of the formation parameters

As we have explained in § 1.4, the properties of porous silicon layers (morphology, pore size, surface area, porosity, thickness) are dependent on the type and level of the crystalline silicon substrate doping and on the anodization parameters. The influence of these parameters on the properties of the formed layer were analysed in order to obtain samples well adapted to our requirements.

First of all, the samples must have a reasonably high porosity and a large developed surface to allow the immobilization of a large amount of enzyme molecules into the pores. Second, the porous layers must keep a good mechanical stability. This is a very important point, since on one hand we need several steps before the immobilization process is complete, and, on the other hand, one of our goal is to fabricate a re-usable biosensor, which is impossible without a good mechanical stability.

4.2.1 Crystalline silicon wafer

The first requirement is to choose a matrix whose pores are large enough to allow the introduction of the enzyme within the pores.

Lipase is a 5 nm-size molecule, therefore the pore size must be of the order of a few tens of nanometers at least.

This condition limits the possibilities in the choice of the crystalline silicon used for anodization, because, as we saw in § 1.4.1, the size and the shape of the pores depend on the concentration and type of the silicon wafer dopant: we can form samples with pore size ranging from nanopores (pore diameter of a few nanometers) to macropores (pore diameter in the 200 nm - 20 μm range).

Among various kind of silicon wafers, *p*-type Si has been excluded a priori because it gives rise to layers with pore diameter of a few nanometers, too narrow for lipase introduction. With *n*-type silicon is possible to realize macroporous samples which are suitable for lipase immobilization. However, the final layer has not a homogeneous morphology in depth, since the first few hundreds of nanometers of the sample are nanoporous, impeding then the introduction of the enzyme in the macropores.

Both n^+-type and p^+-type silicon produce samples with a morphology characterized by long void channels with a diameter of few tens of nanometers, large enough for lipase introduction.

Between them, we chose n^+-type PS, because of a previous knowledge of the material developed during other works of this group[81].

We used Czochralski[80]-grown Si (100) n^+-type ($3 < \rho < 7 \cdot 10^{-3}$ Ωcm) wafers with a thickness of 500 μm, supplied by Siltronix Company.

4.2.2 Porosity

Once chosen the type of silicon wafer to use for anodization, we need to select the best anodization conditions.

For biosensensing applications it is very important to have samples with a large developed surface in order to allow immobilization of large amount of enzyme. In § 1.4.5 we saw that the specific surface is a function of porosity for a given morphology. The exact dependence of specific surface on porosity for n^+- type PS is not known, However, it is a reasonable assumption that, in analogy with the *p*-type case, the specific surface will reach its maximum value for porosities of about 50% and will be decrease for different values. Therefore, we decided to use a material with a medium

porosity (about 50-60%), to have large developed surface for the immobilization of the enzyme while maintaining a good mechanical stability, as we will see in § 4.2.4

The porosity level is a combined function of anodization current density and HF concentration. The influence of these parameters on porosity has been studied for n^+-type samples in a previous work[81], and results are shown in Fig. 4.1:

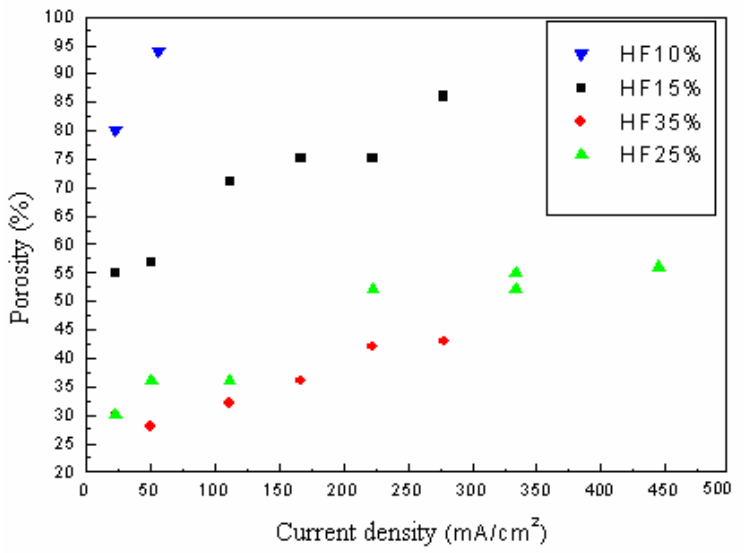

Fig. 4.1: Porosity of n^+-type PS as a function of current density for different HF concentrations [81].

For a given HF concentration the porosity increases with increasing current density, while for fixed current density the porosity decrease with increasing HF concentration.

With fixed current density and HF concentration, porosity increases with thickness and porosity gradients in depth can occur. This is an effect of the extra chemical dissolution of PS layer in HF, but is negligible for thickness smaller than 100 μm.

As we can see from graph in Fig. 4.1, for HF concentrations of 25% and 35% there are only very slow variations of porosity with current density, and even for current densities of the order of 500 mA/cm^2 we can fabricate samples with a maximum porosity of 55%. On the other hand, using HF

concentrations of 10% we cannot obtain samples with a porosity degree smaller than 80% and therefore the resulting layers do not show a good mechanical stability. In many cases samples are so brittle that the stress involved in the drying process after anodization is sufficient for the collapsing of the structure (see paragraph 4.2.4).

The HF concentration which makes accessible the largest range of porosity is 15%, because by varying current densities from a few mA/cm^2 to 500 mA/cm^2, we can obtain porosities in the 50 % to 90% range.

To fabricate samples with a porosity of about 50-60%, we used 15% HF solutions and a current density of 50 mAcm^{-2}.

The reproducibility of the samples' porosity, resulted to be ensured with an error lower that 5%.

In order to ensure a good wettability of the surface and complete diffusion of the HF solution into the pores, a substance capable to reduce the surface tension is always added to the solution. We chose ethanol since it is a standard choice for PS formation[30]. The added tensioactive substance does not have a direct part in the dissolution process, but its role is only to improve aqueous solution diffusion.

In summary the composition of our etching solution is HF, Ethanol and water H_2O in the 15%: 70%: 15% proportion respectively.

4.2.3 Thickness

The thickness of the samples was fixed at 50 μm. This value resulted to be the good compromise between the requirement of a large available surface for enzyme immobilization, of a good stability of the structure and of a homogeneous morphology in depth. In fact, in case of very thick samples the diffusion of liquid solutions in the whole sample's depth could be hindered by capillary forces causing a gradual impoverishment of the solution in F^- ions that will lead to a inhomogeneous morphology.

For a fixed HF concentration in the solution and a fixed current density, the thickness is a linear function of the anodization time. Fig. 4.2 shows the plot[81] of the sample's thickness as a function of the anodization time, for a 15%HF solution and a current density of 50 mA cm^{-2}.

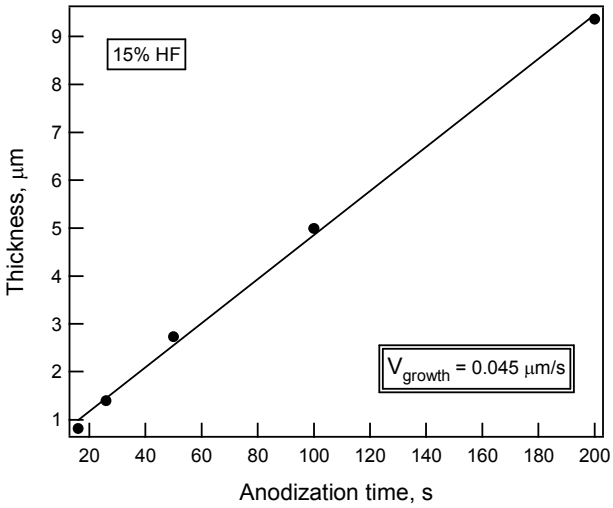

Fig. 4.2: Sample thickness versus anodization time for n^+-type PS, 15% HF solution and current density of 50 $mAcm^{-2}$ [81].

The plot show a linear behaviour, whose slope is the dissolution rate, equal to 0.045 μm/s. To fabricate 50 μm-thick samples the anodization time was fixed at 1110 s.

The optimization of the thickness with respect to the immobilization process has been left to future studies.

4.2.4 Drying Process

The drying of porous silicon films after the rinsing step at the end of the electrochemical etching, is a crucial step in the fabrication process. In general, drying is a problem for samples of high porosity and thickness higher than a critical value[82]. Above this critical value, in fact, when the rinsing water evaporate from pores in the drying process, a cracking of the structure is observed. In Fig. 4.3 is shown an optical microscopy image of the surface of highly porous sample after drying in air.

Fig. 4.3: Optical microscope image of the surface of a highly porosity sample after drying in air.

Macroscopic signs of the film cracking are clearly visible: portions of sample are detached from the wafer and manifestly deformed as a consequence of stress forces. The origin of this phenomenon is due to the large capillary pressure exerted on the porous structure during liquid evaporation, that in case of particularly fragile samples is sufficient to break the structure. Capillary stress can be reduced by replacing water by a drying liquid with lower surface tension, for example pentane[83].

In our case, the good mechanical stability against drying, even without introducing such substances, confirmed the goodness of our choice of a medium porosity and a moderate thickness (50 μm). This result is important for our application since we had to take care to not contaminate the material with substances that could compromise the functioning of the enzyme we want to adsorb onto the pores' internal surface.

4.3 Characterization of PS layers

4.3.1 XRHRD

The first analysis of porous silicon samples was performed by using X-ray diffraction technique. Fig. 4.4 shows a XRD spectrum of a 50 μm- thick

sample, realized by using *D8 discover Bruker-AXS* diffractometer located in "LIMINA" laboratories of Cagliari University.

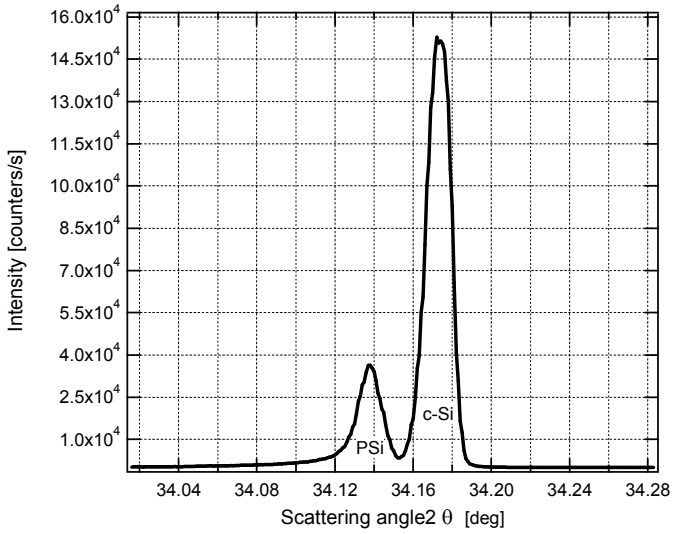

Fig. 4.4: n^+-type PS HRXD spectrum. It consists of two contributions, the crystalline silicon peak and the peak attributed to the expanded lattice of porous silicon

The X-ray diffraction spectra show two distinct contributions: one, with higher intensity and at larger scattering angles, is attributed to crystalline silicon substrate, while the other, shifted towards lower scattering angles, is attributed to the PS layer. This peak in fact indicates the presence of a structure with a larger lattice parameter but with the characteristics of a nearly perfect crystal. The result is in agreement with those[25] obtained for *p*-type porous silicon layers.

Similarly to the case of other kinds of PS layers, even in the case of n^+-type the electrochemical etching leads to a structure with the characteristics of a perfect crystal, but with a lattice parameter slightly different from that of the crystalline silicon substrate used for the anodization.

4.3.2 SEM-FEG

The porous nature of the layer that underwent the electrochemical etch has been confirmed by Field Effect Gun Scanning Electron Microscopy

(SEM-FEG) studies, by using a Zeiss S Ultra 55 microscope located at the CMTC-INP laboratory at the Institut National Polytechnique de Grenoble (France). This instrument allows to obtain images at very high resolution compared to conventional scanning electron microscopes.

As we can see in Fig. 4.5 (a), where a front view image of the surface of the sample is shown, SEM-FEG is able to resolve the fine structure of the surface and reveals the presence of homogenously distributed pores with an approximate size of the order of ten nanometers, compatible with those expected for a n^+-type sample.

Fig. 4.5 (b) shows a cross sectional view of the sample. It is clearly visible the porous layer microstructure consisting of many long void channels propagating in the direction perpendicular to the surface, with numerous side branches. This morphology is the typical structure observed in n^+-type PS[21]. The interface between the porous film and the crystalline silicon is planar, with only local imperfection on a scale comparable to the size of pores. This property is a consequence of the formation mechanism, which consists in a plane dissolution front propagating in a direction perpendicular to the surface. The average pore diameter appears in good agreement with what expected for a mesoporous layer (§1.4.1).

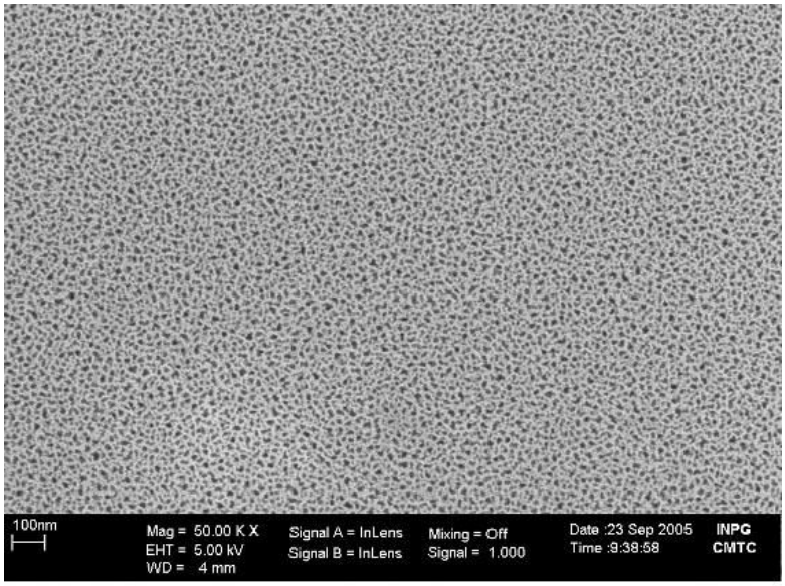

a)

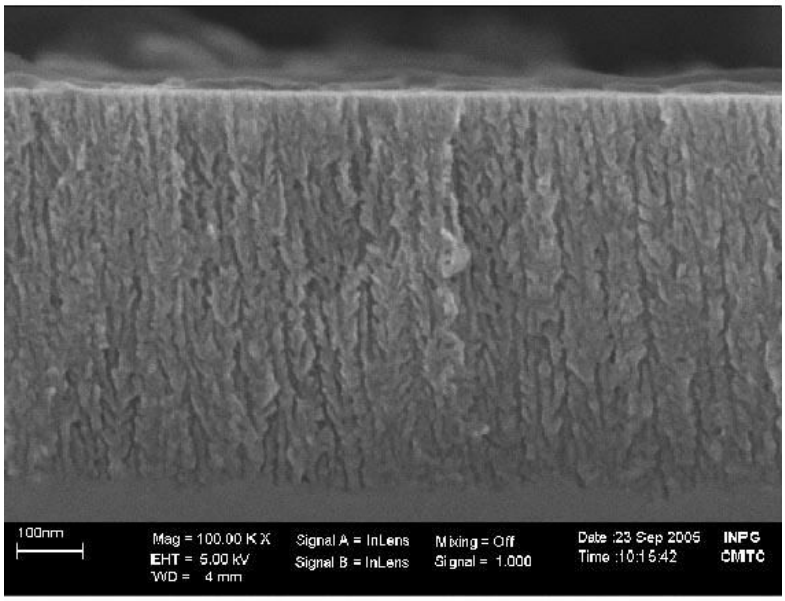

b)

Fig. 4.5: SEM-FEG images of n^+-type porous silicon layer. Front view (a) and cross section (b).

4.3.3 Characterization by BET measurements

The porous nature of our samples has also been investigated by the method of adsorption isotherms of gases at low temperature, that is one of the most common techniques used to obtain a comprehensive characterization of porous materials with respect to the specific surface area, pore size distribution and porosity.

Measurements were done making use of a *SORPTOMATIC 1990* porosimeter by *Thermoquest* at the Industrial Chemistry laboratory of Cagliari University. This device is equipped of a software for the isotherm analysis which calculates information about porosity, developed surface and pore dimension using BET and BJH methods[71, 22].

Fig. 4.6 shows the adsorption/ desorption isotherms obtained at 77K for a 50 μm- thick porous silicon sample:

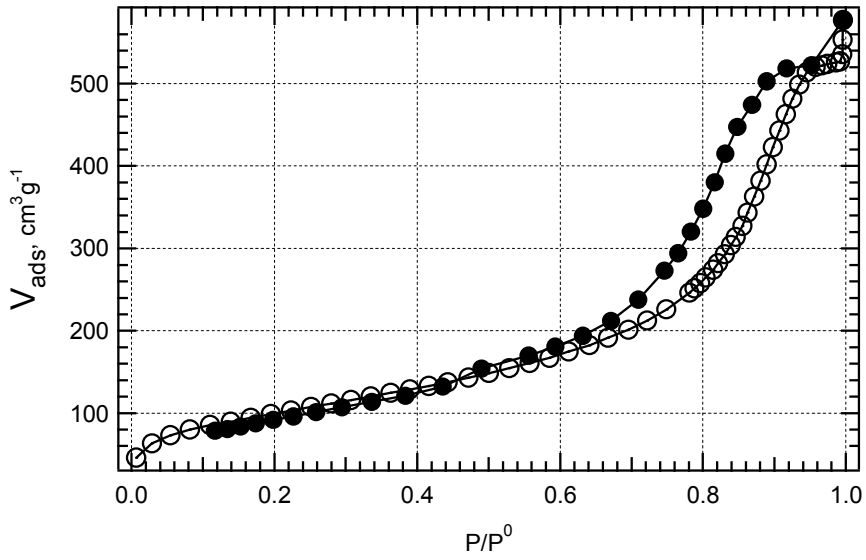

Fig. 4.6: Nitrogen adsorption (○) and desorption (●) isotherms at 77 K obtained for a n^+-type PS sample.

The shape of the curve agrees with the typical trends expected for mesoporous materials, that is for pores of diameter in the 2 – 50 nm range (§ 3.4.3): in the low relative pressure regime, up to 0.7, N_2 molecules are

gradually adsorbed by the surface and the volume of adsorbed gas varies smoothly with pressure. The increase of the relative pressure causes the phenomenon of capillary condensation of gas in the pores, which is clearly distinguishable in the isotherm by the sharp increase of the adsorbed volume.

The distribution of the pore size in the material has been calculated from the isotherms of Fig. 4.6 using the D.H. method[23]. The results are shown in Fig. 4.7, where the volume occupied by pores per gram of material is presented as a function of the pore diameter, and are summarized in Table 3.

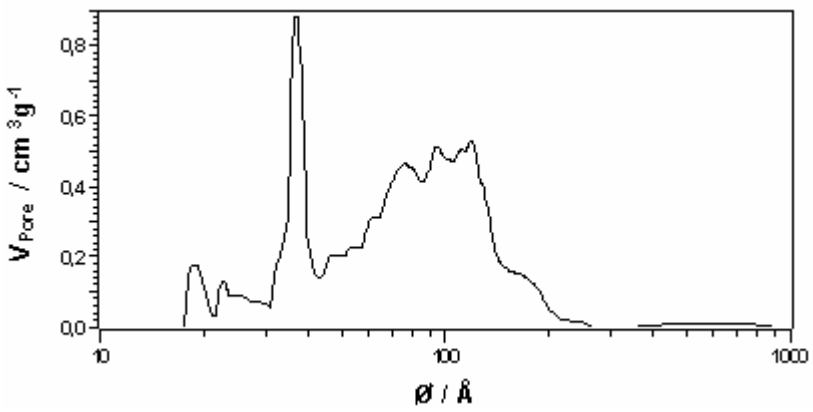

Fig. 4.7: Pore size distribution in n^+-type PS sample calculated by DH method.

Type of pores	Pore diameter (Å)	Pore volume ($cm^3\ g^{-1}$)	Pore volume (%)	BET Specific Surface ($m^2\ g^{-1}$)
micropores	0÷20	0,0058	0,7	361
mesopores	20÷500	0,8341	95,2	
macropores	500÷1000	0,0364	4,1	

Table 3: Pore size distribution and specific surface calculated from adsorption isotherms by DH method.

As we can see in the Table 3, the fraction of the void volume in the material due to micropores, that is pores with diameter inferior of 2 nm, represents only 0.7 % of the total.

The largest part of the pore volume, about 95%, is related to pores with diameters ranging from 2 to 50 nm, confirming the mesoporous nature of n^+-type porous silicon. The pore distribution in this size range is not homogeneous: it is in fact characterized by a narrow peak at about 3.7 nm, and a broader band ranging from 5 to 20 nm, with a maximum at about 10 nm. This results must be interpreted in the light of the information on morphology obtained by SEM-FEG analysis (§ 4.3.2). This studies revealed a microstructure constituted of void channels running in the direction normal to the surface with many branches on the side of each pore. The diameter of void columns was estimated of about few tens of nanometers, while the diameter of branches was estimated to be narrower by a factor of ten with respect to that of the main pores.

Considering this information, we can attribute the large band between 5 and 20 nm to the main columns and the narrow peak at 3.7 nm to the thin branches on the pores' side.

The remaining 4.1% is represented by macropores and corresponds in the curve to the large low band beyond 30 nm.

As lipase dimension is about 5 nanometers, this study demonstrate that, in principle, the vast majority of pores is available for lipase immobilization.

From the values of pores' volume we can deduce the porosity of the sample. Density of bulk silicon is equal to 2.33 g cm^{-3}, and its specific volume is then equal to 0.4292 cm^3g^{-1}. The specific volume found for our samples is instead 0.8763 cm^3g^{-1}. The porosity is given by the ratio of specific volume of bulk silicon to the specific volume of porous silicon and is calculated to be equal to 49%, with an error of 5%. This value is in good agreement with the value of porosity of 50-60% that we had evaluated for our sample from gravimetric study..

The value of the specific surface calculated using the B.E.T equation is 361 m^2g^{-1}, that must be transformed into m^2cm^{-3} to be compared with values shown in literature. With a specific volume of 0.8763 cm^3g^{-1} the calculated specific surface is equal to 412 m^2cm^{-3}.

4.4 Summary: formation and characterization

The anodization conditions and the characteristics of all samples used for enzyme immobilization, if not otherwise specified, are resumed as follows:

Anodization conditions:

Wafer type = n^+ (100); $3 < \rho < 7 \cdot 10^{-3}$ Ωcm

Solution Composition = 15% HF, 15% H_2O, 70% Ethanol

Formation Current Density = 50 mA cm^{-2}

Illumination = No

Morphology:

Mesoporous columnar structure.

Pore diameter = 0.7% with $0 < d < 2$ nm, 95.2% with $2 < d < 50$ nm, 4.1% with $50 < d < 100$ nm.

Chapter 5:

5 PS surface stabilization through oxidation

5.1 Introduction

One of the major problems that we had to solve to realize the biosensor has been the dissolution of porous silicon in aqueous solutions.

In paragraph 1.5.1 we said that 'fresh' porous silicon, that is PS just after formation, is characterized by a hydrophobic surface almost completely covered by Si-H_x groups. This hydrogen-passivated surface exhibits good stability over a period of hours, but it undergoes a significant modification for longer storage in ambient air. This modification consists in a passivation of the surface through natural oxidation and/or saturation of dangling bonds with species coming from atmosphere.

This surface is not at all stable in contact aqueous solution, and a process of dissolution of the layer is observed. This phenomenon has been reported by other authors (§ 1.5.2) for *p*-type PS, but a specific technique to avoid it has not been discussed. Anderson et al. [34] showed that the dissolution rate depends on pH and on porosity. Medium porosity samples (50 ÷ 60%) show evidence of dissolution at pH ≥ 6 after only 24 hours.

We also found that the dissolution process is significantly accelerated by light excitation: just a few minutes in a solution at pH = 7 and under laser

powers of a few tens of mW, were enough to observe a dramatic samples' degradation.

The fact that aqueous solutions at physiological pH values, that is around pH = 7, are the same time the ideal environment for enzymes activity but also a pH in which PS matrix dissolves, imply that we need to find a way to stabilize the pore's surface. As a matter of fact, even if a single measurement would be still possible in this situation, our goal is the realization of a reusable sensing device, and the process of dissolution would prevent this result, because as silicon dissolves the enzyme is lost in the solution.

Among the possible passivation techniques, we chose to oxidize the PS surface, since SiO_2 is a very stable molecule and the oxide surface layer would be able to protect the sample from dissolution.

Moreover, oxidation offers the further advantage that it transforms the PS surface from hydrophobic to hydrophilic, which is more adapted for the diffusion of the aqueous solution into the pores.

We will describe first of all our results for PS oxidation using two simple techniques whose application has been proposed in literature[29]: chemical oxidation by immersion of the sample in H_2O_2 solutions, and dry thermal oxidation in O_2 atmosphere.

5.2 Chemical and thermal oxidation methods

5.2.1 Chemical oxidation in H_2O_2 solution

A first attempt to oxidize the surface was made in a previous work[84] by immersing the sample for 15 minutes in a aqueous solution H_2O_2 diluted at 3%. This treatment leads to a very bland oxidation, that moreover was found to reduce the mechanical stability of the sample.

Fig. 5.1 shows a scanning electron microscope image of the surface of a sample with 55% of porosity and 20μm thick after H_2O_2 treatment. We can see that the sample is clearly damaged in the process.

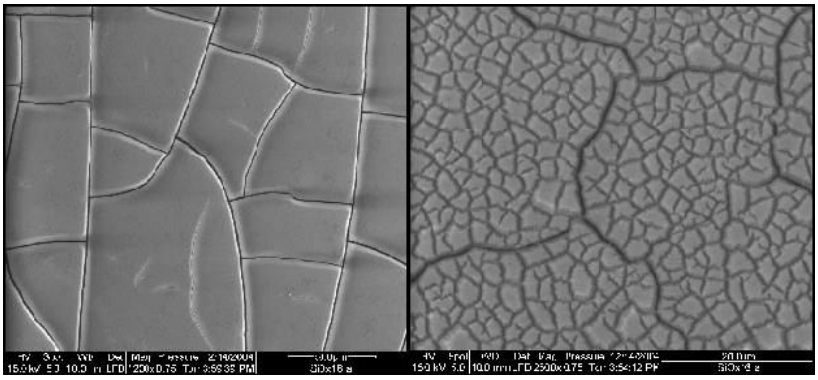

Fig. 5.1: Scanning electron microscope image of the surface of a sample with 55% of porosity and 20μm of thickness. Images are relative to two different magnifications (1200X and 2500X respectively)[84].

Chemical oxidation through H_2O_2 resulted then an inadequate technique to stabilize PS sample before molecules immobilization, therefore other methods were investigated.

5.2.2 Thermal Oxidation

Thermal oxidation was performed by annealing the PS samples at a temperature of 450 °C under controlled under O_2 flow (1L/min).

We prepared four nominally identical samples, that were oxidized using the parameters described above for duration ranging from 30 minutes to 2 hours, with time steps of 30 minutes from one sample to the next ones to study the effect of the length of the oxidation process on the oxidation level. At the end of the process all samples showed a good morphology and no evidence of structural damage. The oxidation levels we were able to obtain will be discussed in detail in § 5.4.1.

5.3 Anodic oxidation of porous silicon

5.3.1 Process description

Electrochemical oxidation of PS is achieved in aqueous electrolyte prepared with de-ionized water with the addition of salts, under anodic polarization conditions.

Anodic oxidation is performed just after the rinsing phase in water that immediately follows the formation process. Water is replaced by a 0.1 M KNO_3 aqueous solution and a constant current density is applied. It is very important that in the process of changing the solutions in contact with the porous layer care is taken to avoid exposing the samples to the air, since fresh-PS is highly hydrophobic and if the pores wall were partially dried, the KNO_3 solution would not be able to thoroughly pervade the pores, leading to a non uniform oxide layer.

The anodization process, which we recall is performed by applying a constant current, can be monitored by recording the evolution of the applied potential with time. Fig. 5.2 shows a plot of the applied potential as a function of time during the anodization of a 50 μm- thick sample using a current density of 6.67 mA cm^{-2}.

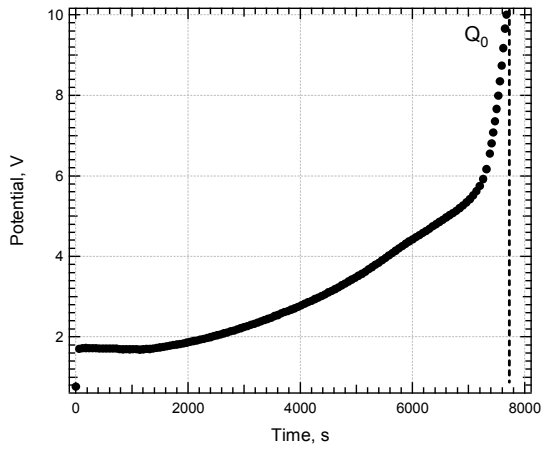

Fig. 5.2: Evolution of the anodization potential during anodic oxidation of a 50 μm-thick sample and 60% of porosity, in KNO_3 0.1 M aqueous solution at constant current density of 6.67 mA cm^{-2}.

In analogy with literature's results for the *p*-type nanoporous PS (§1.5.4), in the oxidation process two regimes are distinguishable: first, the oxidation proceeds with relatively slow variations of the potential during time, until a particular value of potential V_0, in our case about 6V, at which a sharp increase of the potential is observed. This sudden increase of the curve slope is interpreted as an increase in resistivity due the formation of the insulating oxide layer, which eventually leads to the breaking of the electric contact on the porous layer. In our case, the process is interrupted at a potential of 10 V by our experimental setup limitation, but since the slope of the curve in this region is increasing very rapidly, we can suppose that the real interruption of the electric contact would have reasonably occurred after a 1-2 minutes, a time negligible with respect to the total duration of the oxidation process. As a matter of fact, what really counts is not the applied potential value but the time during which the constant current flows into the circuit. The fact that the real interruption of the electrical contact would happen just 1-2 minutes after we actually stop the experiment means that the fraction of Si atoms that would be further oxidized by prolonging the experiment would be irrelevant with respect to the total oxidized Si atoms. For this reason the interruption at 10 V can be assumed as the real breaking of the electrical contact.

The total exchanged charge at the moment of contact breaking, Q_0, can be simply calculated as the product of the current and the anodization duration:

$$Q_0 = J[Acm^{-2}] \times Surface[cm^2] \times Time[s]$$

As we are dealing with a nanoporous electrode, where the electrode and the electrolyte are two interpenetrating phases, the anodic oxidation must be further characterized in order to check if the oxidation process significantly differs from a standard electrochemical process due to the porous nature of the electrode.

In the next discussion we will call the sample oxidized up to 10V as 'fully' oxidized.

5.3.2 Dependence on current density

First of all we want to know if the current density was a critical parameter, or if its influence on the process was negligible. Five identical 50 μm-thick samples were formed and oxidized at five different current densities of 3.33, 6.67, 10, 13.33 and 16.67 mA cm^{-2}. The electrolytic solution used was 0.1 M KNO_3. Fig. 5.3 shows the oxidation curves relative to these five samples:

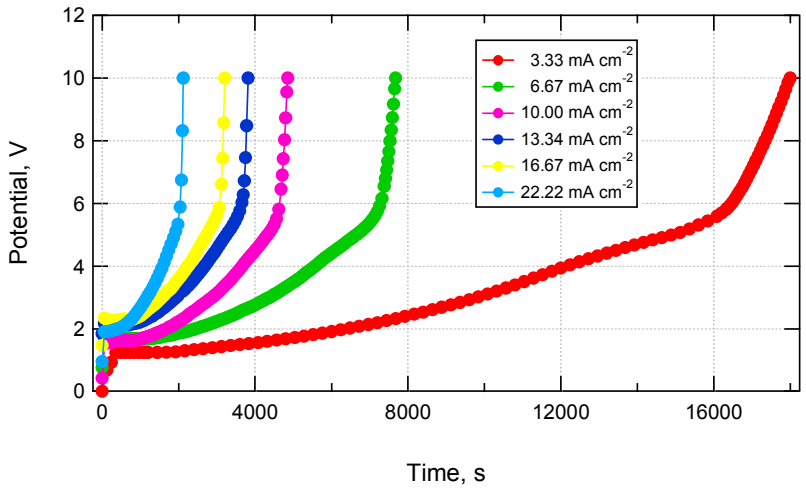

Fig. 5.3: Anodization curves for 50 μm n^+-type PS samples realized at different current densities.

Oxidation curves have qualitatively the same shape for all current densities. The sharp bending of all curves occurs at the same potential, around 6V, and they only differ for the duration of the regime of slow potential variation, that is for the time that is necessary to complete the oxidation process: the process duration increases by decreasing current density. Fig. 5.4 shows the plot of the oxidation time as a function of current density:

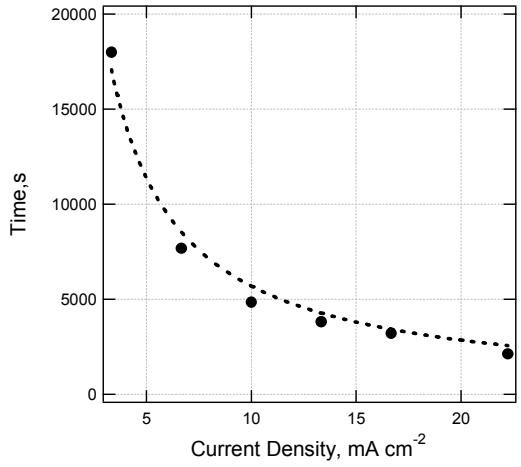

Fig. 5.4: Plot of oxidation process duration as a function of current density for 50 μm-thick samples oxidized in 0.1 M KNO_3 solution at different current densities.

We found that experimental data are in very good agreement with a fit by a hyperbolic function of the form:

$$y - y_0 = \frac{const}{x}$$

This implies that the product of current and time duration is constant for all samples and, being this product equal to the total exchanged charge, that Q_0 *is constant* for all current densities:

$$Q_0 = Current[A] \times Time[s] = (52 \pm 1)C$$

This is an important result because it demonstrates that the oxidation process behaves as a normal electrochemical process: increasing the current density the rate of charge transfer is higher, but the exchanged charge is the same. It implies that in the process the charge diffusion is not limited by the fact the electrode is nanostructured.

In § 5.5 we will see that the average oxygen content in samples fully oxidized using different current densities is the same.

5.3.3 Dependence on the sample thickness

One important problem that emerges from literature is that in the case of *p*-type porous silicon, the oxidation process is interpreted as starting only at the pores' bottom and remaining confined in that region (§1.5.4). If this was also the case for our morphology, that would imply that it would be impossible to anodically oxidize our samples. In fact, in our case the pores structure is not homogeneous in all directions but has a clear asymmetry due to the columnar structure of the pores. If the oxidation process was limited to the pores' bottom that would imply that the oxidation process would mainly affect the region near the porous Si – crystalline Si interface. As a consequence, there would be a large part of the pores' surface that, still not oxidized, would be subject to dissolution in aqueous solution.

In order to study this phenomenon, we investigated the influence of the sample thickness on the oxidation curves. If the oxidation occurs only at the pores' bottom, the oxidation process would be almost the same for all samples' thicknesses, and the plots of voltage vs. time would overlap. By converse, if the oxidation process is homogeneous in the samples' thickness, the plots would differ, and the oxidation type would be proportional to the samples' thickness.

We prepared six samples with thickness of 1, 5, 10, 20, 30 and 50 μm respectively and on each of them we performed the oxidation process until breaking of electric contact, at a current density of 6.67 mA cm^{-2}.

The oxidation curves relative to samples of different thickness are not the same, but the oxidation process duration increases proportionally to the sample thickness (Fig. 5.5). This is an important result because it is a proof of the fact that the process involves all structure and not only on the bottom of pores as observed in the case of nanoporous Si. Besides, it also implies that even if the pores have diameter of few tens of nanometers, there are not capillary forces that prevent the diffusion of the electrolyte into the pores.

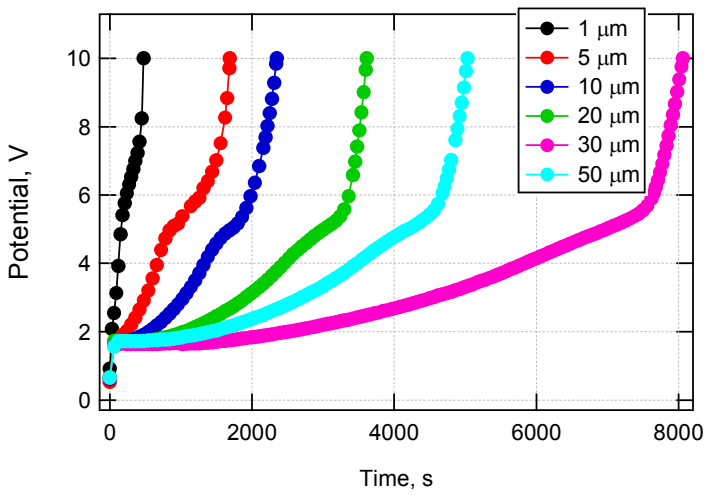

Fig. 5.5: Dependence of anodization curves on the sample thickness.

5.3.4 *Realization of samples with different oxidation levels*

Anodic oxidation allows the preparation of samples with different oxidation level, by simply interrupting the process at given times.

Current density was fixed at 6.67 mA cm^{-2}, and the oxidation process was stopped the applied potential reached the values of 2, 4, 6, 8 and 10 V (see Fig. 5.2). The oxidation level q of these samples can be calculated according to equation:

$$q = \frac{Q}{Q_0}$$

where Q is the charge exchanged up to the moment at which the process is stopped and can be calculated as the product of the duration of the oxidation process and the applied current. NB: the time considered here is the time necessary for the potential to reach the prefixed values of 2, 4, 6, 8, 10 V.

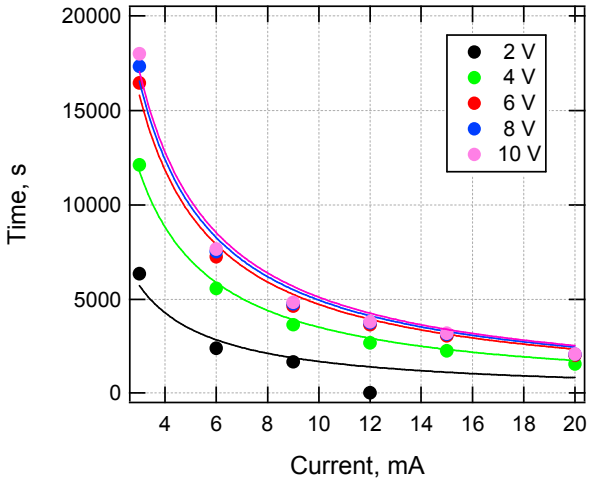

Fig. 5.6: Duration time as a function of current density for oxidation processes stopped at prefixed values of potential of 2V, 4V, 6V, 8V and 10V. Current density of 6.67 $mAcm^{-2}$.

The exchanged charge Q is obtained from the hyperbolic fit of oxidation time-current curves in Fig. 5.6 according to equation:

$$y - A = \frac{Q}{x}$$

where x is the current applied to the system, A is a constant and y is the oxidation time.

The correspondence between exchanged charge, potential and oxidation level of the samples is shown in Table 4.

V	Q	$q = Q/ Q_0$
2 V	(17 ± 2) C	0.33 ± 0.05
4 V	(35 ± 1) C	0.67 ± 0.05
6 V	(47 ± 1) C	0.90 ± 0.05
8 V	(49 ± 2) C	0.94 ± 0.07
10 V	(52 ± 2) C	1.00 ± 0.04

Table 4: correspondence between exchanged charge, potential and different oxidation level of the samples.

5.4 Determination of the oxygen content by means of EDS measurements

The content of oxygen in porous silicon samples after different oxidation treatments was evaluated by Energy Dispersive Spectroscopy (EDS) or X-ray microanalysis.

EDS is an analytical technique for the determination of the chemical composition of solid samples, thin layers or particles under investigation in scanning electron microscopes. It allows to record a spectrum of the X-ray intensity as a function of the X-ray energy, that shows peaks rising above a background composed primarily of scattered X-rays. The energies corresponding to these peaks are the energies of shell binding energies of the chemical elements in the sample, which are unambiguously identified since those energies are different for each chemical element. The relative abundance of the different chemical species in the samples is calculated by a suitable software by taking into account the proper cross section.

Thermally and anodically oxidized samples were analysed. In the two cases the EDS spectra show two peaks: the one with higher intensity, centred at 1.7 KeV, is relative to crystalline silicon, that constitutes the porous silicon skeleton. The other, centred at 0.5 KeV, is relative to oxygen, present at porous silicon surface as an effect of the oxidation.

5.4.1 Thermally oxidized samples

Fig. 5.7 shows the EDS spectra of four samples thermally oxidized for 30 min, 1 h, 1 h 30 min and 2 hours. Measurement where performed on the top of the surface.

Spectra of different samples are nearly perfectly superimposed indicating that thermal oxidation does not allow a high degree of tuning of the oxidation level.

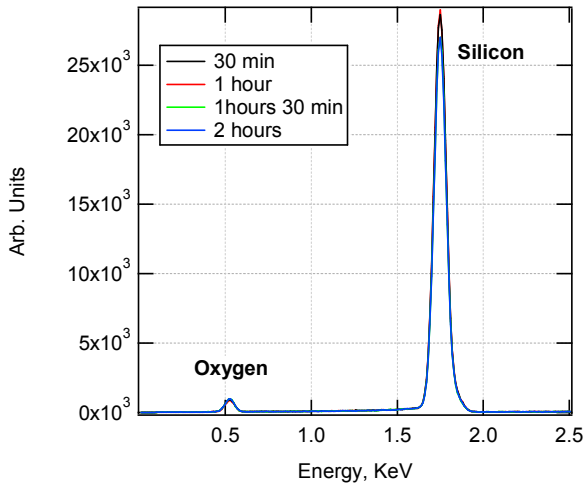

Fig. 5.7: EDS spectrum of 50 µm- thick samples thermally oxidized at 450 °C, under O_2 flow (1L/min) at different oxidation times. Measurement performed on the top of the surface

Fig. 5.8 shows the plot of the oxygen content as a function of the oxidation time for the samples analyzed.

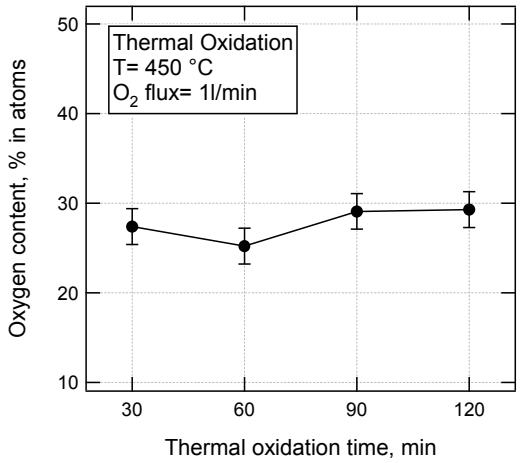

Fig. 5.8: Oxygen content (expressed as atomic percent) of four 50 µm- thick samples thermally oxidized at 450 °C, under O_2 flux of 1l/min, for 30 min, 1 h, 1h 30 min and 2h respectively.

This image clearly shows that even when varying the oxidation times in a wide range, samples do not show appreciable differences in composition, but the oxygen content with respect to the total atoms is comprised in the 25%-30% range. A dependence on the oxidation time is not apparent, indicating that in thermal oxidation we can not control the oxidation level.

5.4.2 *Dependence of oxygen content on the anodic oxidation level*

Energy Dispersive Spectroscopy has also been used to evaluate the oxygen content in samples with different anodic oxidation level. Both top surface and cross section measurements have been performed.

Fig. 5.9 shows the EDS spectrum of the top of four PS samples anodically oxidized at different levels.

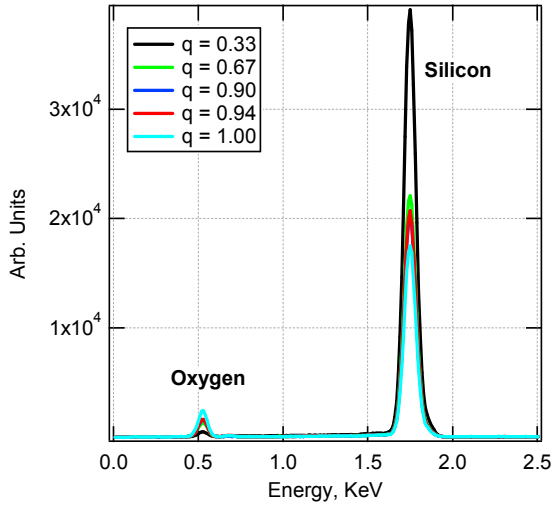

Fig. 5.9: EDS spectra of 50 µm- thick samples anodically oxidized at different oxidation levels. Measurement performed on the top of the surface

Fig. 5.10 presents a enlargement of the oxygen peak, that allows to distinguish differences between samples at different oxidation levels. Measurement where performed on the top of the samples's surface.

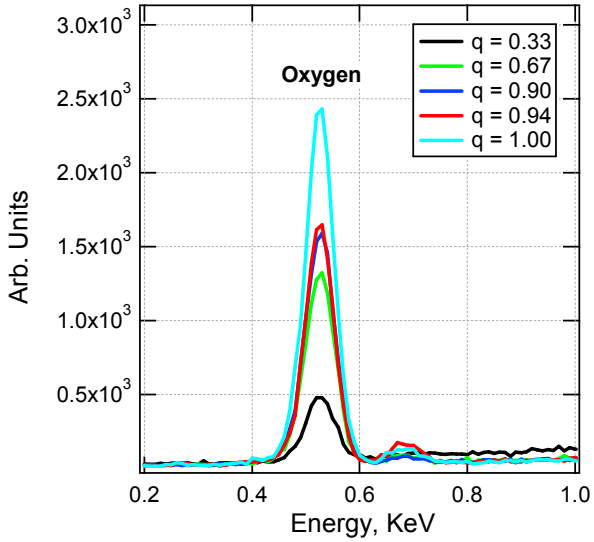

Fig. 5.10: Enlargement of the oxygen peak in EDS spectra showing the different oxygen content in samples anodically oxidized at different levels. The oxygen content increases with the oxidation level. Measurement performed on the top of the surface

In Fig. 5.11 is shown the plot of oxygen content as a function of the oxidation level.

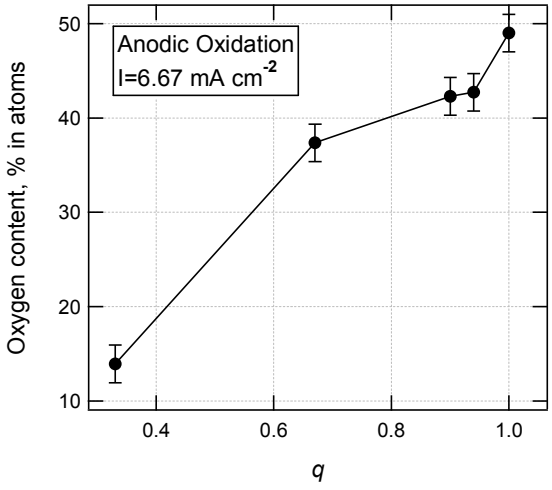

Fig. 5.11: Oxygen content (%) in PS layer as a function of the anodic oxidation level.

If we compare Fig. 5.11 with Fig. 5.8, we can see that anodic oxidation allows a wider range of variation of the oxygen content in the structure with respect to thermal oxidation.

In the next chapter, where we will describe the immobilization of the enzyme on PS, we will see that surface oxidation level affects the process of physical adsorption of lipase; the possibility to tune in a simple way the oxygen content is therefore useful for the characterization of the process.

Another information that we obtained from the EDS study is that even if on a first approximation basis the oxidation process is independent on the applied current density (see § 5.3.2), the samples oxidized using high current values are relatively inhomogeneous, as compared to those oxidized with lower current densities. On the basis of these results, a current density of 6.67 mA cm^{-2} has been used for all samples. In fact, we have observed that on one hand for high value of current density (> 9 mA cm^{-2}) there are some inhomogeneities in the oxygen content on the layer's thickness, on the other hand a density of 3.33 $mAcm^{-2}$ would demand oxidation times excessively long. A current density of 6.67 $mAcm^{-2}$ was then a good compromise between high homogeneity and reasonable durations of the process.

5.5 New information about n^+-PS morphology

The study of the oxidation process has allowed us to find new information about n^+-type PS morphology. In particular results obtained when characterizating oxidation respect to sample thickness and sample depth revealed properties compatible with an inhomogeneity of morphology in depth.

In Fig. 5.12 we reported the time duration as a function of the sample thickness and in Fig. 5.13 the oxygen content in the cross section of the samples, measured by EDS technique.

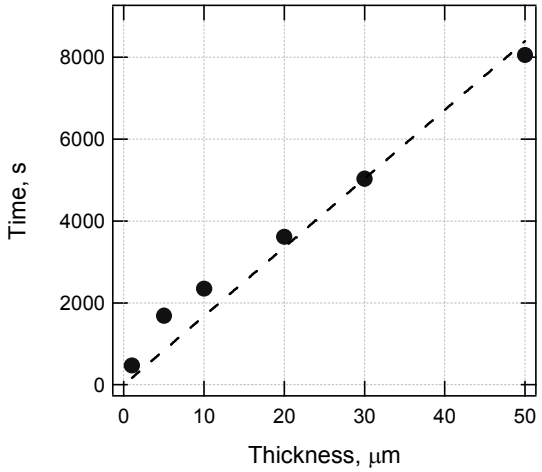

Fig. 5.12: Anodicxidation process duration as a function of sample thickness.

The linear fit is performed imposing the crossing of the origin (thickness=0, time =0) by the fitting line. From Fig. 5.12 it is possible to see that all data points for samples thinner than about 10 μm lie above the fitting line indicating that the behaviour is linear only for higher thicknesses.

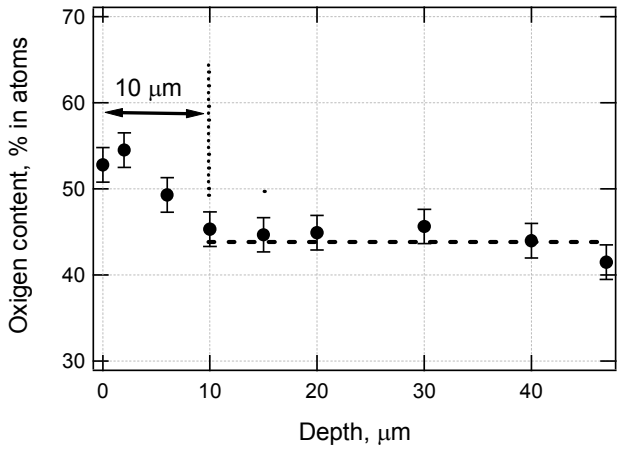

Fig. 5.13: Oxigen content (%) as a function of depth for a 50 μm-thick sample anodicallyoxidized at 6.67 mA cm^{-3} and an oxidation level q = 1. Cross section measurements.

The oxygen content measurements by EDS performed in the cross section of the samples (Fig. 5.13) clearly exclude any diffusion problem of the oxidizing solution since the oxygen content is higher in the first 10 μm , in agreement with higher oxidation times, but is constant in the rest of the depth.

This fact indicates that the oxidation of the first 10 μm of the porous layer below the surface requires more electrons than the porous layer underneath. Since there is no reason for the oxidation process to be slower in the first few μm, the most reasonable explanation is that there are more Si atoms involved in the process.

The most probable explanation is then that the different oxygen contents are related to slight morphological inhomogeneities. In particular, since the oxygen content is higher in the first micrometers under surface than in depth, we can suppose that near the surface the layer is characterize by a greater specific surface, due to a different porosity or to the presence of nanopores. As SEM-FEG did not revealed an evident morphological difference in depth (§ 4.3.2), we can suppose that in the first microns under the surface, the columnar pores have a higher density of nanometer-size ramifications that may significantly increase the specific surface while keeping the porosity almost unchanged.

Chapter 6:

6 Immobilization of lipase on PS

6.1 Introduction

In the previous chapters we described the preparation of porous silicon samples as matrixes for enzyme immobilization. We determined the formation parameters needed to obtain samples with the pore size, porosity, specific surface and thickness suitable for the realization of our biosensor.

Then we described the anodic oxidation treatment, that has been necessary to stabilize our samples against dissolution in aqueous media.

In this chapter we will describe the immobilization of enzymes in the pores' internal surface through physical adsorption and we will study the parameters affecting this process.

6.2 The immobilization process

The immobilization of lipase was performed using simple physical adsorption. We preferred this approach, instead of chemical binding of the

molecules, since physisorption is more gentle and the enzyme molecules are more likely to keep their functionality.

6.2.1 Definition of immobilization parameters

Before describing the optimization of the immobilization process it is worthwhile to make a brief introduction about the parameters useful to characterize the efficiency of an enzymatic device.

In general, the quantitative evaluation of how much enzyme enters the pores during immobilization process is not feasible and, moreover, is not useful to evaluate the device efficiency. In fact, as we have explained in § 3.5.2, the enzyme is rarely pure and part of the immobilized molecules may be in a totally or partially inactive state. For this reason the amount of immobilized enzyme is in general expressed in terms of *activity*.

The definition of the *activity* of an enzyme is based on the velocity of the enzyme-catalysed reaction. In fact, the activity is defined as the number of moles of product formed per time unit and per gram of enzyme.

As we are dealing with immobilized enzymes, the definition of activity should be slightly modified. In particular, we used two parameters to express the catalytic activity:

The immobilized activity.

The device activity.

a) The "immobilized activity" (A_{Imm}) is defined as the difference between the initial (A_i) and final (A_f) activity of the lipase solution[75]used in the immobilization process:

$$A_{\mathrm{Im}m} = (A_i - A_f)$$

This formula is valid only in the assumption that the loss of activity of the enzymatic solution from the beginning to the end of the immobilization process is mainly due to the physisorption of the enzyme into the pores. This is not always true, and particular care must be taken using this definition of activity to evaluate the activity of the enzyme physisorbed into the pores.

In general, the immobilized activity values are referred per unit mass of support. In our case, since all samples we used were nominally identical with a porous layer mass 3.7 mg*, all our measurements are referred to that value.

In this thesis we used this definition of activity only to describe the time evolution of the immobilization process. This study was performed sampling the immobilization solution at given time intervals during the immobilization process. This was done by withdrawing small volumes of solution (e.g. 1 % of total volume for each sample) from the test tube, and measuring their activity using pH-stat method.

b) Once optimized the time duration, all other activity measurements were expresses in terms of " Biosensor Activity". This quantity is the activity of the loaded PS samples measured with "pH-stat method" (§ 3.5.2). These measurements were performed by directly inserting the loaded-PS sample in the tributyrin emulsion as shown in Fig. 6.1.

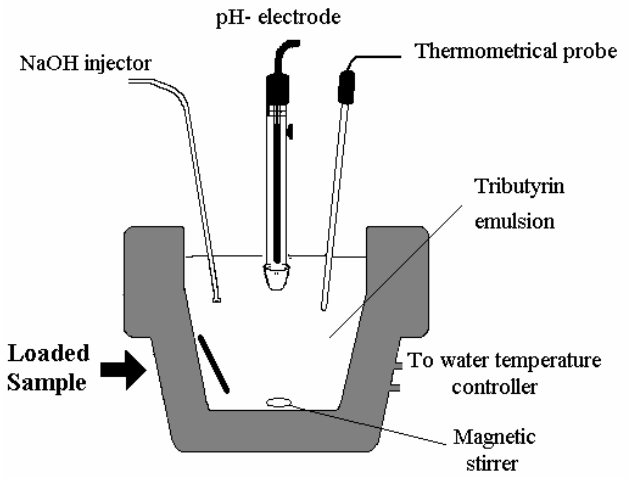

Fig. 6.1: Scheme of the biosensor activity measurement setup.

* The mass of a porous silicon sample can be calculated by multiplying the mass of a cylinder of silicon with volume $V=\pi r^2 \times$thickness by the silicon density (2.33 g cm^{-3}), with the percent of porosity, in this case 49%.

6.2.2 Preparation of the enzymatic solution

Lipase Ay from *Candida rugosa* fungi fermentation was supplied by Amano Enzyme Europe L.T.D. It is put on the market as a powder compound containing, besides the enzyme, lipids, carbohydrates, nucleic acids and salts resulting from process of fermentation and lipase extraction. In principle, we can not exclude *a priori* that all these substances will interfere with the immobilization process, but preliminary test revealed a good enzymatic activity even without enzyme purification. Enzyme purification will be implemented in future work.

Enzymatic solution was prepared by dissolving 0.0125 g of enzymatic powder in 25 mL of buffer solution at different pH (20 mM acetate buffer for pH 4 and pH 5 and 20 mM phosphate buffer for pH 6, pH 7 and pH 8), paying attention to shake the solution gently in order to avoid the denaturation of the enzyme. In a previous work[84] enzyme masses higher by a factor of 10 were used, but the resulting activity was of a factor 10 lower that in our case. This probably indicate that a less concentrated solution enters more easily in the pores, but a systematic study of activity as a function of the enzyme concentration in the immobilization solution has been postponed for future works.

The pH of the immobilization solution was fixed at pH = 7 at the beginning of the study, since at this pH value the enzyme activity is maximum. A comparison of the immobilization as a function of the pH of the lipase solution will be described in the following paragraphs.

6.2.3 Physical adsorption of lipase on PS

The freshly prepared enzymatic solution was inserted in a test-tube, whose capacity was about 14 mL, together with the porous silicon sample as indicated in Fig. 6.2.

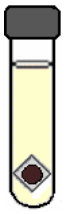

Fig. 6.2: Scheme of the test-tube used for enzyme immobilization on PS samples.

The test-tube is then placed in rotating agitator (see Fig. 6.3) and left under weak and continuous stirring in order to favour the introduction of lipase molecules into pores. As for the preparation of the enzymatic solution, we have to take care that the rotation velocity is not too high, so to avoid the denaturation of the enzyme. The immobilization process is carried out at room temperature.

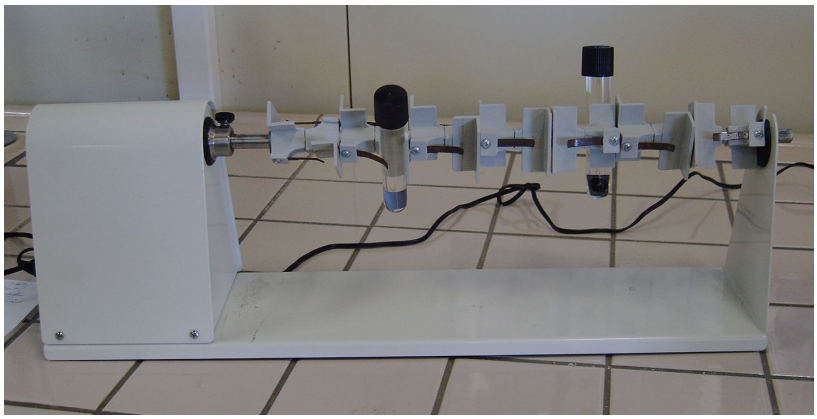

Fig. 6.3: The rotating agitator used for lipase immobilization process.

6.3 Optimization of the immobilization parameters

6.3.1 Immobilization duration

The first step for optimizing the immobilization process, is the determination of the time necessary to maximize the porous silicon enzyme load[84].

A_f was determined by withdrawing small volumes of solution at different time intervals. In particular, the sampling of the solution was performed after 50 min, 1 h, 15 h, 33 h, 36 h, 52 h, 57 h, 123 h.

In order to consider negligible the variation of the volume of the immobilization solution during the analysis, the sum of withdrawn volumes has been kept below 7% of the initial volume. For seven time steps, this condition is satisfied for withdrawals of 100 μL each.

Fig. 6.4 shows dynamic evolution of the immobilized activity during time for a 20 μm- PS sample. We can see that the immobilization process requires very long time to reach the thermodynamic equilibrium. However, after 24h, the immobilized activity was about 90% of its maximum value. The immobilization time was then fixed at 24h, as a compromise between maximum load and reasonable duration of the immobilization process.

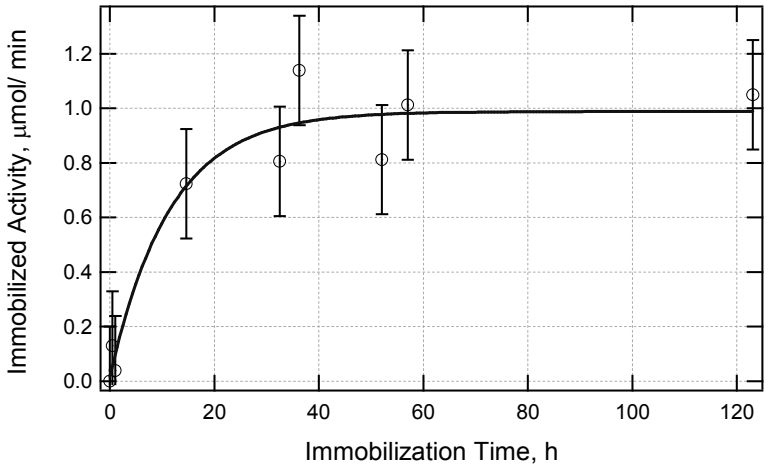

Fig. 6.4: Immobilized activity versus time[84] for a PS sample loaded with the Candida rugosa lipase at pH = 7.

In order to remove all non-adsorbed enzyme molecules, the lipase-loaded PS was submitted to two rinsing cycles of 1 hour each, with the same buffer used for the immobilization process. The check of the released activity showed that already after the first rinsing cycle the released activity was below the detection limits of the pH-stat. This confirms the reaching of a stable lipase-PS preparation.

6.3.2 Influence of pH

We stated at the beginning of this chapter that the immobilization process was performed initially at pH = 7 since this was the optimum pH value to maximize the lipase' activity. However, the physical adsorption process may be dependent on the pH value and be optimum for a different pH value. In fact, physical adsorption is due to a cooperation of intermolecular forces (electrostatic, dipole-dipole, hydrophobic interaction etc.) that can be modified by pH changes in a way that is not predictable a priori. The study of the effect of the pH of the enzyme solution on the immobilization process and on the device' performances was then necessary.

In principle, it is possibile to guess the optimum pH value by analysing charge states on the porous silicon surface and enzyme molecules immersed in different pH. Unfortunately, this study implies the knowledge of the isoelectric points (pI) that, in our case, is not known. In a previous work[84] an attempt to deduce pH influence on immobilization was presented, based on values of silica pI recovered from literature[85] (and given equal to 2) and on pI of enzyme provided by producer specification. However, the results based on this analysis disagreed with experiments, probably because porous silicon isoelectric point does not match that of silica even if a thin layer of oxide is present on the surface.

The direct measurements of the operation of the biosensor was chosen as the best method to evaluate the ideal pH condition. We prepared six buffer solutions at pH values of 3 (3.02), 4 (4.08), 5 (5.01), 6 (6.04), 7 (7.00), 8 (7.91), that were used to prepare six enzymatic solutions.

Fig. 6.5 show the plot of loaded PS activity as a function of the immobilization pH.

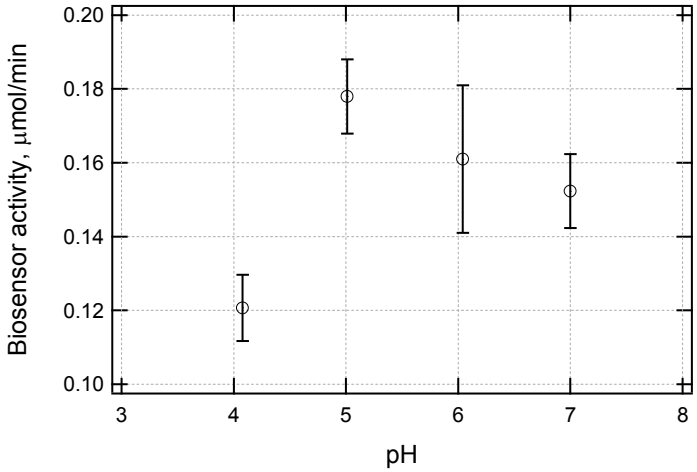

Fig. 6.5: Biosensor Activity as a function of the immobilization pH for a 50 µm-PS sample.

Biosensor activity is quite dependent on immobilization pH. It shows a maximum at value of pH between 5 and 6. This result is in agreement with previous studies[84]. pH = 5 was then chosen as reference value for all immobilizations and storage of the samples.

We also explored other methods to improve the enzyme immobilization. For instance, we added a small amount of ethanol to improve the diffusion into the pores, but the presence of even a few percents of ethanol dramatically reduced the overall enzyme activity[84].

6.3.3 Influence of the oxidation level

We already discussed the fact that PS oxidation is needed to avoid the samples' dissolution in aqueous media. However, the presence of the oxide layer modify the properties of the surface of the pores, and its Effect on the immobilization process must be investigated. Four samples oxidized at different oxidation levels *q* (see §5.3.4), were used for lipase immobilization and the final biosensor activities of the samples were compared. The results are shown in Fig. 6.6;

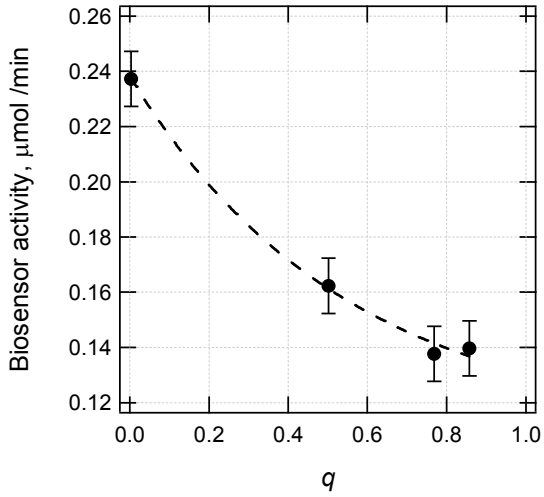

Fig. 6.6: Biosensor activity as a function of the anodic oxidation level.

The biosensor activity decreases by increasing the oxidation level and is reduced by a factor of two when going from the $q \sim 0.1$ to $q \sim 0.9$. Is important to note that the activity values reported for highly oxidized samples are still very good values to fabricate a performing biosensor.

If we compare the plot of Fig. 5.8 with that of Fig. 5.11 for the oxygen content as a function of oxidation level we can observe that the higher the oxidation level the lower, all others parameters being the same, the final activity.

Since the oxidation causes a transformation of the pores' surface from hydrophobic to hydrophilic, we can suppose that the interactions which lead to physical adsorption are weaker in case of oxidized surface.

Even if the activity measured for the highest oxidation level show a still good activity value, we chose for the oxidation an intermediate value ($q \sim 0.33$) that, while still protecting the surface from rapid degradation, allowed a high final activity.

6.4 Sensitivity to substrate concentration

After the study of the behaviour of our biosensor as a function of parameters such as the immobilization pH and the oxidation level of the porous silicon layer, we had to study its sensitivity to substrate concentration, in order to compare the behaviour of the immobilized enzyme with that of a free enzyme. One way to obtain this information is to verify if the enzyme kinetics follows the Michaelis Menten model. This study has been the subject of a Laurea degree stage in our group[84].

The initial velocity V_0 of the hydrolysis reaction for a free lipase into a tributyrin emulsion follows the Michaelis-Menten (MM) equation:

$$V_0 = \frac{V_{MAX}[S]}{K_M + [S]}$$

where V_{MAX} is the maximum velocity, [S] is the substrate concentration and K_M is the Michaelis-Menten constant, equal to the concentration at which the velocity is half maximum. The MM equation describes the behaviour of most enzyme-substrate couples, and states that there is an univocal correspondence between the initial reaction velocity and the substrate concentration for substrate concentrations below a critical value.

In fact, according to the MM equation, V_0 increases with [S] for substrate concentrations below $2K_M$, indicating that the first part of the Michaelis-Menten plot can be used for the calibration a biosensor. For [S] exceeding $2K_M$, instead, V_0 reaches a maximum value and becomes independent on the substrate concentration.

The reaction velocity was measured with the pH-stat method, by using the experimental configuration for biosensor activity measurements described in paragraph § 6.2.1.

The result of the study performed with a lipase-loaded PS sample immersed in tributyrin emulsions at different concentration are reported in Fig. 6.7.

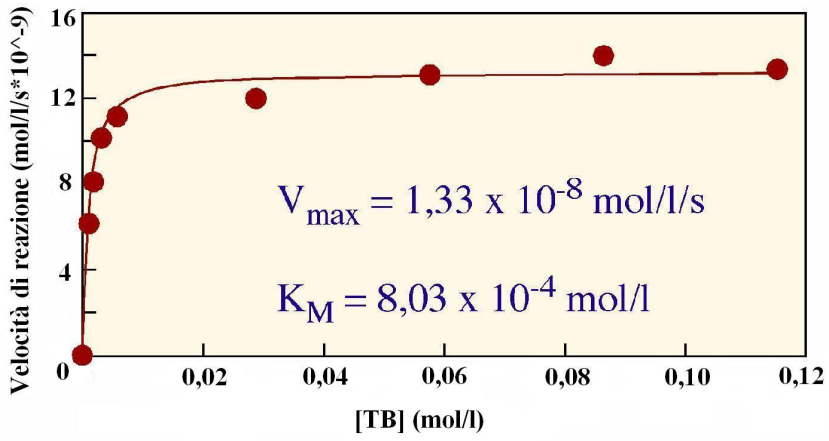

Fig. 6.7: Reaction velocity (expressed as the number of mole hydrolyzed per litre of emulsion in the time unit) as a function of tributyrin concentration in the emulsion. The biosensor has been realized with a PS samples with oxidation level $q = 0.92$, and using a enzymatic solution containing 0.125 g of enzymatic powder in 25 mL of pH = 7 buffer solution[84].

We can see the very good agreement between the data points and the solid curve fit obtained using a MM equation with $V_{max}= 1.33 \cdot 10^{-8}$ mol/l/s and $K_M= 8.03 \cdot 10^{-4}$ mol/l.

The fact that the physisorbed enzyme kinetics follows the Michaelis Menten equation is very important because it indicates that its behaviour is the same as that of the free enzyme, and therefore that there are no limitations to the solution diffusion within the pores.

We have therefore demonstrate that porous silicon is a good matrix for enzyme immobilization.

6.5 Device storage and stability

One of the objectives of this work was the realization of a reusable device. To verify this property we tested our samples' lifetime in the short and long period stability. In the intervals between the measurements the samples are preserved immersed in pH = 5 buffer solution at 4°C.

The results for a sample oxidized at $q \approx 0.33$ are shown in, Fig. 6.8, where the measured activity is plotted versus time.

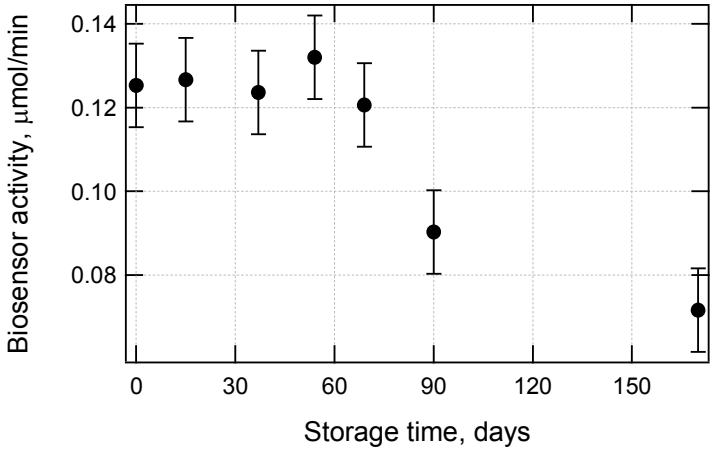

Fig. 6.8: Biosensor activity as a function of storage time in pH = 5 buffer solution and temperature T = 4°C.

We can see that the device maintains an unaltered activity for the first two months. However, after this period the activity of the biosensor significantly decreases, probably as a consequence of the fact that an oxidation at $q \approx 0.33$ is not enough to completely prevent the layer's dissolution, even if the rate is noticeably reduced. We then decided to use a higher oxidation level, that is $q \sim 0.9$.

We studied the stability of the biosensor activity for repeated measurements. Each reported measurement consists in the average of three measurements of five minutes each. Between each measurement the sample was rinsed in water. The results are shown in Fig. 6.9.

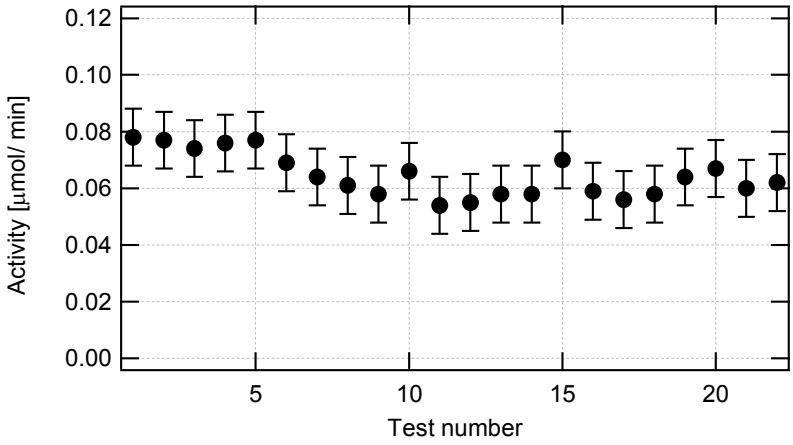

Fig. 6.9: Reusability test: biosensor activity for 22 consecutive tests in a 0.12 M tributyrin emulsion. Each reported measurement is the average of three measurement of a duration on five minutes each. The total biosensor working time exceed 5 hours.

We can see that the catalytic efficiency of the biosensor is reasonably stable for all tests, and we can therefore conclude that the biosensor can be reused many times, for a total operation time that is surely longer than 5 hours.

The long-period stability and verification of the goodness of storage conditions is at this time an ongoing measurement.

Chapter 7:

7 Realization of an *n^+-type* Porous Silicon based potentiometric quantitative biosensor for triglycerides analysis

7.1 Introduction

In previous chapters, we described all steps involved in the preparation of porous silicon samples and in the immobilization of lipase on their surface. We discussed all the problems involved in the matrix preparation and the solution we chose for them.

The final step of our work is now the realization of a proof-of-principle device for the quantitative determination of the triglycerides concentration in a given emulsion. We chose to develop a potentiometric biosensor, that is to measure the pH variations induced by the hydrolysis reaction by measuring the open circuit potential (OCP) of the cell. OCP is the potential measured on the cell when no current is flowing We will describe this procedure in detail in the next paragraphs.

7.2 Operation principle

Our prototype biosensor consists in an electrochemical cell, where the hydrolysis of triglycerides takes place, and a high impedance voltmeter for the potentiometric measurements. The porous silicon samples loaded with lipase are inserted in the electrochemical cell and used as the working electrode, while a platinum electrode acts as counter electrode; the reference electrode was a saturated calomel electrode. The triglycerides emulsion is kept under constant stirring to favour its diffusion into the PS matrix.

The operation principle may be described as follows: when triglycerides emulsion enters the pores where the lipase is immobilized, the hydrolysis reaction starts producing fatty acids and leading to the reduction of the pH of the emulsion. As we saw in § 1.2.2, this pH variation affects the flat band voltage of the semiconductor/electrolyte interface and then the open circuit potential of the cell. The determination of the triglycerides concentration is then made by studying the pH change rate. As a matter of fact, for triglycerides' concentrations that do not saturate the active lipase molecules available, the pH change rate is proportional to the fatty acids production rate, which is itself directly related to the triglycerides concentration in the emulsion.

7.3 The PS/ Electrolyte interface

If the semiconductor/electrolyte interface has been extensively reviewed[6], there are very few data available about the PS/ electrolyte interface. Nanocrystalline electrodes could have unusual properties as a consequence of the fact that the electrode/electrolytic solution system consists of two interpenetrating contiguous phases. To verify that, for our applications, the system behaves as a normal semiconductor/electrolyte interface we first characterized the interface through photocurrent measurements.

7.3.1 Photo-electrochemical characterization

The porous silicon/electrolyte interface has been first investigated by photoelectrochemistry.

A PS sample was used as electrode in an electrochemical cell containing a pH = 7 buffer solution as electrolyte.

First of all we measured the OCP value in the dark for our experimental setup, that was equal to about 650 mV. The sample was then polarized at a voltage equal to OCP and the photocurrent spectra was taken for exciting wavelengths in the 300-700 nm range using a Hg lamp. The maximum of photocurrent was found at $\lambda = 450$ nm (see Appendix A). A cyclic voltammetry was then performed under controlled illumination using a 450 nm radiation and polarization voltage ranging from -200 mV to +200 mV with respect to OCP (that is ranging from 450 to 850 mV) (Fig. 7.1). The *i-V* characteristic confirms that the interface behaves as a normal *n*-type semiconductor/ electrolyte interface. The photocurrent has a maximum when the polarization voltage equals the open circuit potential voltage, while for cathodic polarization with respect to OCP the photocurrent decreases due to the flattening of the bands. The applied voltage that leads to zero photocurrent is the flatband potential. For anodic potential ranging from 0 to 200 mV respect to OCP, photocurrent decreases to a minimum value and then increases again. We did not exceed 200 mV polarization with respect to OCP in order to avoid surface' modifications. In fact, it is possible to see in Fig. 7.1 that when we reduce the applied voltage towards cathodic polarization, for anodic potentials the photocurrent value is slightly reduced, indicating that anodic oxidation of the surface has occurred. This can be understood since the formation of an oxide layer onto the surface creates an insulating barrier which prevents charge diffusion and causes a decrease of the photocurrent. For this reason the photoelectrochemical characterization of PS was performed on non intentionally oxidized samples.

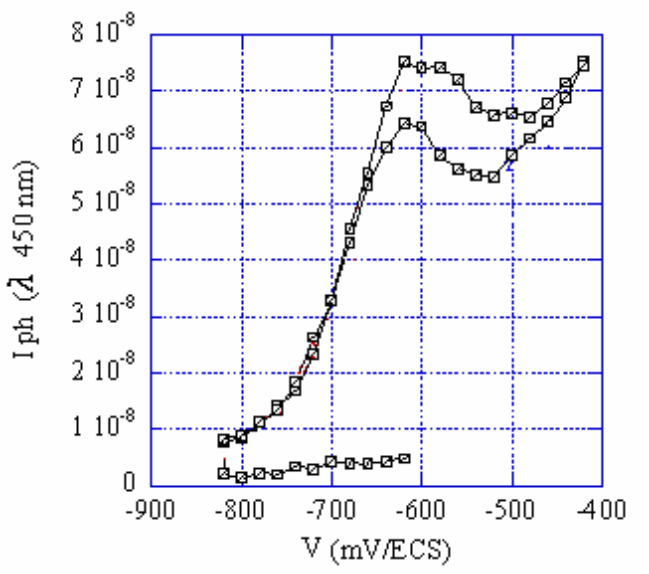

Fig. 7.1: *i-V* characteristics of non oxidized PS/electrolyte interface under illumination (λ = 450 nm).

7.3.2 Dependence of the open circuit potential on pH

As we have seen in the first chapter (§ 1.2.2), the flat band potential V_{fb} of a semiconductor/electrolyte interface is affected by the pH of the electrolyte and is sensitive to reactions occurring at the electrode. A good parameter that can be used to follow the variations of V_{fb} is the open circuit potential (OCP). OCP is in fact equal to V_{fb} apart from a constant value that depends on the details of the experimental setup and that can be considered independent on the reaction occurring in the cell. Moreover, we are not interested in the absolute value of the OCP, but only in its variations due to hydrolysis reaction. As a matter of fact, the parameter that will give information about the triglycerides concentration in a given emulsion is the rate of the production of the fatty acids, and this value is related to the *variation* of the pH and not to its absolute value. This means that our results will be independent from the value of the offset constant.

The dependence of OCP on pH was investigated for different kind of samples:

Samples with a partial anodical oxidation (q < 1);

Samples with a full anodical oxidation (q = 1);

Samples thermally oxidized.

Six buffer solutions with pH values ranging from 4 to 8 were prepared and used as electrolytes. For pH 4 and pH 5 we used 20 mM acetate buffer, while for pH 6, pH 7 and pH 8 we used 20 mM phosphate buffer.

For each pH value, the measurements where carried out for several minutes, in order to verify that at a given pH and when no reaction is taking place the OCP value remains constant. The results are shown in Fig. 7.2.

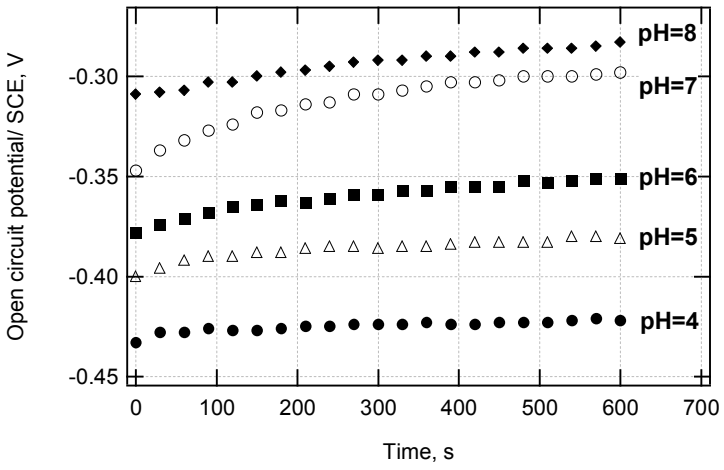

Fig. 7.2: Plot of OCP as a function of time for different pH.

where we can see that OCP is constant after a few minutes, indicating that the interface reaches equilibrium in a short time (probably the time necessary for the solution to pervade the pores). The stable OCP values are, as expected, a function of pH, as shown in Fig. 7.3.

The plot of open circuit potential as a function of pH is linear, in agreement with theory, but the slope is different for samples with different oxidation levels.

The results show that we can divide the samples in two groups, depending on the observed slope. First, at a slope of about 70 mV/pH there are all samples with an oxidation level $q < 1$, and, second, there are all samples with an oxidation level $q = 1$ (fully oxidized samples). Thermally

oxidized samples (full squares in the plot) show a behaviour identical to that of fully anodically oxidized samples.

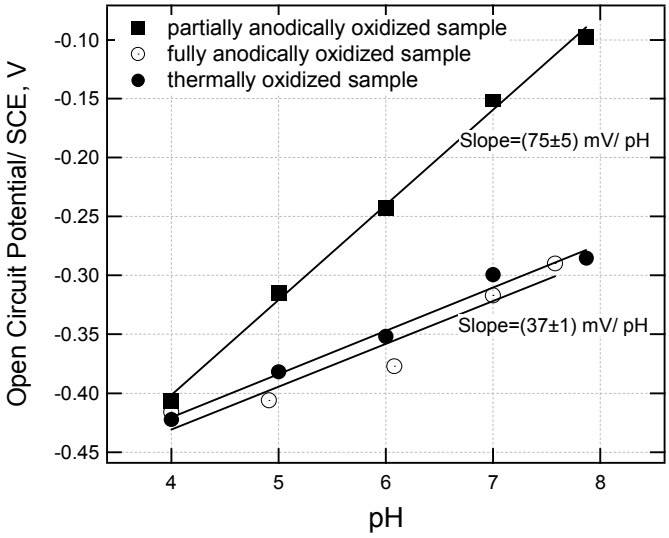

Fig. 7.3: Plot of OCP as a function of pH for samples oxidized at different levels.

We discussed in Chapter 1 the pH dependence of the V_{fb} of semiconductors covered by a thin oxide layer as mainly due[8] to the different charge that can accumulate on the surface depending on the pH of the solution.

Generally, a dependence of 59 mV per pH unit is expected for these systems, in agreement with Nernst equation, but deviation from the nernstian behaviour are often observed[86]. For instance, in the case of silicon covered with a thin oxide, Madou et al.[87] reported a slope of only 30 mV, attributing this result to the amphoteric behaviour of the Si–OH sites, that can both accept a proton yielding a $Si–OH^+_2$ group, and donate a proton, yielding a $Si–O^-$ group.

In our case, the observed behaviour for both fully and partially oxidized samples deviates from what is predicted by the Nernst law.

We interpret our experimental results by referring to two different phenomena that are very likely to occur at the same time in our samples:

first, the amphoteric behaviour of the surface oxide, and, second, the silicon dissolution in aqueous solution.

Literature results (§1.5.3) show that the thermal oxidation of porous silicon is homogeneous over all the available surface, and we can expect that, even if not all the internal skeleton of silicon is transformed in silica, the surface is uniformly covered by an oxide layer and no unoxidized silicon is exposed to the electrolyte. In this case we expect a dependence of OCP on pH close to 30 mV in agreement to Madou et al.[87]. This is actually the case for the observed value of 37 mV/ pH.

In case of partial anodic oxidation, the PS surface is not uniformly covered by a thick oxide layer and there could be some regions where unoxidized silicon atoms are in direct contact with the electrolyte. In these regions the surface is subjected to the dissolution process that passes through an intermediate step of oxidation of silicon atoms. The exact chemistry of this process is not known, but being a red-ox reaction we expect a behavior governed by the Nernst equation.

$$E = E_0 + \frac{0.059}{n} \log \frac{[ox]}{[red]}$$

However, since the samples' surface is partially covered with silica, we expect that when put in contact with the aqueous solution this portion of the surface will show amphoteric Si-OH groups, that will contribute to the curve slope by an amount of 37 mV.

In a first approximation we can reasonably suppose that the two contributions (from the Si atoms oxidation and from the amphoteric behaviour of silica) simply add. The value of slope resulting from this sum is in our case 75 mV/ pH. If our approximation is correct, the oxidation reaction, which contributes to the total slope together with the 37 mV / pH deriving from the amphoteric groups, would involve two electrons (~30 mV / pH), that is not coherent with the formation of SiO_2. A further investigation of the surface composition, for example through IR absorption spectroscopy, is required to give a proper interpretation of our data.

In case of fully anodically oxidized samples, since the measured slope is the same as in case of thermal oxidized samples, we can reasonably suppose that also for anodic oxidation the surface is fully covered with Si oxide.

The presence of two reactions in partially oxidized samples is supported by the fact that they degrades after a few month in aqueous solution (ref. to § 6.5), while fully oxidized samples are stables even after a time span of more than one year.

On the basis of our experimental results, we can then conclude that, while the OCP values show a well defined response to different pH values, well beyond measurements errors for both partially and fully oxidized samples, the best reproducibility is obtained for fully oxidized samples, since the absence of corrosion leads to a much higher stability.

7.3.3 Variation of OCP during hydrolysis

With the information about the OCP sensitivity to pH variations, we can proceed to OCP measurements in triglycerides emulsions. The triglyceride we chose for this work as the substrate for the lipase is tributyrin, a small triglyceride whose hydrolization leads to the formation of glycerol and butyric acid.

The lipase-loaded PS samples were used as electrodes in the electrolytic cell containing the triglyceride emulsion, in the same configuration used for the OCP sensitivity determination with the lipase-free PS samples.

For results presented in this work, samples oxidized at an oxidation level $q = 0.9$ were used. These samples are stable over a time span of several months, during which the biosensor can be used without noticeable corrosion. A tributyrin emulsion 0.028 M was prepared and titrated at pH = 7 through addition of little amounts of NaOH 0.1 M. In fact the as-prepared emulsions have a pH value that is around 4.5 due to a natural partial hydrolization of tributyrin that occurs during shelf preservation. However, since lipase has its maximum activity at pH = 7 we correct the natural pH of the emulsion to ensure optimum enzyme functioning. Moreover, our biosensor will be mainly used in physiological media that have pH values around 7.

Fig. 7.4 shows the time evolution of OCP using a 0.028M test emulsion.

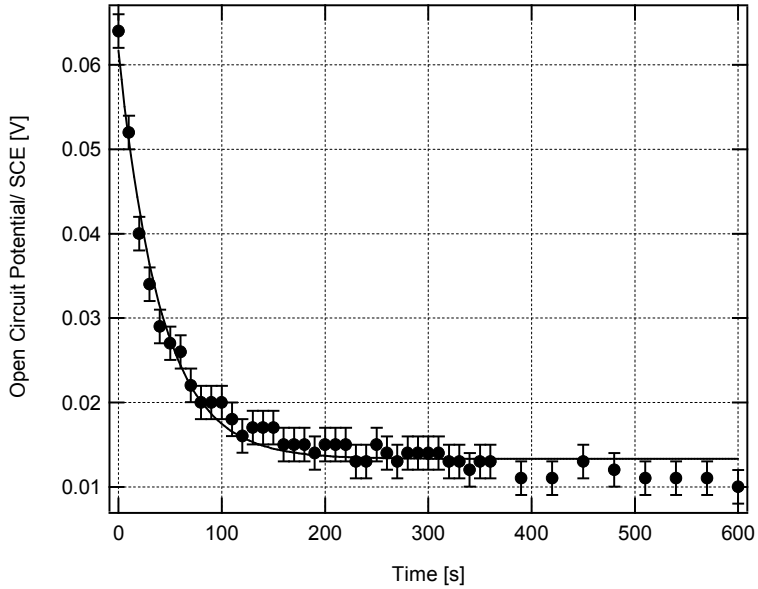

Fig. 7.4: Variation of OCP during time for a loaded PS samples using a 0.028 M test emulsion.

An exponential variation of OCP with time is observed. This is coherent with what is expected for first order reactions[88]. What happens here is that the lipase catalyze the hydrolysis reaction of the available tributyrin molecules, whose concentration is such that the lipase molecules are not saturated. With time, the tributyrin concentration decreases and at the same time the rate of formation of butyric acid slows down, so that the emulsion pH will eventually stabilize.

The total OCP variation (about 30 mV in 5 minutes), using the calibration curve of the previous paragraph, corresponds to a pH variation of about 0.4 units. This conclusion was confirmed by direct pH measurement. This is a very important point, since this confirmation indicate that the surface phenomena that lead to the OCP variations stay unaffected in presence of lipase molecules within the pores.

This results demonstrate that OCP measurements using a lipase-loaded PS samples are a valid alternative to direct pH variation measurements for the determination of triglycerides' concentration in an emulsion.

7.3.4 Sensitivity of the system to different triglycerides concentrations

To calibrate the biosensor, once known the pH sensitivity, we need to perform a series of measurements using a number of emulsion with different tributyrin concentrations.

In our case we want to express the reaction velocity, in terms of the rate of variation of the OCP that must depend itself on the substrate concentration.

To verify this, we proceeded as follows: to plot the variation of OCP during time for each emulsion was plotted, since we can not measure the value of the tangent to OCP vs time curve exactly at the starting moment, because system needs a few tens of seconds to stabilize, we averaged the value of ΔOCP variation rate in the first minute.

The obtained value were plotted against tributyrin concentration, as shown in Fig. 7.5

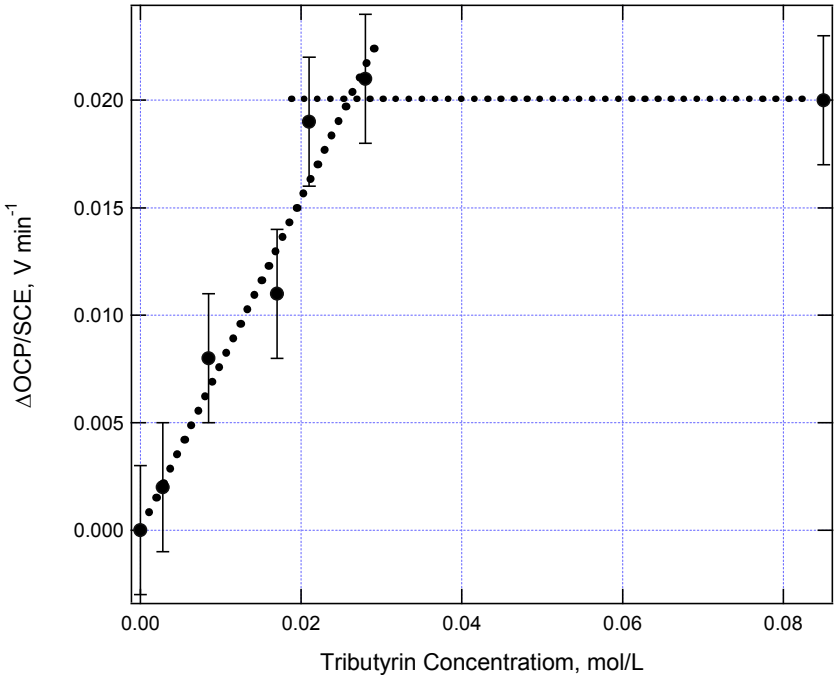

Fig. 7.5: Values of ΔOCP averaged in the first minute of reaction as a function of tributyrin concentration.

The curve presented in Fig. 7.5 shows that the rate of variation of OCP is dependent on the substrate concentration. The $\Delta OCP/\Delta t$ is a linear function of the tributyrin concentration, until a critical value is reached. Above this substrate concentration the rate of variation of OCP with time is independent on the substrate concentration and remains constant, indicating that all lipase active sites are saturated.

The univocal correspondence between OCP variation rate and substrate concentration is then in the 0 - 0.03 mol/ L range, and give the calibration curve for our biosensor. This measurement range is compatible, for instance, with the usual human blood triglycerides concentrations.

We must specify that the substrate concentration at which the lipase saturation occurs depends on the loaded PS layer parameters, and that this upper limit is valid only for the samples fabricated in our standard conditions. It may be interesting, for instance, to lower or raise the limit value to improve the biosensor sensitivity to, respectively, lower or higher substrate concentrations in the emulsion that must be characterised.

The upper detection limit can be easily reduced, for instance, by reducing the immobilization time, and may be easily increased by using larger PS layer or, possibly, by increasing the PS layer thickness and/or with a detailed optimization of the immobilization process.

These results demonstrate that we were able to realize a fully functional biosensor prototype for the quantitative determination of triglycerides using porous silicon as impregnation matrix.

8 Appendix A: PS matrix as drug carrier

8.1 Introduction

In 1.6.1 we said that the biocompatibility and non toxicity of porous silicon has suggested its use in the field of drug delivery.

One of the research lines that we are now developing focuses on the application of PS silicon for the realization of a drug delivery system for tretinoin. The work is developed by our group in collaboration with the Dept. Farmaco Chimico Tecnologico of the Cagliari University directed by Prof. Anna Maria Fadda.

Tretinoin (*trans*-retinoic acid, TRA) is a natural retinoid widely used in proliferative and inflammatory skin diseases, such as psoriasis, acne and skin cancer. Due to the severe side effects when systematically administered, tretinoin is almost exclusively topically employed. It can in fact cause photoreactions, allergy, scaling, erythema, stinging, as a consequence of the formation of degradation products due to the TRA high instability in the presence of air, light and heat [89].

The availability of a carrier able to protect tretinoin from degradation would reduce the side effects involved in the use of this powerful drug.

The aim of the work is to evaluate the potential of porous silicon as a topical delivery system capable of improving the photostability of tretinoin and to obtain a controlled drug release.

8.2 Building a drug delivery PS system

The realization of a porous silicon drug delivery system consist in two phases: the material preparation and the drug loading.

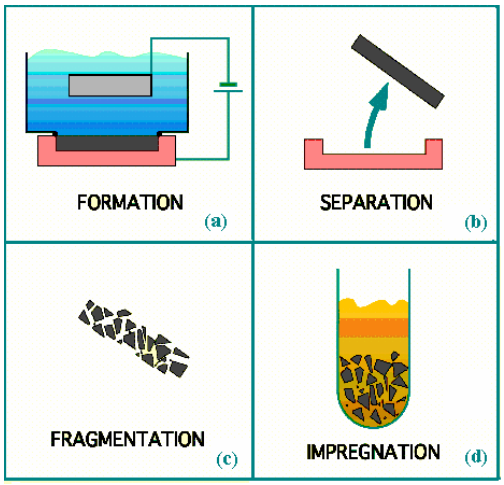

Fig. 8.1: Steps involved in the building of a PS carrier for the drug delivery.

8.2.1 Porous silicon preparation

Porous silicon samples were prepared from n^+-type silicon with a resistivity of 3-7 $\cdot 10^{-3}$ Ω cm. PS layers were obtained, by using an HF solution containing 15% of HF, 15% of water and 70% of ethanol. Anodization current was fixed at 45 mA cm^{-3} and the anodization time at 3000 s. The obtained samples had a porosity of 50-60% and a thickness of 150 μm. After formation, the samples were detached from the crystalline silicon substrate through electropolishing. The free standing layer was then fragmented and reduced to a powder. No preventive oxidation step was required since tretinoin is better mixed in non aqueous solution that don't dissolve PS and better diffuse in this case af hydrophobic surface [ref]

8.2.2 Drug loading

Drug loading into porous silicon is achieved by soaking the PS powder in a methanolic saturated solution of tretinoin, for two days, at room temperature, under continuous stirring.

The determination of the drug load is determined by analysing the concentration of tretinoin after and before the loading process. The solvent,

in fact, is separated from loaded - porous silicon by centrifugation and analysed by HPLC, using a liquid chromatograph Alliance 2690 (Waters), equipped with a photodiode array detector and a computer integrating apparatus (Millennium 32).

The amount of drug loaded by porous silicon has been determined as the amount of impregnated drug (%w/w) with respect to the mass of the porous silicon matrix. We found that drug loading was about 20%.

8.3 Drug release study

After loading the samples are dried in an oven at 65°C and then used for the release test.

The release study has been performed *in vitro* by using a hydrophobic membrane (Perthèse®), composed by a donor compartment and a receiver compartment. TRA-loaded porous silicon was suspended in a gel and placed on the membrane surface in the donor compartment.

The receiver compartment had a volume of 7 cm^3 and an effective diffusion area of 0.785 cm^2 and was filled with a hydroalcoholic solution. The solution was constantly stirred with a magnetic bar and thermostated at 37°C throughout the experiments. In this way the behaviour of the human skin is simulated.

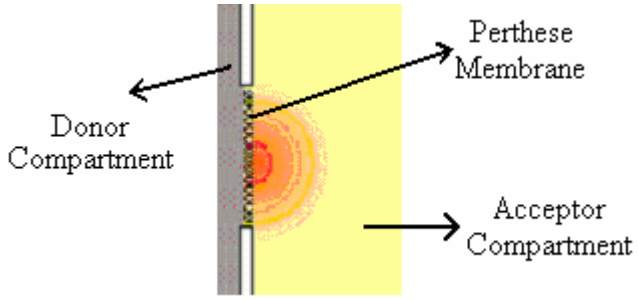

Fig. 8.2: Scheme of the membrane used for the drug release test.

The drug release has been controlled during 24 h and at fixed time intervals (1, 2, 6, 8, 24 h), samples of the receiving solution were withdrawn

to measure the tretinoin content. The profile of the release during time is shown in Fig. 8.3. The study revealed that 40% of the loaded drug was released in 24 h. The amount of tretinoin released is a linear function of time, that is the velocity of release is constant. This is a very important result in the perspective of real applications, because it would imply the possibility to guarantee a constant administration of drug to the patient.

We also performed the study of the stability of tretinoin loaded in PS. We already said that one of the main agent which causes tretinoin degradation is illumination with light in the visible and UV range. Since these wavelength are within the absorption band of porous silicon, we can expect that the matrix can protect the molecules loaded within the pores from degradation. To study the degradation, we exposed loaded samples to UV light and we then analyzed the released drug with HPLC. The results show no trace of degraded TRA molecules, indicating that the drug was successfully protected from light degradation when inserted with the PS pores.

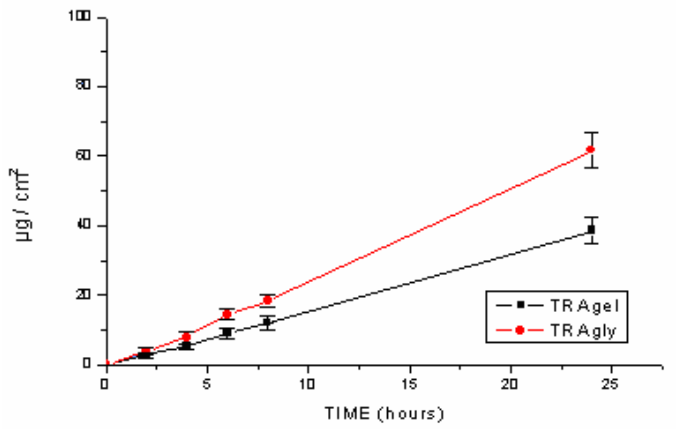

Fig. 8.3: Curve of the tretinoin release from porous silicon dispersed in two different media.

While being only preliminary results, all these observations demonstrate the potentiality of PS applications in drug delivery and encourage further studies.

In particular the first step would by to verify the reproducibility of the process of drug load and release, in order to predict the amount of drug that

the device can release per time unit. The subsequent study would be to study if the maximum load and the release velocity can be tuned by modifying the characteristics of porous silicon structure, i.e. the porosity, the pore size etc.

Also the study of tretinoin stability under UV illumination have to be investigated.

9 Appendix B: Photoelectrochemical characterization of PS for DNA sensing

9.1 Introduction

This work has been developed during a six months stage which took place at the LEPMI (Laboratoire d'Electrochimie et Physico-chime des Materiaux et des Interfaces) of the Institute Nationale Polytecnique de Grenoble (France), finalized to the verification of the feasibility of a PS-based photoelectrochemical biosensor for DNA sensing.

The idea is to use photoelectrochemistry as a technique for DNA recognition. The interest in this study comes from the property of PS / electrolyte interface to produce electric current when illuminated with radiation of energy larger than its gap. This property is strictly connected to the band bending and its reasonably itself affected by reaction occurring at the interface (§1.2.2). The operation basics are the following: we immobilized a particular DNA sequence on PS samples and then we exposed the sample to a solution containing other DNA sequences. We expected a different response in photocurrent when the sequence is the complementary to that immobilized or not.

Two different research groups were involved in the work, besides our: The CMESSIE (Couches Minces et Spectroscopie des Surfaces et des Interfaces Electrochimiques) group directed by Dr. Thierry Pagnier and the POE (Photo et Opto-Electrochimie) group directed by Prof. Didier Delabouglise.

9.2 Photoelectrochemical characterization of the PS / electrolyte interface

Here we present preliminary results obtained from the photoelectrochemical characterization of the PS/ electrolyte interface.

9.2.1 Experimental setting

The scheme of the photocurrent measurements experimental setting is shown in Fig. 9.1. The light source is an Hg lamp, L indicates lens, C is the chopper, MC is the monochromator and M is a mirror. A monochromator allows the choice of particular wavelengths in the lamp spectrum.

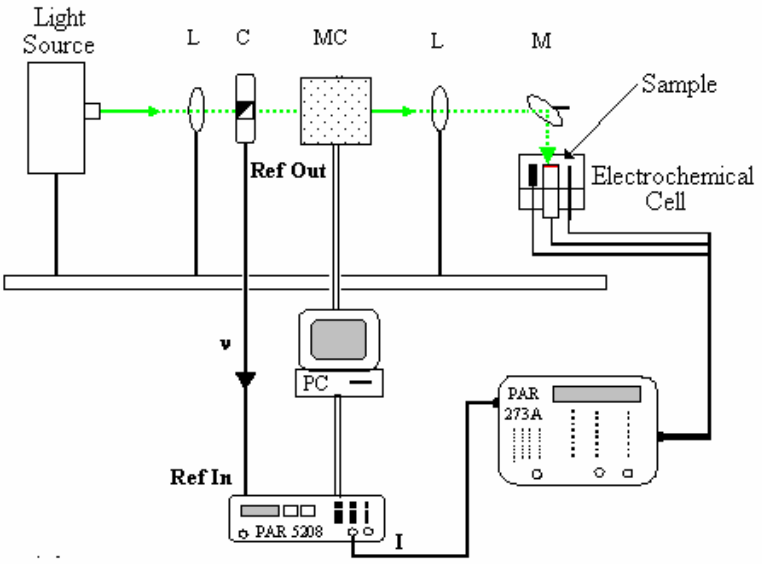

Fig. 9.1: Scheme of the apparatus used for photoelectrochemical measurements.

9.2.2 Results

In § 7.3.1 we have seen that the photocurrent has its maximum for a polarization voltage equal to the OCP; therefore we first determined the OCP of the cell, and then we polarised the interface at that value for all

measurements. The spectrum of photocurrent as a function of the excitation energy is shown in Fig. 9.2, where a comparison with the spectrum of a crystalline silicon sample is shown. The first observation is that porous silicon exhibits higher efficiency as compared to crystalline silicon.

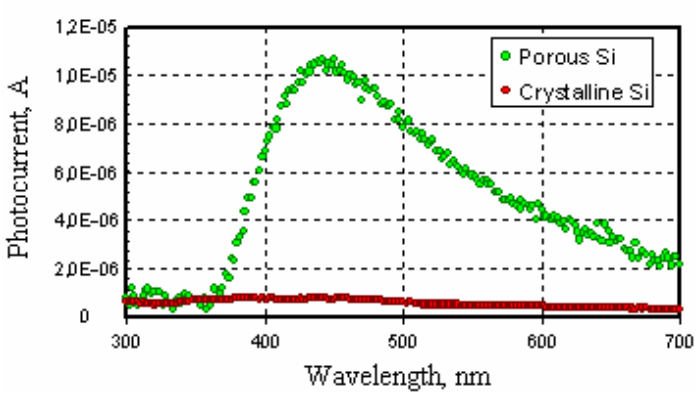

Fig. 9.2: Photocurrent spectrum of PS.

According to literature[90], we can observe a large band in the visible range with a maximum at $\lambda = 450$ nm. The energy at which light begins to be absorbed form porous silicon is compatible with a value of the indirect energy gap of 1.2 eV (Fig. 9.3).

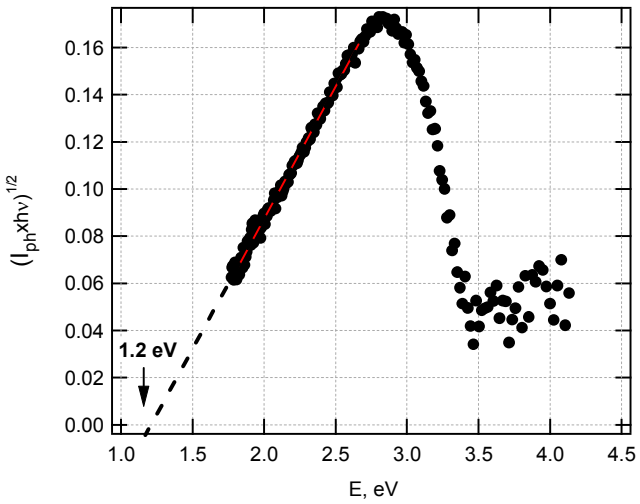

Fig. 9.3: Photocurrent spectrum of PS with the photon energies as x axis.

Once determined the photocurrent maximum, measurements were performed by exciting the samples with the 488 nm ray of an Argon laser of power equal to 20 mW. Photocurrent was measured by alternating periods of dark and enlightening of 100 s each (Fig. 9.4). We can see that for a power of 20 mW the photocurrent (given by the difference between the dark current and the light current) is quite constant and equal to 400nA.

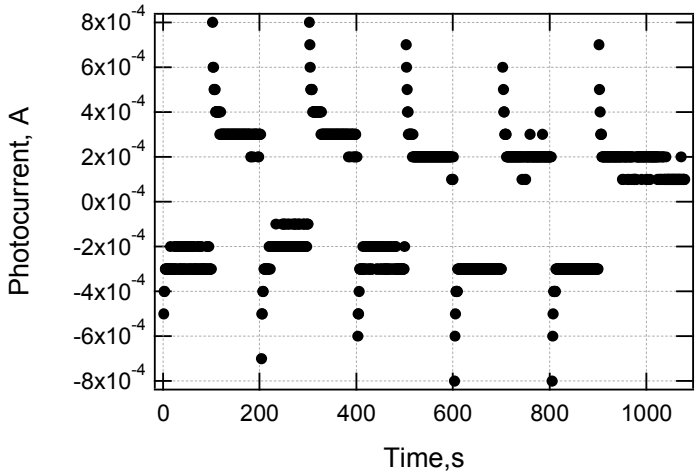

Fig. 9.4: Photocurrent as a function of time, alternating dark and enlightening.

The value of photocurrent as a function of the laser power is shown in Fig. 9.5. For laser powers lower than 60 mW, photocurrent increasess linearly with power. For impinging powers larger than 60 mW a saturation is observed, due to the fact that the increase of the sample temperature causes thermal agitation which favour the recombination of electron hole pairs, which do not diffuse to give further contribution to photocurrent..

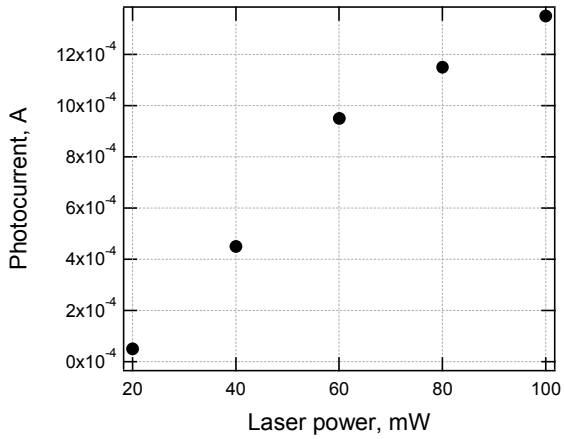

Fig. 9.5: Photocurrent as function of the laser power.

We observed that surface oxidation is a critical parameter for photoconductive property of PS. In fact the presence of an oxide layer on the surface, that is indispensable to prevent dissolution in aqueous media, creates an insulating barrier which prevents charge diffusion and causes a strong decrease of photocurrent. The only way to stabilize the surface using oxidation is to fully oxidize the samples, because partially oxidized samples immersed in aqueous solutions are stable only for short periods of time (§ 6.5). In order to form samples stables and suitable for the construction of a photoelectrochemical biosensor, other techniques of surface stabilization must be developed in alternative to oxidation.

9.2.3 DNA sensing

Preliminary characterizations were performed using samples naturally oxidized, which guarantee stability for a period of a few days.

We immobilized a single strand of DNA on porous silicon samples, by passive immersion in dilute physiological solution for 24h. We have tested the photocurrent evolution during in situ injection of other DNA strands, i.e. complementary strand (Fig. 9.6) or non complementary strand. The response is clearly different in the two cases.

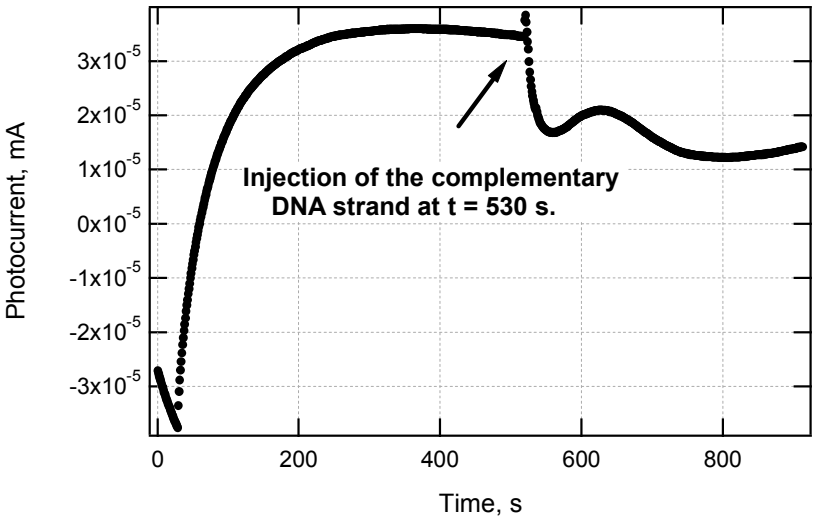

Fig. 9.6: Photocurrent plot of DNA-loaded PS layer during time. A DNA strand complementary to that immobilized in the pores is injected in the electrolyte at a time t = 530 s.

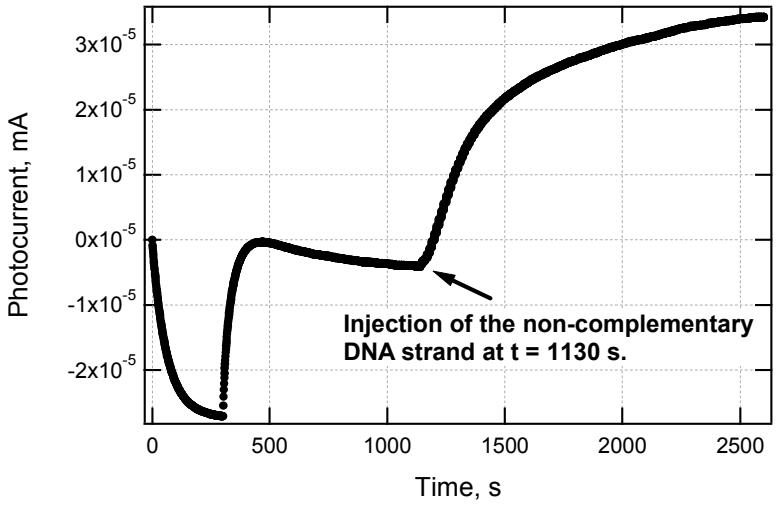

Fig. 9.7: Photocurrent plot of the DNA-loaded PS layer during time. A DNA strand non-complementary to that immobilized in the pores is injected in the electrolyte at a time t = 1130 s.

These results are very promising and will need further experiments.

10 Conclusions

In this Ph.D. work we fabricated a porous silicon-based proof-of-principle potentiometric biosensor for the detection of tryglicerides that is compact, easy to use, efficient, re-usable. This result was obtained in a close collaboration with the group 'Biocatalisi' directed by Prof. Maura Monduzzi of the Chemical Sciences Department of Cagliari University,

The device is based on the coupling between PS with an enzyme (lipase) able to catalyze the hydrolysis of triglicerides. It is constituted by a PS electrode, on which the lipase is immobilized, that is immersed in the solution to be analysed. The parameter used for the detection is the *open circuit potential* (OCP), that is the potential of the PS electrode referred to a reference electrode, with no current flow. OCP is in fact a parameter characteristic of semiconductor/electrolyte systems that is very sensitive to reactions occurring at the interface.

For the realization of our biosensor we required that the material to be used had a large developed surface for the immobilization of large amounts of bioactive molecules, pore dimension adapted to the molecules' size, good mechanical and chemical stability. In this view, porous silicon showed most of the desired attributes. The structural properties of our PS layers were then characterized by means of HRXRD, SEM-FEG and N_2-adsorption measurements, in order to verify their fit for the realization of the biosensor and for the optimization of the formation parameters.

A major drawback during the first tests of enzyme immobilization was the observed dissolution of the porous layers in aqueous media, which prevents the realization of stable and reusable devices. This problem was overcame by performing anodic or thermal oxidation of the porous layers just after formation, that lead to samples stability in aqueous solution for

time periods longer than one year. The detailed study of the anodic oxidation process has lead to new insights in the understanding of the PS formation process. In particular, we observed a slight morphological inhomogeneity in the porous layers, since it appears that the layers first ten micrometers have a higher porosity likely due to a larger amount of nanosized pores in this region. This morphology inhomogeneity is not visible by SEM-FEG investigation, but can be deduced from the oxygen content determination.

The immobilization process has been optimized, using standard analytical techniques, to obtain the greatest device efficiency in terms of thenzymatic activity. The sensitivity of the loaded- PS matrix to the triglycerides concentration showed a behaviour that almost perfectly fit the Michaelis – Menten equation. Since this equation refers to a free enzyme in a solution, this result demonstrate that the immobilized enzyme behaves as a free enzyme and that there are no diffusion problem within the pores, which is very important to fabricate a well performing device.

The sensitivity of the porous silicon / electrolyte interface to changes in pH was tested by OCP measurements using buffer solutions with different pH, and showed a dependence well above the instrumental sensitivity and well fitted for standard applications. This OCP dependence on pH was found to be independent on the presence of immobilized lipase onto the pores's surface, at least within the pH range of the triglycerides emulsions we used in our test.

For all triglycerides concentration measurements we used a short chain triglyceride, tributyrin, commonly used for this kind of tests.

The biosensor was calibrated performing a series of measurements using emulsions with different tributyrin concentrations. The rate of variation of OCP was found to depend on the substrate concentration, with a response time shorter than 5 minute. The biosensor response to different tributyrin concentrations in the 0-0.03 mol/ L range, that is compatible, for instance, with the usual human blood triglycerides concentrations, was univocal and well defined.

Study on life time and reusability of the device have been made, showing that the device can be safely stocked in a pH = 5 buffer at a temperature of 4 °C, and reused for a total working time correspondent to more than 100 assays without loss of efficiency.

We were then able to fabricate a prototype biosensor that match all our objectives, since the device show an univocal and well defined fast response to different tributyrin concentration, united with a high degree of reusability. Moreover, the reduced size of the samples united with the simplicity of OCP measurements will allow the fabrication of compact-size devices.

In the course of this thesis, we also investigated two others applications of porous silicon in biotechnology, that have been presented in the appendices of this manuscript since they are at a very early stage: the use of PS matrices as carriers for drug delivery (in collaboration with the 'Farmaco Chimico Tecnologico' department of Cagliari University) and the study of a PS biochip for DNA recognition based on photoelectrochemical measurements (developed during a six-month stage at the INPG of Grenoble, France). Both applications show very interesting preliminary results that are very encouraging for continuing their development.

11 Perspectives

The first development in the development of the PS-based triglycerides biosensor would be the check of the functioning for longer chain triglycerides and the application to real situations (analysis of blood samples for example). Second, it would be interesting to develop chemical immobilization techniques to improve the biosensor performance. For instance, we cited the possibility to functionalize the inner pores' surface by means of some chemical species adapted for the chemical bonding of the lipase. This possibility may be very interesting to improve the amount of enzyme molecules bonded to the pores' surface, but it demands a great care to keep the enzyme molecules functionality reasonably unchanged.

For a complete understanding of the reactions occurring at the oxidized PS / electrolyte interface an accurate investigation of the surface bonds, for example through FTIR, would be required.

12 References

1 J. Wang, Analyst, **130**, 421 – 426 (2005).

[2] A. Uhlir, Bell Syst.Tech.J. **35**, 333 (1956).

3 G. Vincent, Appl. Phys. Lett. **64**, 2367 (1994).

4 A. H. Mayne et al. Phys. Stat. Sol. (a), **182**, 505-513 (2000).

5 L.T. Canham, Appl. Phys. Lett. **57**, 1046 (1990).

6 A. J. Bard and L. R. Fanlkner, Electrochemical methods: Fundamentals and applications. John Wiley & Sons, NawYork (2000).

7 H. Gerischer, Advance in electrochemistry and electrochemical engineering I, Ed. P. Delahay, C. W. Tobias, Interscience Publ., New York. 139- 162 (1961).

8 Teaching notes of Prof. J. E. Moser at the École Politechnique Fédérale of Lausanne, Switzerland : http://photochemistry.epfl.ch/EDEY/JEM_3.pdf.

9 J. van de Lagemaat, J. Appl. Phys. **83**, 6089-6095 (1998).

10 M.J. Madou et al. Surf. Sci. **108**, 132-152 (1981).

11 H. F. Okorn-Schmidt, J. Res. Develop. **4**, 351 (1999).

12 M.M Rieger, P. A. Kool, J. Electrochem. Soc. **145**, 1490 (1995).

13 R. Memming, G. Schwandt, Surf. Sci. **4**, 109- 124 (1966).

14 V. P. Parkhutik et al.Surface technology, **20**, 265-277 (1983).

15 M.I.J. Beale et al. Appl. Phys. Lett. **46**, 86 (1985).

16 V. Lehmann, U. Gösele, Appl. Phys. Lett., **58**, 956-858 (1991).

17 H. Foll, Appl. Phys. **A. 53**, 8 (1991).

18 M.I.J. Beale et al. J. Crystal Growth **73**, 622-636 (1985).

19 N.–J. Chazalviel et al. Materials Science and Engineering B, **69**, 1–10, (2000).

20 Hans Joachim Lewerenz, Jaroslaw Jakubowicz and Helmut Jungblut, Electrochemistry Communications, **6**, 1243–1248 (2004).

21 R. L. Smith and S. D. Collins, J. Appl. Phys. **7**, R1-R22 (1992).

22 E.P. Barett, L. G. Joyner, P.P. Halenda, J. Am. Chem. Soc. (USA) 73, 373 (1951).

23 Dollimore D., G.R. Heal, J. Appl. Chem. 14, 109 (1964).

24 R. Hérino, G. Bonchil, K. Barla, C. Bertrand, J. L. Ginoux, Journal of Electrochemical Society, 134, 8 (1987).

25 K. Barla et al. J. Crystal Growth **68**, 721 (1984).

26 M. Mynbaeva et al. Appl. Phys. Lett. **78**, 117-119 (2001).

27 S. I. Romanov et al., Appl. Phys. Lett. **75**, 4118-4120 (1999).

28 Huang Yi-Ping et al. *Chinese Phys. Lett.* **18**, 1507-1509 (2001).

29 L. T. Canham, *Pore type, shape, size, volume and surface area in porous silicon*. From: Properties of Porous Silicon, Edited by L. Canham, Institute of Engineering and technology (1997).

30 A. Halimaoui, Porous silicon science and technology, Lecture 3 of "Porous silicon sciences and technology", Les editions de Physique, 1994.

31 J. –N. Chazalviel and F.Ozanam, *Surface modification of porous silicon*. From: Properties of Porous Silicon. Edited by L. Canham, Institute of Engineering and technology (1997).

32 E.A. Petrova et al. Materials Science and Engineering B **69**, 152–156 (2000).

33 L. T. Canham, Phys. Stat. Sol. (a) **182**, 521–52 (2000).

34 S.H.C. Anderson, Phys. Stat. Sol. (a) **197**, 331– 335 (2003).

35 Claudia Steinem, Tetrahedron **60**, 11259–11267 (2004).

36 Petrova-Koch et al. Appl. Phys. Lett. **61**, 943 (1992).

37 O. Bisi et al. Surf. Sci. Rep. **38**, 1-126 (2000).

38 J.L. Cantin et al., Thin Sol. Films, **276**, 76-79 (1996).

39 A.Bsiesy et al. Surf. Sci., **254**, 195 (1991).

40 A.Bsiesy et al. J. Electrochem. Soc. (USA), **138**, 3450-6 (1991).

41 I. Mihalcescu, PhD Thesis at Joseph Fourier University of Grenoble, France, (1994).

42 M. A.Hory et al. Thin Sol.Films, **255**, 200-203 (1995).

43 R.Herino, *Luminescence of porous silicon after electrochemical oxidation*, Lecture 4 of "Porous silicon sciences and technology", Les editions de Physique, 1994.

44 A. Nakajima et al. Appl. Phys. Lett. (USA) **61**, 46-8 (1992).

45 C. Peng et al. Metr. Res. Soc. Symp. Proc. (USA) **298**, 179 (1993).

46 X. Wang. Appl. Phys. Lett. (USA) **63**, 2363-5 (1993).

47 L.T. Cahnam, *Chemical composition of intentionally oxidized porous silicon*. From: Properties of Porous Silicon, Edited by L. Canham, Institute of Engineering and technology (1997).

48 L. T. Canham, *Biomedical applications of porous silicon*, From: Properties of Porous Silicon, Edited by L. Canham, Institute of Engineering and technology (1997).

49 L. T. Canham et al. Adv Mater. **7**, 1055 (1995).

50 L.T. Canham et al. phys. stat. sol. (a) **182**, 521 (2000).

51 Jeffery, L. Coffer, phys. stat. sol. (a) **197**, 336– 339 (2003).

52 V. Chin et al. Adv. Mater.,**13**, 1877 (2001).

53 J. M. Schmeltzer and J. Buriak. *Recent development in the Chemistry and Chemical Applications of Porous silicon*. From 'The Chemistry of nanomaterials: Synthesis, Properties and applications', Volume2, WILEY-VCH (2004).

54 Blum, J.L.; Coulet P.R.; Biosensor: Principle and Application, Oxford Univ. Press, NY (1989).

55 C. Jianrong et al., Biotechnology Advances **22**, 505–518 (2004).

56 W. Vastarella, PhD thesis at the Bari University (2001).

57 M. Bengtsson et al., phys. stat. sol.(a) **182**, 495 (2000).

58 N. Alonso et al., J. mol. Catal., B Enzym, **135**, 57-61 (2005).

59 K. Wannerberger, Dissertation, Lund University (1996).

60 Salis, A. Et al., Langmuir, **21**, 5511 (2005).

61 I. Schechter et al., Anal. Chem., **67**,3727-3732 (1995).

62 R. W. Bogue, Biosensors & Bioelectronics, **12**, R 27 (1997).

63 V. S.-Y. Lin et al., Science, **278**, 840-843 (1997).

64 G. Di Francia et al., II Workshop on chemical sensors and biosensors, ENEA-Casaccia, Rome, Italy (1995).

65 S. Chan et al., Materials Science and Engineering C, **15**, 277–282 (2001).

66 S. Chan et al., phys. Stat. sol. (a) **182**, 541 (2000).

67 M. Thust et al., Measurement Science and Technology, **7**, 26-29 (1996).

68 M. Thust et al., Journal of molecular catalysis B: Enzymatic **7**, 77-83 (1999).

69 R. Reddy et al., Biosensors & Bioelectron. **16**, 313-317 (2001).

70 R. Reddy et al., Applied Physics **3**, 155-161 (2003).

71 S. Brunauer, P. H. Emmett, E. Teller, J. Am. Chem. Soc. (USA) **60**, 309 (1938).

72 R.Herino, *Pore size distribution in porous silicon*. From: Properties of Porous Silicon, Edited by L. Canham, Institute of Engineering and technology (1997).

73 K.-E. Jaeger et al. Curr. Opin. Biotechnol., **13**, 390-397 (2002).

74 A. Salis, M. Monduzzi, V. Solinas, Biocatalysis: Chemistry and Biology; Trincone, A., Ed.; Research Signpost: Kerala, 29-53 (2005).

75 A. Pandey et al., Biotechnol. Appl. Biochem. **29**, 119-131 (1999).

76 P. Grochulski, et al., M. Protein Sci. **3**, 82-91 (1994).

77 P. Grochulski et al., J.Biol.Chem. **268,** 12843-12847 (1993).

78 From producer's specification sheet.

79 D.M. Lawson et al., Protein Eng. **7,** 543–550 (1994).

80 J. Czochralski, Z. Phys. Chem. **92**, 219-221 (1918).

81 Valeria Demontis, Tesi di laurea at the Università degli Studi di Cagliari (2003).

82 O. Belmont et al., Thin Sol. Films, **276**, 219-222 (1996).

83 D. Bellet, *Drying of porous silicon*. From: Properties of Porous Silicon, Edited by L. Canham (1997).

84 Silvia Salis, Tesi di laurea at the Università degli Studi di Cagliari, (2005).

85 Y.-J Han et al., J. Mol. Catal. B **17,** 1 (2002).

86 J. van de Lagemaat, J. Appl. Phys., **83**, 6089-6095, (1998).

87 M. J. Madou and S. R. Morrison, Chemical Sensing with Solid State Devices (Academic, Boston, 1989).

88 D. Voet, J. Voet, C. Pratt, Fondamenti di biochimica, Zanichelli (2001).

89 D. J. Elbaum, J. Am. Acad. Dermatol. **19**, 486-491 (1988).

90 B. Unal et al., J. Appl. Phys. **87**, 3547 (2000).